# THE INFLUENCE OF ANGLED SURVEY LINES ON THE DATA AND RESULTS OF 2D ERT SURVEYS USING THE WENNER (α) ARRAY

Unarine Mukhwathi

Submitted in fulfilment of the requirements for the degree

*Magister Scientiae in Geohydrology*

in the

Faculty of Natural and Agricultural Sciences

(Institute for Groundwater Studies)

at the

University of the Free State

Supervisor: Dr FD Fourie

January 2020

## *DECLARATION*

I, Unarine MUKHWATHI, hereby declare that the dissertation hereby submitted by me to the Institute for Groundwater Studies in the Faculty of Natural and Agricultural Sciences at the University of the Free State, in fulfilment of the degree of Magister Scientiae, is my own independent work. It has not previously been submitted by me to any other institution of higher education. In addition, I declare that all sources cited have been acknowledged by means of a list of references.

I furthermore cede copyright of the dissertation and its contents in favour of the University of the Free State.

Unarine MUKHWATHI

22 January 2020

## *ACKNOWLEDGEMENTS*

First and foremost, I would like to thank the Lord Almighty for the favour He has bestowed upon my life and blessing me with the opportunity to do my degree at the University of the Free State (Institute for Groundwater Studies), and for giving me wisdom and strength that kept me striving towards completing this study. Without Him everything within this dissertation would not have been possible.

I would like to thank the Institute for Groundwater Studies for accepting me as a student.

I have always thought that conducting research was an impossible task when I faced difficulties during this dissertation write-up process. However, I found it very interesting because of the help, sustained support, and guidance I received from the following individuals;

- Firstly, I would like to express my sincere gratitude to my supervisor Dr FD Fourie for his continuous support throughout this study, for his patience and immense knowledge. His guidance has helped me all the time during my research process and writing of this dissertation.
- My heartfelt gratitude goes to my mother Mrs T.M Mukhwathi, for her love, support and encouragement. I would also like to thank my late father Mr A.E Mukhwathi who passed away few months before the submission of this dissertation for his continuous support, motivation and words of encouragement. To my siblings, this dissertation would not have been completed without your love and moral support.
- This dissertation owes its existence to my friends in Bloemfontein who assisted me a lot with the fieldwork.

## *TABLE OF CONTENTS*

## *LIST OF FIGURES*

# *LIST OF TABLES*

# *LIST OF ABBREVIATIONS*

| | |
|---|---|
| 1D | One-dimensional |
| 2D | Two-dimensional |
| 3D | Three-dimensional |
| CBD | Central business district |
| ERT | Electrical resistivity tomography |
| VES | Vertical electrical sounding |

# CHAPTER 1:
# INTRODUCTION

## 1.1 BACKGROUND

The electrical resistivity method was first developed in the 1920s but has been widely used since the 1970s due to advances in the technology to collect, analyse and process data (Loke, 1999). This geophysical technique is one of the main methods used to investigate the subsurface resistivity distribution. Until recently, electrical resistivity surveys were mostly conducted in a one-dimensional (1D) mode, either by performing *vertical electrical sounding* (VES) where resistivity variations with depth are investigated, or *horizontal profiling* where lateral resistivity variations are studied.

However, 1D surveys have several limitations. VES allows the modelling of only horizontally layered earths and it does not provide tangible information for the interpretation of structures and the extent of subsurface features (Loke *et al*., 2013). Horizontal profiling, in turn, assumes a constant depth of investigation along the profile, which is not strictly true since the depth of investigation is dependent on the subsurface resistivities. To overcome the limitations of a 1D surveying, two-dimensional (2D) and three-dimensional (3D) resistivity methods were developed. These methods are more accurate, convenient, and field worthy, since they are more technologically advanced and easier to use than the 1D modes of investigation.

The 2D electrical resistivity tomography (ERT) method has become one of the most widely used geophysical technique in investigating near-surface structures. This method was developed to satisfy the need for new technologies that can generate high-resolution sections of the sub-surface (Daily *et al*., 2005). The ERT method is based on the fact that different geological units or structures in the earth's subsurface are more or less sensitive to electrical current flow and that different geological units have different electrical conductivity (Milsom and Ericksen, 2011).

During 2D ERT surveys, apparent resistivity data are collected by using numerous collinear electrodes inserted into the earth along a straight line. The measured resistivity data are later edited, processed, and inverted using 2D inversion software to yield models of the subsurface resistivity distribution. The 2D ERT technique has been recently applied to address a number of engineering, geological and geo-hydrological problems such as detection of faults and fractured zones, investigation of the slope stability, and delineation of cave systems (Yadav, 1988; Kumar, 2012; Obi, 2012; Mohamaden and Ehab, 2017)

In geohydrological studies, the main applications of the ERT technique are to investigate 1) the presence of geological structures potentially associated with groundwater, 2) the movement of

groundwater and 3) the presence and migration of contaminants in the subsurface. The technique has been widely used in this field because quality water resources have become a primary concern in many societies due to increasing population and industrialisation (Donnenfeld *et al.*, 2018). To increase water supply and sustain industrial demands, economic growth and growing population, all potential water resources should be appropriately utilised and managed. Groundwater often forms a large component of the total water supply to communities. However, unlike surface water that can be seen or measured, groundwater is generally not visible from surface. In addition, the occurrence of groundwater is localised and often associated with geological structures. The ERT method may be used to investigate the subsurface and locate sites where production boreholes have a high probability of intersecting high-yielding aquifer systems, thereby avoiding the wasteful expenditure of drilling unsuccessful production boreholes.

Studies conducted by Woodford and Chevallier (2002) in the Karoo Basin, show that dolerite intrusions (dykes and sills) are considered as the main targets for groundwater exploration. Dolerite dykes in the Karoo Basin are linear or circular (ring-dykes) geological bodies that intruded the sedimentary country rock during the Jurassic Age. According to Makhokha and Fourie (2016), the intrusions were associated with the high temperatures and pressures, causing fractured zones along the margins of the intrusive bodies. Moreover, the fractured zones are often associated with significant permeability and high-yielding aquifers (Woodford and Chevallier, 2002).

Since large resistivity contrasts generally exist between the dolerite intrusives and the sedimentary country rock, the 2D ERT method is well-suited to locating and delineating such intrusives. However, a major assumption of the method is that the survey lines are straight and electrodes are collinear. Due to the presence of surface infrastructure or other surface constraints (e.g. rivers, vegetation, large outcrops, and steep topographic gradients) it is not always possible to conduct 2D ERT surveys along straight lines. The study investigates the influence of angled survey lines on the data recorded and the resistivity models obtained when using the Wenner (α) array. This array is one of the most commonly used arrays in resistivity surveying and has a high signal-to-noise ratio compared to the other commonly used arrays.

## 1.2 PROBLEM STATEMENT

Two-dimensional ERT surveys typically employ multiple electrodes laid out along a straight line. The systems used for surveying employ protocols that control switching between various electrode pairs to take measurements at different positions along the survey line. The standard protocols assume that the survey lines are straight and the electrodes are collinear. However, it is often not possible to conduct 2D ERT surveys along straight lines, and the collinear assumption of the protocols breaks

down. When survey lines are angled, the resistivity data and results may be affected for measurements where electrodes straddle the position of the angle in survey lines, since the assumed distances between some of the electrodes are larger than the actual (true) distances. This may result in:

- Incorrect geometric factors and apparent resistivities,
- Incorrect estimation of the depths of investigation,
- The volumes of the subsurface sampled may be displaced from the survey line and the recorded apparent resistivity data may be the representative of the subsurface at positions displaced from the survey lines.

Therefore, the need exists to investigate the impact that angled survey lines have on ERT data and the resistivity models derived from these data.

## 1.3 AIMS AND OBJECTIVES

The aim of this study is to investigate the impact of angled survey lines on the 2D ERT data and resistivity models obtained with the Wenner (α) across different geological structures typically found in the Karoo Basin.

To address the aim of this research, the following objectives are defined:

- To review the geological and geohydrological conditions of the Karoo rocks, with specific focus on the structures that may act as or be associated with aquifers,
- To review the 2D ERT method focusing on the fundamental theory of the resistivity method, the sensitivities and depths of investigation of the various electrode arrays, and lastly, the effects of electrodes misplacement on the recorded resistivity data.
- To investigate through theoretical considerations, the influence of angled survey lines on the geometric factors, apparent resistivities, depths of investigation and volumes of the subsurface investigated.
- To use numerical models to calculate and evaluate the influence of angled survey lines on the resistivity models obtained for both small and large angles in the survey lines.
- To perform field surveys along straight and angled survey lines across known geological structures to confirm the results of the theoretical predictions and numerical models.
- To make recommendations, based on the results of the investigations, for the processing and interpretation of ERT data recorded along angled survey lines.

## 1.4 RESEARCH METHODOLOGY

The research methodology followed to achieve the aim and objectives of this study is divided into four components described below:

- **Literature review:** performing a review of the literature on the geological and geohydrological conditions of the Karoo Supergroup, on a regional scale and within the location of the study areas. This also incorporates a review of the electrical resistivity method.
- **Theoretical investigations:** studying the influence of angled survey lines on the geometric factors, apparent resistivities, depths of investigation and volumes of the subsurface sampled during ERT surveys from a theoretical perspective. The percentage errors in the geometric factors and apparent resistivities for angled survey lines are investigated and calculated by taking into account the true or calculated geometric factors. The depth of investigation is investigated in terms of the median depth by following the methodologies of Roy and Apparao (1971) and Edwards (1977). The volume of the subsurface investigated by calculating the three-dimensional (3D) Fréchet derivative for electrodes along angled survey lines.
- **Numerical modelling:** modelling of the ERT responses across potential groundwater targets typically encountered in Karoo rocks (dykes, sills, contacts, weathered zones) for straight and angled survey lines by forward and inverse modelling. The responses for the angled survey lines are evaluated against the response for the straight survey line.
- **Field surveys:** conducting surveys across known geological structures along straight and angled survey lines and comparing the results.

## 1.5 STRUCTURE OF DISSERTATION

This dissertation is structured as follows:

**Chapter 1** gives an introduction to the study and describes the aim and objectives of the research, as well as the research methodology followed to achieve the aim of this study.

**Chapter 2** is a literature review of publications relevant to the current study. The literature review comprises a review of the geology and geohydrological conditions of the Karoo Supergroup, a review of the electrical resistivity method, and lastly a review of the effects of electrode misplacement on electrical resistivity surveys.

In **Chapter 3** the influence of angled survey lines on ERT data is discussed from a theoretical perspective.

**Chapter 4** discusses the results of numerical modelling of the ERT responses over different geological structures typically encountered in the Karoo rocks for straight and angled survey lines. The results are obtained using forward and inverse modelling software.

**Chapter 5** discusses the results of field ERT surveys conducted at three sites across known geological structures for both straight and angled survey lines.

In **Chapter 6** the conclusions drawn from the study are discussed. Recommendation for further studies are also made.

# CHAPTER 2:
# LITERATURE REVIEW

## 2.1 INTRODUCTION

In this chapter, a review of the literature relevant to the current study is done. Since the fieldwork component of the study is done on the rocks of the Karoo Supergroup, the literature review begins with a discussion of the geology and geohydrology of the Karoo Supergroup. The aim is to give an overview of the lithological conditions encountered in the Karoo Supergroup, with a particular focus on the groundwater occurrence within Karoo rocks. This is followed by the discussion of the principles of the electrical resistivity methods, together with the description of the effects of electrode misplacements on recorded resistivity data.

## 2.2 GEOLOGY OF THE KAROO SUPERGROUP

The rocks of the Karoo Supergroup cover more than 50% of the land surface of South Africa and form a thick pile of sedimentary successions or sedimentary strata that were deposited over the period of 310 to 182 million years ago (late Carboniferous to the middle Jurassic periods) (McCarthy and Rubidge, 2005). This supergroup originated millions of years ago when an intracratonic and foreland basin on Gondwanaland was filled with sediments. During those periods Gondwanaland drifted from polar to tropical latitude (Smith, 1990). This caused sedimentation to occur under different depositional environments (Herbert and Compton, 2007), which resulted in a supergroup that consists of different sedimentary strata each resembling its physical properties.

The sedimentary strata are made up of sedimentary rocks that were formed through the deposition and lithification of sediments, mainly sediments transported by ice (glaciers), water (rivers, lakes and oceans), and wind (Truswell, 1977). Lithification led to sedimentary rocks of the Karoo Supergroup with low permeability, low porosity, and reduced elasticity (Botha *et al*., 1998). Sediments of the Karoo Supergroup are divided into groups, and these groups are described as aggregates of two or more formations that share specific lithological characteristics. They are named: the Dwyka, Ecca, Beaufort, Stormberg, and Drakensberg Groups. These groups were named according to the climatic conditions and the depositional environment on Gondwanaland (McCarthy and Rubidge, 2005). The distribution of different groups in this supergroup is shown in Figure 2.1.

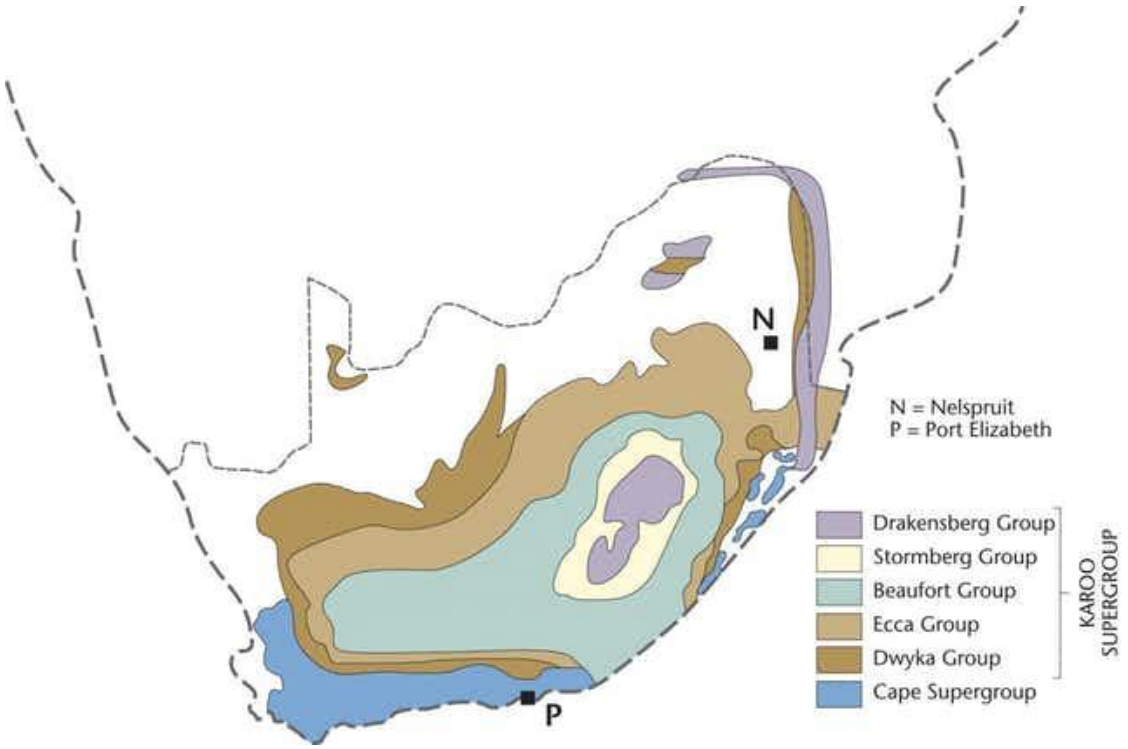


**Figure 2.1: Geological map showing the occurrence of the Karoo Supergroup in South Africa (McCarthy and Rubidge, 2005)**

The Karoo stratigraphic sequence (Figure 2.2) shows the occurrence of the different groups and their formations with the time of deposition. A north-south cross-section through the rocks of the Karoo Supergroup is shown in Figure 2.3. This cross-section shows the thickness of the pile of rocks in different groups and how that pile thins towards the north which is caused by the mountain-building episodes in the Cape Fold Belt, as well as the nature of the underlying lithosphere.

According to Woodford and Chevalier (2002), the geology of the main Karoo Basin was controlled by four major geodynamic events:

- Deposition of the Karoo sediments and the upliftment of the Cape Fold Belt,
- The intrusion of Karoo basalt and dolerite (dykes and sills), and the break-up of Gondwanaland,
- The intrusion of kimberlite and mantle up-welling, and,
- Modern geomorphology, deposition of recent sediments, uplift, and cessation of regional tectonism.

Some of the aspects of these four major geodynamic events will be explained in the upcoming sections.

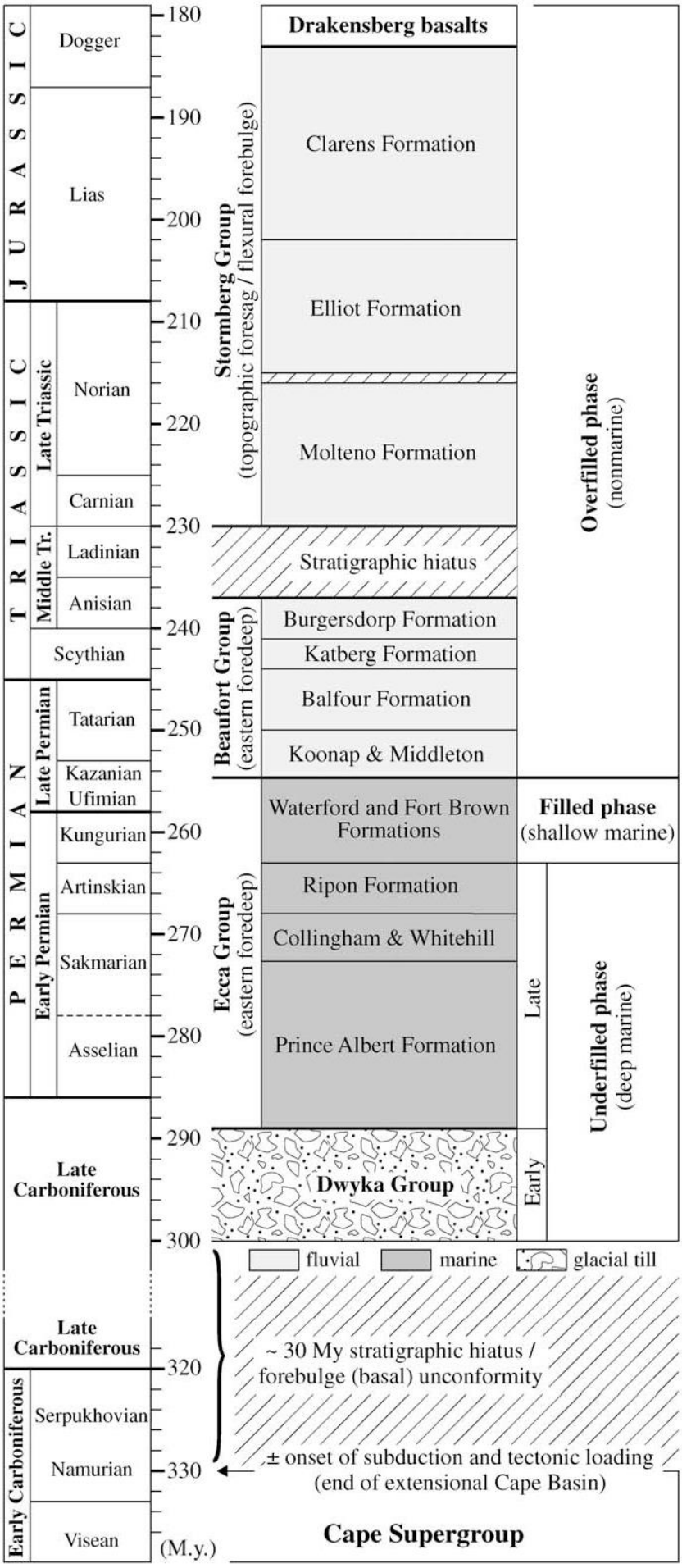


**Figure 2.2: Geological sequence of the main Karoo basin (Catuneanu *et al.*, 2005)**

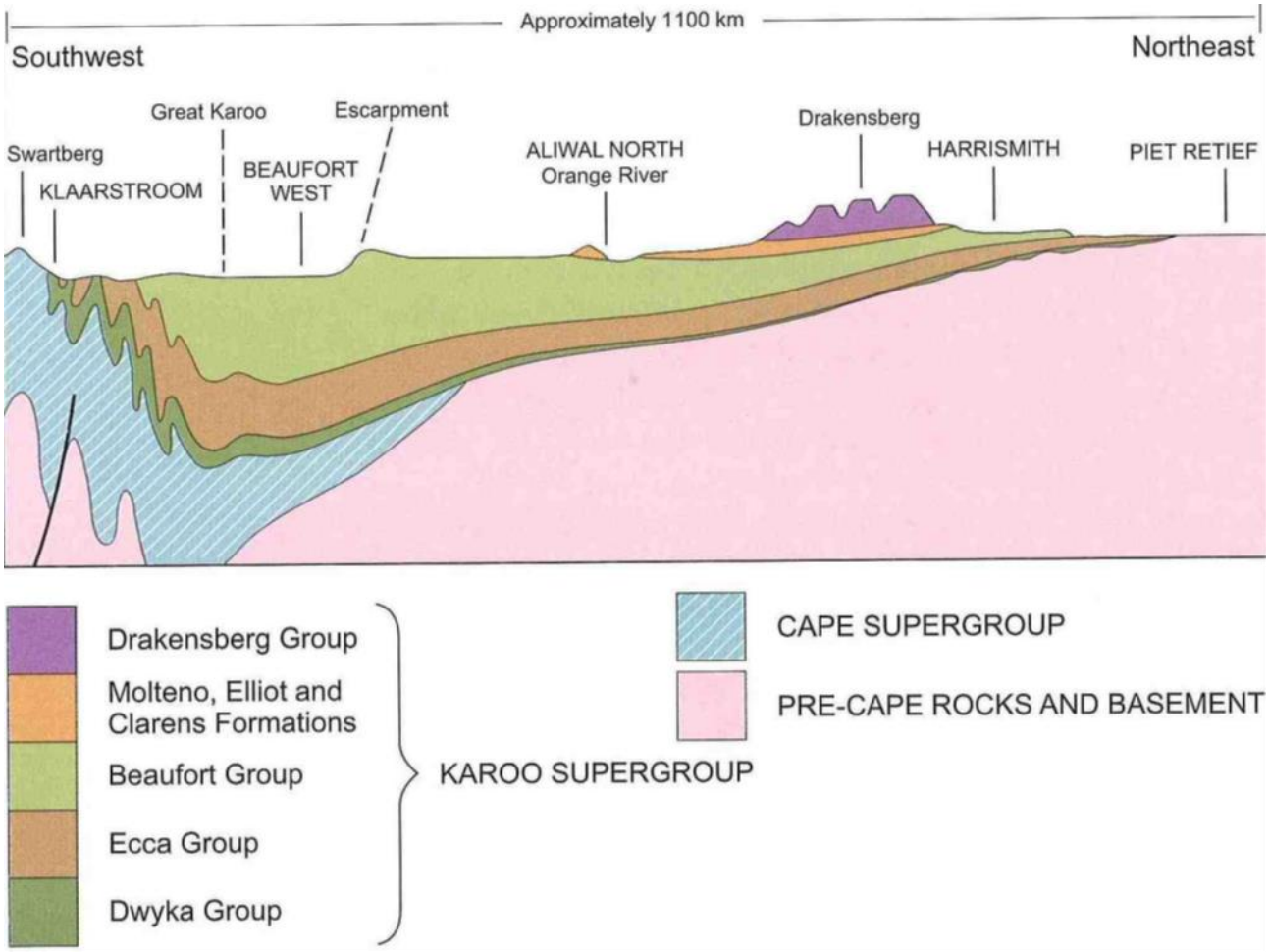


**Figure 2.3: Cross-section through the main Karoo Basin (Van Tonder, 2012)**

## 2.3 GEOLOGICAL AND GEOHYDROLOGICAL OVERVIEW OF STRATIGRAPHIC UNITS IN THE KAROO SUPERGROUP

### 2.3.1 Dwyka Group

#### 2.3.1.1 Deposition

The Dwyka Group is the first deposited and oldest deposit in the Karoo Supergroup basin. This group was formed in the late Carboniferous to an early Permian period (McCarthy and Rubidge, 2005; Smith, 1990). It was formed when the glacial deposits, which include diamictite, shale, and mudstone with conglomerates and fluvioglacial gravel, were left behind when glaciers melted and retreated (Linol and de Wit, 2016). These glacial deposits formed poorly sorted Dwyka tillite/ diamictite, which formed the first sediments deposits in the developing Karoo Basin (Smith, 1990).

In the southern part of the basin, the diamictite displays distinctive 'tombstone' morphology as a result of selective weathering along axial-plane cleavage (Woodford and Chevallier, 2002). This morphology was influenced by the Cape Fold Belt. The diameter of the clasts in the Dwyka diamictite is usually larger in the northern facies as compared to the southern facies (Botha *et al.*, 1998). Moreover, the clasts in the north facies tend to fine upwards.

#### 2.3.1.2 Geohydrological properties

This group is composed mainly of shale and diamictite with very low hydraulic conductivities and no primary voids. Conductivities range from $\sim 10^{-11}$ to $10^{-12}$ $m.s^{-1}$, and the water is confined within narrow fractures and joints (Woodford and Chevallier, 2002). It is regarded as a non-ideal unit for the development of the large-scale groundwater (Botha *et al*., 1998).

### 2.3.2 Ecca Group

#### 2.3.2.1 Deposition

The Ecca Group consists mainly of shale and sandstone deposited during the Permian period as clastic sediments (Botha *et al*., 1998). It was deposited in a broad and shallow inland sea by marine deposition. Three geographical zones or facies are identified namely: the Northern Facies with alternating layers of silts, sands, shale, and coal, the Western Facies which was developed in the south-western side of the basin consisting of bluish-black shale and sandstones, and the Southern Facies with greenish-grey shale and greywacke sand (Truswell, 1977). To expand, this group comprises several formations namely: the Prince Albert, Collingham, Vischkuil, Laingsburg, Ripon, Skoorsteenberg, Fort Brown, Waterford, Tierberg, Kookfontein, Pietermaritzburg, Vryheid, Volksrust and Whitehill Formations. According to Woodford and Chevallier (2002) the Ecca Group sediments were predominantly derived from:

- Clastic sedimentary material from the Cape Fold Belt,
- Volcanic ash exhaled from the magmatic arc situated along the Gondwana plate subduction zone, and,
- Sediments reworked in the Basin.

The Ecca sediments were deposited within the trough of a foredeep basin by prograding submarine fans and turbidites leading to the formation of the following formations: the Prince Albert, Collingham, Vischkuil, Laingsburg, Ripon and Skoorsteenberg Formations. The Fort Brown, Waterford, Tierberg, Kookfontein Formations were deposited as prodeltas and deltas. Furthermore, continental provenance located north and northeast of the basin supplied fluvial to deltaic sediments to the Prince Albert, Pietermaritzburg, Vryheid and Volksrust Formations (Woodford and Chevallier, 2002), as well as to the shallow lake deposits also known as the Whitehill Formation.

#### 2.3.2.2 Geohydrological properties

The Ecca Group is composed mainly of shale with thicknesses varying with location from 1500 m in the south to 600 m in the north (Botha *et al*., 1998). Since the shale is very dense it is often overlooked as an essential source of groundwater. The density of shale is highest in the southern parts and lower

in the northern regions. Therefore, there is a possibility that an economically viable aquifer may exist in the north region of the areas underlain by Ecca shales. Botha *et al*. (1998) suggested that the Ecca Group should not be neglected as possible source of groundwater since large quantities of water are pumped from the Ecca shales in some areas.

## 2.3.3 Beaufort Group

### 2.3.3.1 Deposition

The Beaufort Group covers the largest part of the Karoo Supergroup compared to the other groups (Truswell, 1977). It overlies the Ecca Group and it was deposited through fluvial processes during the Triassic age (Ahiakwo *et al*., 2018). The rocks were deposited by a large northward-flowing meandering river (Figure 2.4). It consists of a thick upward fining succession of sandstones and mudstones containing numerous thin layers of chert bands and rich tetrapod fauna remains. The sediments were produced from the fast-rising Cape Fold Belt. This group is subdivided into two subgroups, namely the Adelaide and Tarkastad Subgroups.

The Tarkastad Subgroup is subdivided into two formations namely; the Burgersdorp Formation, which is composed of brightly coloured red, blue and green mudstones, and the lower Katberg Formation, which consists of thick layers of sandstone, but also contains brightly coloured shales and mudstone (Botha *et al.*, 1998).

The Adelaide Subgroup consists mainly of grey, green, bluish, red mudstones and fine-grained sandstones. It is further divided into the Teekloof, Abrahamskraal and Balfour Formations.

Two fluvial processes (meandering and braided streams) were responsible for the deposition of Beaufort Group. The mudstone and sandstones are commonly red due to highly oxidised fluvial slopes on which the deposition occurred, and also due to the seasonal global temperature increase. In addition, the area of Bloemfontein where the study areas are located are underlain by the upper beds of the Adelaide Subgroup (Botha *et al.*, 1998).

### 2.3.3.2 Geohydrological properties

The aquifers in the Beaufort Group are multi-layered and multi-porous with variable thicknesses due to the lateral migration of the meandering materials over the flood plain. Thus, pumping of the multi-layered aquifer will cause faster drop in the piezometric pressure of the more permeable layers than of the less permeable layers. Therefore, it is possible to deplete the more permeable layers of the aquifer without materially affecting the piezometric pressure in the less permeable layers. Furthermore, the studies conducted by Botha *et al*. (1998) shows that a borehole drilled in a Beaufort

Group aquifer has a significant yield if it intersects the bedding-parallel fracture. Therefore, the bedding-parallel fractures plays an important role in the occurrence of groundwater.

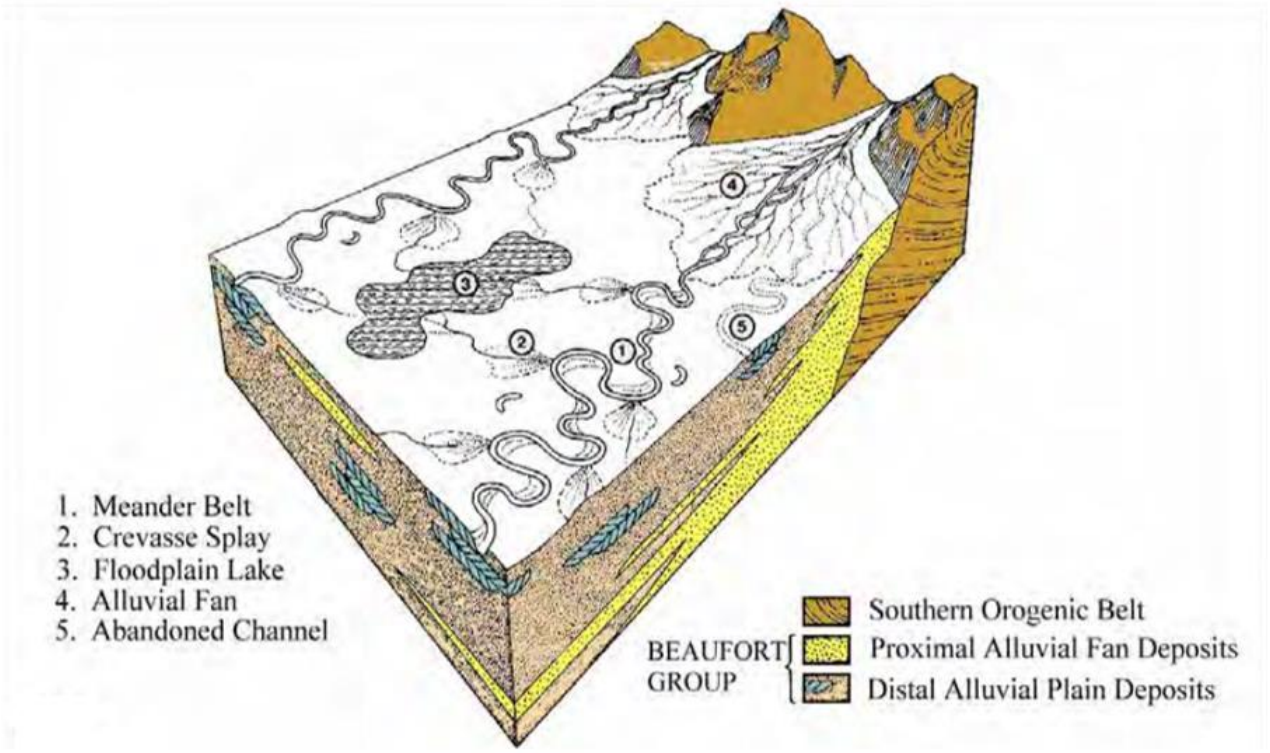


**Figure 2.4: Depositional environment of the Beaufort Group in the Southern Karoo Basin (Woodford and Chevallier, 2002)**

## 2.3.4 Stormberg Group

### 2.3.4.1 Deposition

The Stormberg Group is composed of the Molteno, Elliot, and Clarens Formations, from oldest to the youngest. The Molteno Formation is composed of sandstones that are tabular sheets of medium- to coarse-grained sediments that formed in a braided stream environment on a vast braid plain. The deposition in this formation was predominately bed-load from rivers. The Elliot Formation overlies the Molteno Formation. This formation comprises an alternating sequence of red mudstones and subordinate fine- to medium-grained sandstone (Figure 2.5). The reddish mudstone shows that the formation was deposited when the climate was changing to arid conditions (Smith, 1990).

**Figure 2.5: Alternating sequence of red mudstones and fine to medium-grained sandstone of the Elliot Formation in a road cutting on Wolfhuis pass**

Lastly, the Clarens Formation which was deposited in a desert environment, as indicated by fine-grained Aeolian sand dune deposits composed of fine-grained sandstones, sandy siltstones and mudstones (Figure 2.6). Minor basaltic lava flows interlayered with sandstone occur in the uppermost part of the formation. This signals the commencement of magmatic activity that led to the termination of sedimentation in the Karoo Basin.

**Figure 2.6: Layers of sandstones, sandy siltstones and mudstones of the Clarens formation sand dune**

### 2.3.4.2 Geohydrological properties

In the Molteno Formation, the sedimentary bodies are sheet-like and more persistent than those of Beaufort Group. Therefore, it is not likely to site high-yielding boreholes in this formation. The Elliot

Formation consists of relatively impermeable but highly porous rocks (Botha *et al*., 1998). Lastly, the Clarens Formation consists of well-sorted, medium-grained sandstones deposited as thick consistent beds. This formation is more homogeneous when compared to other Karoo formations. It also has high and uniform porosity. Furthermore, it comprises low permeability materials, since the rocks are poorly fractured. Therefore the formation may store a large volume of water, but is unable to release it quickly due to lack of fractures to allow the passage of groundwater (Botha *et al*., 1998).

### 2.3.5 Drakensberg Group

#### 2.3.5.1 Deposition

Sedimentation in the Karoo depression was terminated when the compression that prevailed throughout the deposition of the sediments of the Karoo Supergroup relaxed, which according to McCarthy and Rubidge (2005) happened approximately 182 million years ago after the start of the Jurassic period. The supercontinents of Gondwana drifted apart causing extension of the tectonic plates, resulting in the process called fissure eruption in which magma flows up onto the earth's surface through fissures in the earth's crust. The magma upwells to the surface of the earth along a complex system of fractures. Magma crystallises within these fractures forming basalts, dolerite sills and dykes. The volcanic activity produced massive thick lava piles along the Drakensberg Mountain range which cover a large area of Lesotho and central South Africa (Johnson *et al*., 1996).

#### 2.3.5.2 Geohydrological properties

In the Drakensberg Group, the aquifers are expected to be poorly developed in the upper massive and thick lava sequences. Furthermore, the rocks are characterised by a low permeability. The base of the Drakensberg lavas is composed of paleo-reliefs and inter-bedded sediments, and forms the most favourable zone for groundwater storage and movement. There are numerous springs formed at the contact zone between the Drakensberg Group and the Clarens Formation. Woodford and Chevallier (2002) concluded that boreholes drilled within the Drakensberg basalt often intersect water at the fractured and weathered zone contact with the sediment.

## 2.4 KAROO DOLERITE MAGMATISM

As previously mentioned, sedimentation in the Karoo Supergroup was ended by a widespread volcanism at the beginning of the Jurassic Age. Karoo magmatism occurred approximately 182 Ma ago (McCarthy and Rubidge, 2005). It is presumed to be related to the successive breakup of Gondwanaland during the early-middle Jurassic period. During the breakup of Gondwanaland the crust ruptured forming long crack-like fissures in the earth's crust, in which huge volumes of basaltic

lava upwelled (Manninen *et al*., 2008). The magma flowed through the fissures of the earth's crust and crystallised to form dolerite intrusion (Tankard *et al*., 2009).

Dolerite can be defined as a fine- to medium-grained crystalline igneous rock, typically with mafic and holocrystalline texture. It is similar to volcanic basalt or plutonic gabbro, and it consists of plagioclase and pyroxene (Chevallier *et al*., 2001). It usually occurs in the form of dykes, plugs and sills. Only dolerite dykes and sills will be discussed for the purpose of this study.

### 2.4.1 Dolerite dykes and sills

According to Botha *et al*. (1998) sills in the Karoo formations are sheet-like forms of dolerite intrusions that actually follow the sedimentary beds of the formations. They were formed when magma was injected under pressure into the horizontal sedimentary strata of the Karoo rocks, where it crystallised to form dolerite sills (McCarthy and Rubidge, 2005). Dolerite sills often protect the underlying sedimentary strata from erosion. Dolerite dykes were formed when magma solidified in fissures or fractures to form linear ridges extending across the Karoo landscape.

Botha *et al*. (1998) further suggested that sills are not regarded as a good source of groundwater since they intruded during an extremely active magmatic phase. Therefore, magma was generated at extremely high temperature. The magma partaking in the formation of sills was so hot that it metamorphosised the Karoo sediments instead of baking them (Botha *et al*., 1998). Linear dolerite dykes were formed during the less active phases of Gondwanaland's fragmentation, and did not have enough energy to cause metamorphosis of the country rocks.

### 2.4.2 Dolerite dykes: geometry, structure and mechanism of emplacement

Dolerite dyke intrusions were emplaced in the Karoo during the period of extensive magmatic activity that took place over the entire subcontinent of South Africa. Dolerite dykes form vertical to inclined intrusive igneous bodies that cut across the country rocks (Woodford and Chevallier, 2002). These geological structures are more dominant within the rocks of the Karoo Supergroup than in other rock units of South Africa (Chevallier *et al*., 2001).

Figure 2.7 shows the distribution of dolerite dykes in the Karoo Supergroup. During dolerite dyke intrusion, the country rocks fracture in the contact zones between the dolerite and the country-rock due to high temperatures and pressures (Woodford and Chevallier, 2002). The structures are also fractured into a system of joints usually columnar in shape, which result in the formation of secondary permeability to the rock strata (Singhal and Gupta, 2010). According to Woodford and Chevallier (2002) the average thickness of dolerite dykes ranges from 2 to 10 m, and the width of a dyke is a function of its length: the wider the dyke, the greater its lateral extent.

In many cases, dyke outcrops are not visible on the earth's surface; however, occasionally they are well exposed in stream beds. In some areas where dyke outcrop is visible, it can be traced by lines of green vegetation and slight changes in the topography, since vegetation growing on dolerite structures is generally thicker than vegetation of the surrounding area. In addition, water for the vegetation growing on dolerite dyke structures is often available, since the altered zones adjacent to the intrusions often allow the collection of water in the fractured material along the structures. Furthermore, dolerite intrusions are usually impermeable, and form barriers to groundwater flow in the direction perpendicular to their strikes restricting groundwater to move any further (Woodford and Chevallier, 2002). Thus, dolerite dykes have been and still are the preferred exploration and drilling target for groundwater in the rocks of the Karoo Supergroup.

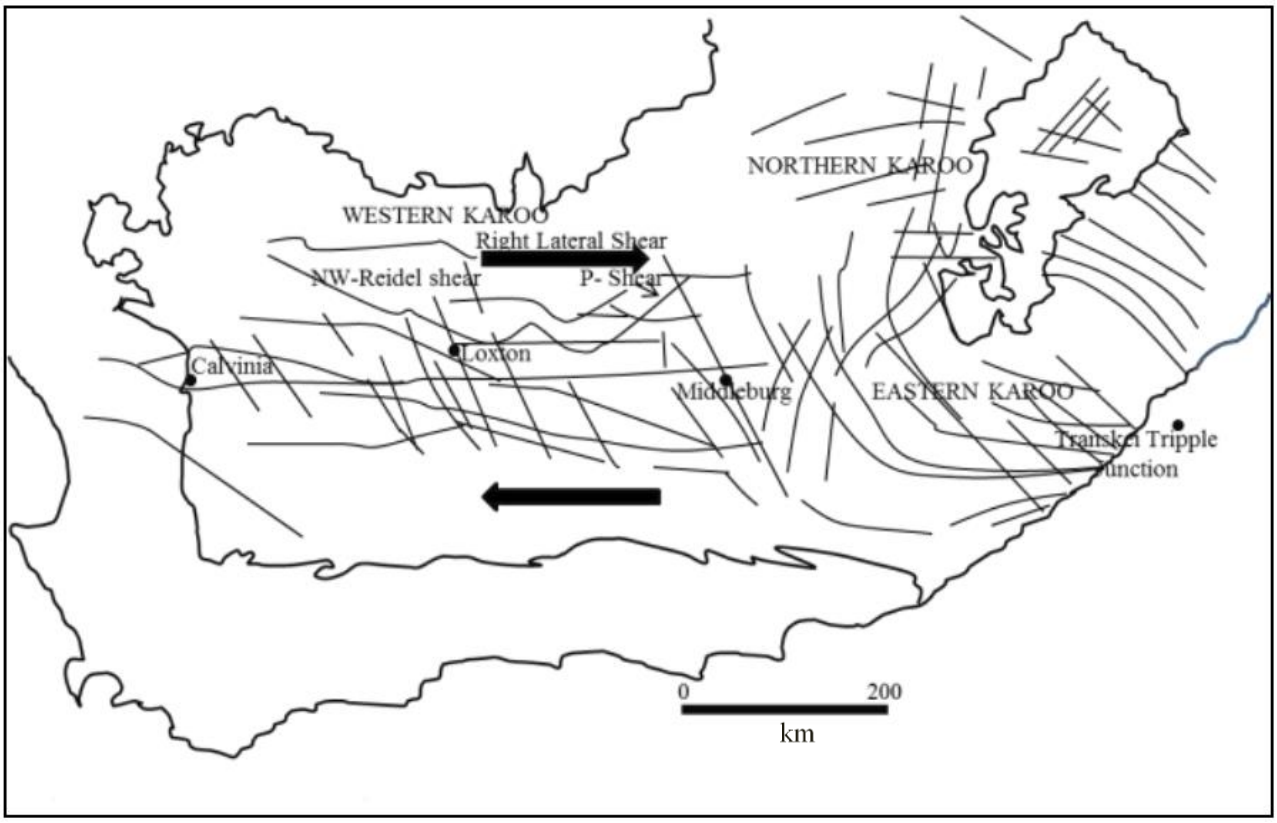


**Figure 2.7: Structural domains and mechanism of emplacement of dolerite dykes of the Karoo Basin (Chevallier *et al.*, 2001)**

### 2.4.3 Fracturing related to dolerite dykes

According to Woodford and Chevallier (2002), the country rock is fractured during and after dyke emplacement. Furthermore, the fractures form sets of master joints parallel to the strike of the dyke (Figure 2.8). The dolerite dykes are also affected by columnar or thermal jointing perpendicular to their margins. These thermal joints also extend over a small distance into the host rock, creating more fractures in the host rocks which may channel groundwater flow.

Since fractures are usually regarded as the main source of groundwater in the Karoo formations, the density of fractures plays the most important role in the prediction of the quantity of water available within an aquifer. The density of fractures is higher near linear dolerite dykes than in undisturbed country rocks. The presence of fractures near the linear dykes is caused by the hot magma that baked the Karoo rocks during the intrusion causing them to fracture more easily (Botha *et al*., 1998).

**Figure 2.8: Highly fractured dolerite dyke intruded through sandstone layers**

Fractures, faults and joints also contribute to the secondary porosity of the rock material and allow the storage of groundwater (Chandra, 2015). They also act as conduits which may extend to greater depths to allow movement of deep-seated groundwater (Meinzer, 1923). Many geothermal streams occur within the Karoo Supergroup; these are often formed by deep faults that allow deep-seated hot water to reach the surface.

## 2.5 GROUNDWATER OCCURRENCE AND FLOW IN THE KAROO ROCKS

The Karoo formations occur mainly in semi-arid to arid regions of South Africa where there is a lack of major rivers and other surface water sources (Woodford and Chevallier, 2002). The Karoo region is characterized by low rainfall which is highest in the eastern part of the basin and it decreases to the west (Woodford and Chevallier, 2002). Groundwater is considered the most crucial source of water in the Karoo due to its significant contribution to high demand for quality water resources. Unfortunately, Karoo aquifers have very unpredictable and complex behaviours, and groundwater

occurrences differ with respect to the geology of the area (Botha and Cloot, 2004). Karoo aquifers are generally characterized by the low permeability of the different formations forming these aquifers.

When conducting groundwater exploration, there are some target features associated with the availability of groundwater in the Karoo environment. Woodford and Chevallier (2002) and Murray *et al*. (2012) listed some of the important features to consider when exploring for groundwater, namely:

- Dolerite intrusions,
- Structural features other than those associated with dolerite intrusion,
- Horizontal or near-horizontal fractures along bedding planes and formation interfaces,
- Other fracture and joint systems,
- More porous sedimentary successions,
- Shallow groundwater associated with near-surface calcrete layers, and,
- Alluvial deposits associated with ephemeral rivers and streams.

As discussed previously, many of these features were formed during the break up of Gondwanaland where there was a widespread magmatic activity which caused Jurassic dolerite dykes and sills to intrude the Karoo Supergroup. These intrusions caused extensive fracturing which resulted in the water-bearing characteristics of Karoo rocks (Figure 2.9).

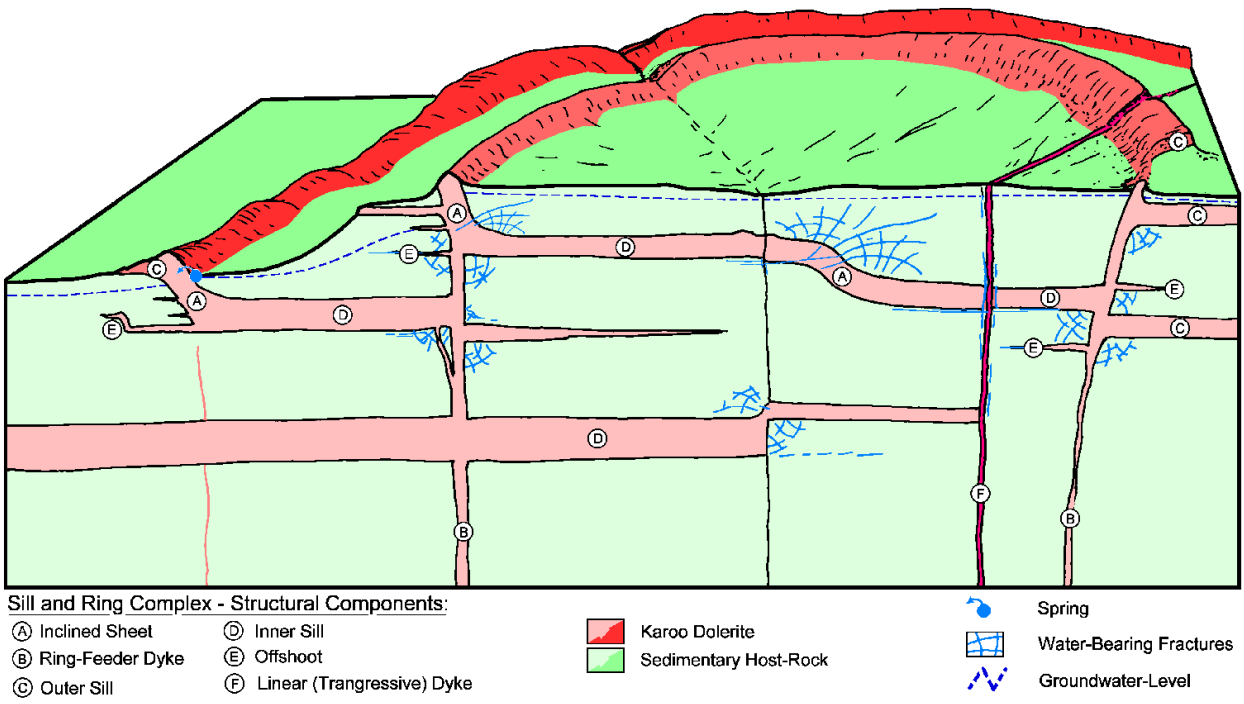


**Figure 2.9: Dolerite dykes and sills acting as water-bearing formations (Woodford and Chevallier, 2002)**

According to Botha *et al*. (1998), Woodford and Chevallier (2002) and Murray *et al*. (2012), dolerite dykes and sill structures are the primary targets for groundwater in the main Karoo Basin. Furthermore, the fractures in the Karoo Supergroup serve primarily as the preferential flow paths during the recharge of the aquifer and not as groundwater storage units. This is caused by the fact that the physical dimensions of the fractures do not allow large quantity of groundwater to be stored within the fractures themselves. In a borehole that intersects the fracture, the main water supply is from the sedimentary rock matrix that surrounds the fracture, as shown in Figure 2.10. These structures do not only provide the conduits for water flow to and from the aquifer, but also play a prominent role in the interactions responsibility for the behaviour of these aquifers (Woodford and Chevallier, 2002).

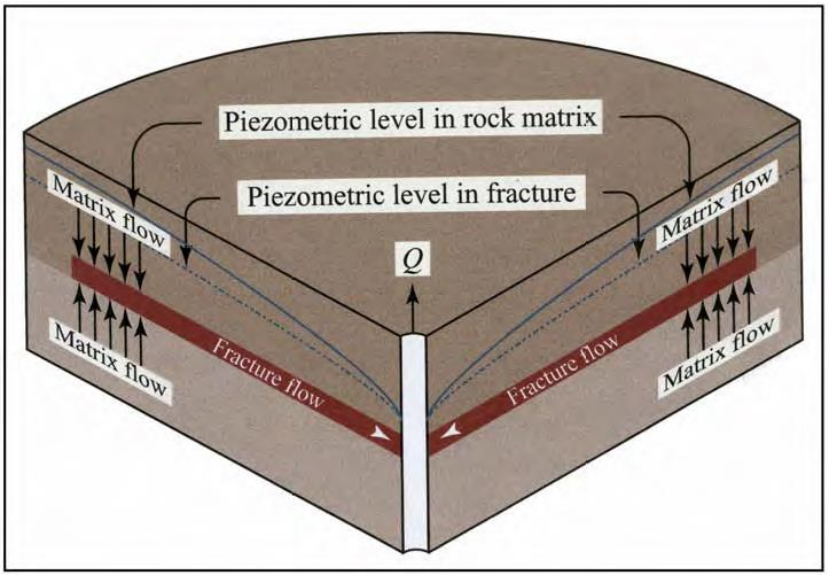


**Figure 2.10: Schematic illustration of groundwater flow towards a borehole in a Karoo aquifer (Woodford and Chevallier, 2002)**

## 2.6 GEOHYDROLOGICAL CONDITIONS ASSOCIATED WITH DOLERITE DYKES

Dolerite dykes are vertical to inclined discontinuities that act as impermeable to semi-permeable barriers to restrict groundwater flow within the aquifer (Woodford and Chevallier, 2002). Dolerite dykes are often preferred as drilling target for groundwater in the Karoo and aquifer yields of around 2 to 3 L/s are common (Chevallier *et al*., 2001). There are many reasons why dykes are preferred for groundwater exploitation namely (Woodford and Chevallier, 2002):

- Higher probability of drilling a wet or high-yielding borehole in or next to a dyke than in the host rock away from the dyke, because highly fractured zones often surround the dykes,
- Easier to detect dykes since they are highly magnetic, and they can be detected by simple geophysical techniques. They are also often clearly visible in the field (i.e. if not outcropping, they are often visible as lines of vegetation),

- It is easy to conceptualise and site an exploration borehole in the field, because of the relatively simple and regular 3D geometry of the dykes, and,
- They are thus a very cost-effective groundwater target during exploration.

According to Woodford and Chevallier (2002), the highest borehole yields are obtained within 1 m of the dyke contact. When siting a drilling position, it is also very important to consider the dip of the dyke to ensure that the borehole intersects that fractured contact zone with the host rock. Sami et al. (2002) reported that boreholes drilled adjacent to dolerite dykes have yields that are significantly higher compared to elsewhere in the Karoo Basin.

## 2.7 WEATHERING OF DOLERITE INTRUSION OF THE KAROO SUPERGROUP

The degree of weathering in the Karoo rocks gives information about the composition and the age of the main lithologies, volcanic intrusions, and regional tectonism. There is a gradational change in the degree of weathering with an increase in depth: the rocks in the deeper section of the crust tend to weather slowly compared to the rocks found near or on the earth's surface.

Weathering of the Karoo dolerite intrusions can however impart secondary permeability and porosity to varying extent, and is influenced by the following factors: the degree of fracturing, climate, the width of the intrusion, the cooling rate and the grain size (Woodford and Chevallier, 2002).

The degree of fracturing in the rock strata is controlled by tectonic reactivation and thermal jointing. If only jointing is present, the dolerite intrusion remains relatively solid and intact. However, if tectonic reactivation of dolerite has taken place, the rock mass appears shattered and consist of small boulders usually set in fine-grained matrix (Woodford and Chevallier, 2002). Development of weathered zones is prominent with intense fracturing and deep weathering is initiated by the structural deformities (Chandra, 2015). Deep weathering occurs slowly, since the deeper depth materials are protected by overburden strata. Most weathered materials occur near the surface since weathering of earth material starts from the surface downwards and is influenced by climatic conditions.

The cooling rate, grain size and the width of the dyke are interrelated and have an effect on the permeability of dolerite intrusions. Wide dykes usually exhibit an important chill-margin containing fine-grained rocks that weathers to produce small well rounded white speckled boulders. The central portion of the dyke consists of medium- to coarse-grained rocks that decompose to form uniform gravelly material, exhibiting exfoliation weathering patterns. This part of a dyke tends to weather more intensely than fine-grained dolerite dykes (Botha *et al.*, 1998). Narrow dykes usually consist of fine-grained rocks that tend to be more resistant to weathering than thicker dykes. The outcrop of

narrow dykes usually display a uniform pattern of shrinkage joints, and the dykes also weather to produce small rounded, white speckled boulders set in an angular fine groundmass.

From observations of dolerite dykes and sills in the Karoo Basin, weathering seems to be more prominent and severe in the eastern parts since rainfall is highest in these parts (Woodford and Chevallier, 2002). The western part of the Karoo Basin is dry and receives less rainfall compared to the eastern part. Hence, dolerite in the western part of the basin weathers slowly (Figure 2.11). In addition, Woodford and Chevallier (2002) further suggested that the western parts of the Karoo Basin are known for their relatively poor soil cover, which is caused by the slow weathering of rocks in this part of the basin.

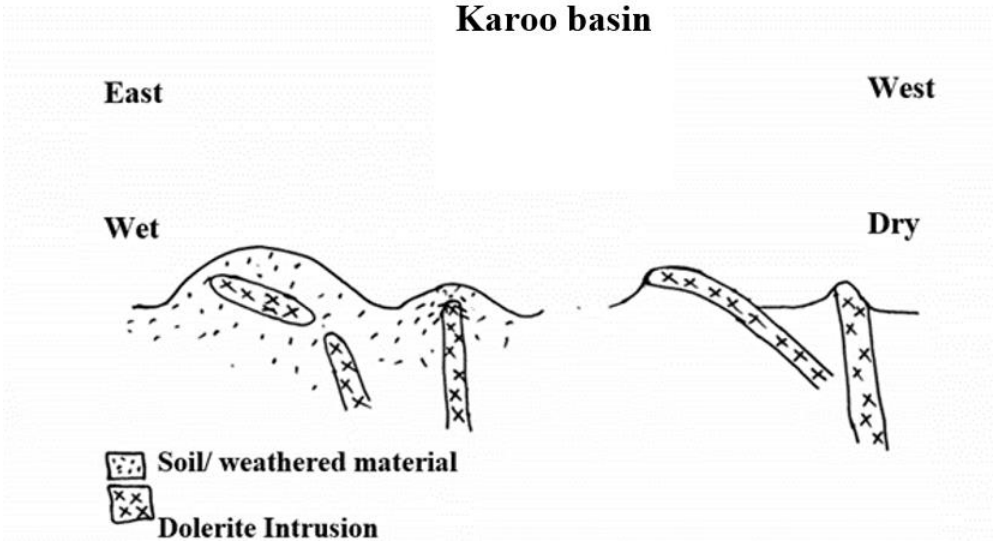


**Figure 2.11: Schematic illustration of dolerite weathering occurrence in parts of the Karoo Basin**

### 2.7.1 Influence of weathering of dolerite dyke on the groundwater occurrence

From a groundwater perspective, the hydraulic properties of the weathered dolerite dykes is important, since weathering of dolerite intrusions influences the groundwater occurrence in Karoo aquifers. The transmissivity and storativity of Karoo dolerite dykes decline with depth as the degree of weathering diminishes with depth. According to Van Wyk (1963) and Vegter (1995) the porosity and permeability of Karoo rocks are highest in the upper 30 m of the crust, since the rocks are generally more weathered than the deeper rocks.

According to observations made during drilling programmes at Philippolis and Rouxville by Botha *et al*. (1998), high-yielding boreholes were located near the highly weathered dykes. Furthermore, the contact zones between dolerite dykes and the host rock within the weathered zone remains the most favoured target for groundwater exploration (Vegter, 1995).

## 2.8 THE ELECTRICAL RESISTIVITY METHODS

Electrical resistivity surveys have been widely used for many decades in industries such as; mining, hydrogeological and geotechnical (Loke, 1999). It is a technique that is non-intrusive, and it is intensively used in determining the subsurface resistivity distribution by using measurements taken on the ground surface (Kirsch, 2006). The method is based on the fact that different geological units or structures in the earth's subsurface are more or less sensitive to electrical current flow and that different geological units have different resistivity values. Resistivity is influenced by different geological parameters such as the degree of water saturation in rocks, porosity concentration of dissolved salts, fluid and mineral content (Wilkinson *et al*., 2010). Accordingly, this section gives a general background on the resistivity method, different electrode arrays, electrical resistivity sounding and profiling, the 2D ERT method and also describes some of the effects of electrode misplacement on electrical resistivity surveys.

### 2.8.1 Fundamental theory of resistivity methods

Dey and Morrison (1977), Parasnis (1986) and Loke (2004) give descriptions of the basic resistivity theory. Ohm's law is the fundamental physical law that governs the flow of electrical current in earth materials during resistivity surveys. The assumption is made that the materials exhibit linear behaviour (Ferry, 2012). In a continuous medium, Ohm's law is given in a vector form as:

$$\mathbf{J} = \sigma\mathbf{E} \tag{1}$$

where $\sigma$ is the conductivity of the medium, $\mathbf{E}$ is the electric field intensity, and $\mathbf{J}$ is the electrical current density. The resistivity ($\rho$) of a material is the inverse of its conductivity ($\rho = 1/\sigma$). The relationship between the electric field intensity and the electric potential ($\phi$) is given by:

$$\mathbf{E} = -\nabla\phi \tag{2}$$

Combining Equations 1 and 2 gives:

$$\mathbf{J} = -\sigma\nabla\phi \tag{3}$$

In resistivity survey, current sources are generally in the form of point sources. An elemental volume ($\Delta V$) surrounding a current source ($I$) located at ($x_s$, $y_s$, $z_s$) in Cartesian space gives Equation 4, which represents the relationship between the current density and the magnitude of the current (Dey and Morrison, 1977):

$$\nabla \cdot \mathbf{J} = (\frac{I}{\Delta V})\delta(x - x_s)\delta(y - y_s)\delta(z - z_s) \tag{4}$$

where $\delta$ is the Dirac delta function. Equation 4 can then be written for a generalized three-dimensional space as:

$$-\nabla \cdot [\sigma(x,y,z)\nabla\phi(x,y,z)] = (\frac{I}{\Delta V})\delta(x-x_s)\delta(y-y_s)\delta(z-z_s) \quad 5$$

Equation 5 gives the potential distribution in the ground caused by a point current source (Loke, 2004). Consider a homogeneous earth with a single electrode injecting electrical current into the ground. This electrode acts as a point source of electrical current. The electrical current flows radially outward originating from a point source. Thus, the current distribution is equal and similar everywhere on the equipotential surfaces. The equipotential surfaces are semi-spherical shaped, and the current flows at right angle to the equipotential surfaces, as shown in Figure 2.12.

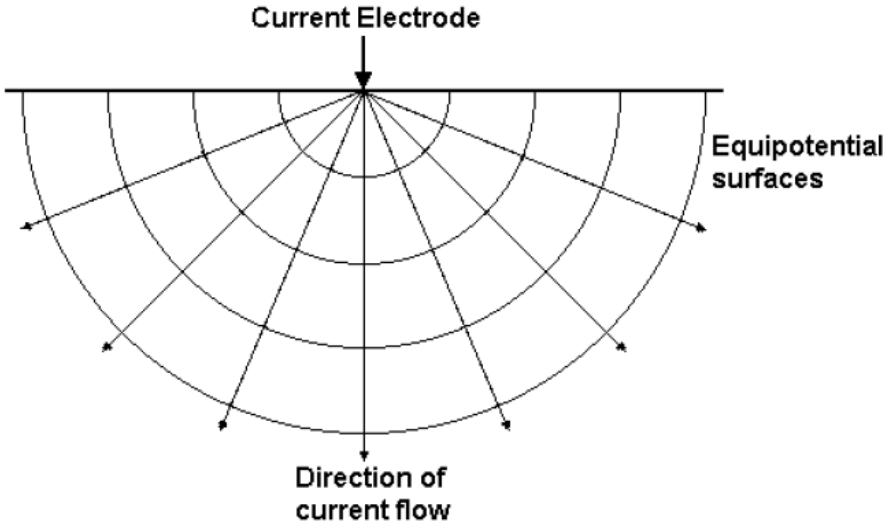


**Figure 2.12: The flow of current from a point current source and the resulting potential distribution (Loke, 2004)**

The electric potential $(v)$ at a distance $r$ from the current source is given by:

$$v = \frac{\rho I}{2\pi r} \quad 6$$

For two current electrodes (one injecting current and one removing current) the equipotential surface is no longer spherical and the current flow paths are therefore no longer radial, as shown in Figure 2.13.

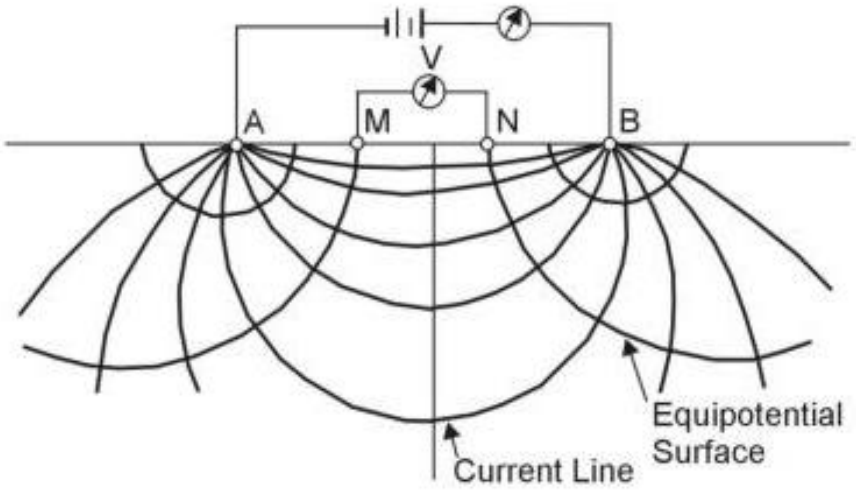


**Figure 2.13: The potential distribution caused by a pair of current electrodes in a homogeneous half-space (Loke, 2004)**

For two current electrodes, the electric potential at a subsurface position is given by:

$$v = \frac{\rho I}{2\pi}\left(\frac{1}{r_A} - \frac{1}{r_B}\right) \qquad 7$$

where $r_A$ and $r_B$ are the distances from the first and second electrodes to the subsurface position. The most basic electrode setup used in resistivity surveys typically employs four electrodes: two current electrodes (A and B) and two electrodes used to measure the electric potential difference (the potential electrodes, M and N). For such a four-electrode setup, the electrical potential difference between the electrodes may be calculated by applying Equation 7 for each of the two potential electrodes. The electrical potential difference $\Delta v$ can then be written as:

$$\Delta v = \frac{\rho I}{2\pi}\left(\frac{1}{r_{AM}} - \frac{1}{r_{BM}} - \frac{1}{r_{AN}} + \frac{1}{r_{BN}}\right) \qquad 8$$

where $r_{AM}$ is the distance between current electrode A and potential electrode M, and so forth. For real earth materials, the subsurface is inhomogeneous. Therefore, Equation 8 cannot be applied to determine the true resistivity of the subsurface, but only an apparent resistivity ($\rho_a$):

$$\rho_a = \frac{2\pi\Delta v}{I}\left(\frac{1}{r_{AM}} - \frac{1}{r_{BM}} - \frac{1}{r_{AN}} + \frac{1}{r_{BN}}\right)^{-1} \qquad 9$$

The apparent resistivity is the resistivity of a hypothetical homogeneous half-space giving the same ratio of $\Delta v$ to $I$ for the same electrode geometry. Equation 9 is often written in the form:

$$\rho_a = K\frac{\Delta v}{I} \qquad 10$$

where $K$ is known as the geometric factor which depends on the arrangement of the four electrodes on the ground surface. The geometric factor is given by:

$$K = 2\pi\left(\frac{1}{r_{AM}} - \frac{1}{r_{BM}} - \frac{1}{r_{AN}} + \frac{1}{r_{BN}}\right)^{-1} \quad 11$$

## 2.8.2 Electrode arrays

There are numerous arrays that can be employed during the electrical resistivity survey. The arrays that are most commonly used are: the Wenner array, the Schlumberger array, the dipole-dipole array and the pole-dipole array. According to Griffiths and Barker (1993) and Loke (2004), the following factors need to be considered when choosing an array:

- The sensitivity of the array to vertical as well as horizontal changes in the subsurface resistivity,
- The horizontal coverage of the data,
- The depth of investigation,
- The signal strength, and,
- The type of structure to be mapped.

The sensitivity of the array to vertical and horizontal changes in the subsurface resistivity tells us the degree to which a change in the resistivity of a section will influence the potential measured by the array (Ahzegbobor, 2010). Higher values of the sensitivity function imply greater influence of the subsurface region on the measurement.

### 2.8.2.1 The Wenner array

The Wenner array was first proposed for geophysical investigations by Wenner in 1916, and was popularized by the pioneering work carried out by a research group at the University of Birmingham (Loke, 1999). In the Wenner array, the adjacent electrodes are separated by an equal distance ($a$). Three different Wenner arrays exist, depending on the order of the current and potential electrodes: the Wenner (α) array (AMNB) (Figure 2.14), the Wenner (β) array (ABMN), and the Wenner (γ) array (AMBN). However, of these arrays, the Wenner (α) array is the most commonly used since it results in the largest electrical potential difference of the three arrays, and thus the highest signal strength.

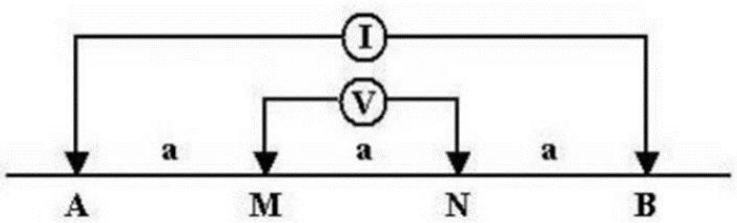


**Figure 2.14: Electrode geometry of the Wenner (α) array (Morrison and Gasperikova, 2012)**

From Equation 9 it is clear that the geometric factor of the Wenner array is simply $2\pi a$ since the spacing between the electrodes is constant. Therefore, the apparent resistivity for the Wenner array can be calculated from Equation 9 as:

$$\rho_a = 2\pi a \frac{\Delta v}{I} \qquad 12$$

The Wenner array also have some limitations. Firstly the array is considered less sensitive to horizontal changes in the subsurface resistivity compared to some of the other commonly used arrays; however, it is very sensitive to vertical changes (Herman, 2001). It is therefore a good choice for detecting horizontal layering in the subsurface. Furthermore, when compared to other arrays, the Wenner array has the highest signal strength.

#### 2.8.2.2 The Schlumberger array

The electrode geometry of the Schlumberger array is shown in Figure 2.15. The potential electrodes (M and N) are separated by a distance $a$, while the current electrodes (A and B) are placed a distance $b$ from the nearest potential electrode.

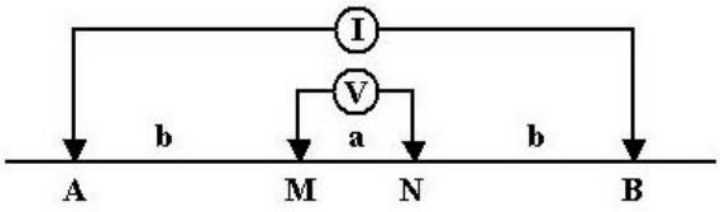


**Figure 2.15: Electrode geometry of the Schlumberger array (Morrison and Gasperikova, 2012)**

The apparent conductivity for the Schlumberger array is given by:

$$\rho_a = \frac{\pi}{a}(b^2 - a^2/4)\frac{\Delta v}{I} \qquad 13$$

The Schlumberger array generally has a better lateral resolution than the Wenner array and allows a greater probing depth.

#### 2.8.2.3 The dipole-dipole array

The dipole-dipole array consists of four electrodes, two current electrodes (electrodes A and B) and two potential electrodes (electrodes M and N), as shown in Figure 2.16 below.

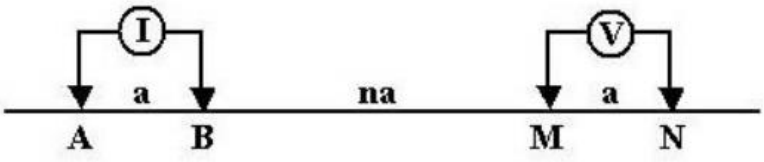


**Figure 2.16: Electrode arrangement for the Dipole-dipole array (Morrison and Gasperikova, 2012)**

In the dipole-dipole array, an equal distance for both the current and potential electrode spacing is maintained all the time as a positive integer multiple of $a$, and the distance between the B and M electrodes is $na$. Then the distances between the electrodes are given by: $r_{AM} = r_{BN} = (n+1)a$, $r_{AN} = (n+2)a$, and $r_{BM} = na$. Substituting these values into Equation 9 gives:

$$\rho_a = \pi[n(n+1)(n+2)a]\frac{\Delta v}{I} \qquad 14$$

The dipole-dipole array is very sensitive to horizontal changes and relatively insensitive to vertical changes in the subsurface resistivity (Okpoli, 2013). Therefore, this makes it the most preferred array for mapping vertical structures such as dykes and faults. In addition, it is the most sensitive array to 3D structures compared to other arrays. The depth of probing is one of the limitations of this method, because it probes to comparatively shallow depths. Another limitation is caused by the decrease in signal strength as the distance between the dipole pair increases. This array can be used where a good horizontal coverage is required (Herman, 2001).

#### 2.8.2.4 The pole-dipole array

The pole-dipole array is similar to the dipole-dipole array. It also uses four electrodes: two potential electrodes and two current electrodes. One of the current electrodes is, however, placed so far from the other three electrodes that its influence is negligible. The distance between the two potential electrodes is represented by $a$ while the distance between the current electrode and the closest potential electrode is denoted by $na$ as shown in Figure 2.17. The distances between the different electrodes are: $r_{AM} = na$, $r_{AN} = (n+1)a$, $r_{BM} \to \infty$ and $r_{BM} \to \infty$. Substituting these values in Equation 9 gives:

$$\rho_a = 2\pi[n(n+1)a]\frac{\Delta v}{I} \qquad 15$$

The pole-dipole is very sensitive to vertical structures, and it has a good horizontal coverage and higher signal strength compared to the dipole-dipole array (Ahzegbobor, 2010). It also allows greater depths of investigation than the dipole-dipole array. However, it has lower signal strength compared to the Wenner and Schlumberger arrays (Okpoli, 2013).

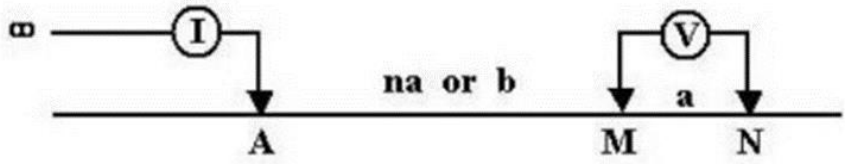


**Figure 2.17: Electrode arrangement for the Pole-dipole array (Morrison and Gasperikova, 2012)**

## 2.8.3 Electrical resistivity sounding and profiling

Resistivity surveys may be used to investigate both the vertical and lateral changes in the resistivities of the subsurface. Vertical changes are investigated through sounding while lateral changes are studied through profiling. These modes of investigation are described below.

### 2.8.3.1 Vertical electrical sounding (VES)

VES surveys are used to detect changes in the resistivity with depth in a geological formation (Koefoed and Mallick, 1979; Chandra, 2015). The subsurface is assumed to consist of horizontal or near-horizontal layers, each with its specific resistivity (Pozdnyakova *et al*., 2001). In addition, it is assumed that the resistivity of each layer does not change in horizontal directions. VES is therefore assumed to be a one-dimensional (1D) investigation of the changes in resistivity with increase in depth.

This survey is typically done using four electrodes, two electrodes injecting current (the current electrodes) and two electrodes measuring the electrical potential difference at a specific surface position (Loke, 2004). Electrical current is injected into the ground through the two current electrodes, causing current to flow through the subsurface. The voltage drop (electrical potential difference) is then measured between the potential electrodes (Reynolds, 1997; Adli *et al*., 2010).

For the Schlumberger array, the current electrode separation is constantly increased while the centre point of the array remains fixed. By increasing the current electrode separation, the effective depth of investigation is increased accordingly as a larger volume of the subsurface is surveyed (Seaton and Burbey, 2002). This array is commonly used for VES surveys because of its simplicity with respect to the electrode arrangement, since only two electrodes are shifted for each and every measurement. However, other configurations, such as the Wenner array with equal spacing between the electrodes, can also be used, although it will require shifting all four electrodes for each and every measurement.

The recorded apparent resistivity is normally plotted on a double logarithm graphs against electrode spacing. The obtained results are then matched against theoretical curves, which are commonly referred to as master curves (Parasnis, 1986). The turning point in the curves is interpreted as an indication of the interface between two different layers. The shape of the curves depends on the

differences in resistivity between the two layers and more than two layers can be interpreted using the auxiliary point diagrams (Loke, 2004). The results obtained for a 1D VES survey yield information on the thicknesses and resistivities of different layers in the subsurface.

Over the last few decades, various software packages have been developed to replace the graphical methods of interpretation. Software packages typically allow both forward modelling and inverse modelling. During forward modelling, the user changes the layer thicknesses and resistivities to obtain modelled responses that approximate the measured responses. Inverse modelling makes use of an inversion algorithm to find the best fit between the modelled and measured responses. Some software packages (such as IPI2WIN; Bobatchev *et al*., 2001) allow the inclusion of data from multiple sounding centres. Since coherent interpretations of the subsurface layering are required that make sense geologically, the data recorded at each sounding centre effectively limits the possible models at nearby sounding centres. By including data from several sounding centres, a two-dimensional section of the subsurface resistivity distribution may be obtained.

Since VES assumes homogeneous layers of infinite lateral extent, the sounding assumption breaks down in the presence of vertical structures. Sounding data recorded in the vicinity of such structures could lead to incorrect models of the subsurface.

#### 2.8.3.2 Electrical profiling

Electrical profiling used the same four electrodes as in the standard setup, i.e. two electrodes injecting current (the current electrodes) and two electrodes measuring the electrical potential difference. It differs from the VES in that it uses constant spacings between the electrodes to effectively investigate the subsurface resistivity distribution up to a specific depth. All four electrodes are moved along a profile in order to detect lateral variations of the subsurface (Parasnis, 1986). The recorded data are usually presented as profile plots or contour maps (in the case of several parallel profiles).

Profiling can be conducted using any array, but it is generally conducted using Wenner, dipole-dipole, and Wenner-Schlumberger arrays (Chandra, 2015). When the geological strike in an area is known, profiling surveys are conducted approximately perpendicular to the strike to obtain profiles that clearly show the positions of lateral changes in the subsurface resistivities.

### 2.8.4 Electrical resistivity tomography

Two-dimensional (2D) electrical resistivity tomography (ERT) is a technique of measuring apparent resistivity data in both the horizontal and vertical directions (Okpoli, 2013). ERT can therefore be thought of as resistivity surveys during which both sounding and profiling data are recorded to provide information on the subsurface resistivities in 2D sections underlying the survey lines. For these surveys it is assumed that the resistivities do not change in directions perpendicular to the survey

line. This assumption is usually reasonable, especially for surveys that are completed over elongated geological structures.

The equipment used for ERT surveys typically consists of 1) multi-core electrical cables laid out along the survey line, 2) numerous electrodes inserted at constant spacings along the survey line and connected to the multi-core cable, 3) an electrode selector which switches between the different electrodes during the different measurements, and 4) an instrument that measures the current injected between two selected current electrodes, and the potential difference between two selected potential electrodes to calculate an apparent resistivity.

The way 2D ERT data are measured to obtain a 2D section of the apparent resistivities is demonstrated in Figure 2.18 for the Wenner (α) array. For the shallowest measurements, the smallest AB separation is used. This corresponds to using four adjacent electrodes, as in the top image of Figure 2.18. Current is injected through electrodes A and B, while the potential difference between electrodes M and N is measured to calculate an apparent resistivity for this measurement. The apparent resistivity value is assigned to a position halfway between the current electrodes and at a pseudo-depth (discussed in Section 3.3). The electrodes are then all shifted one position to the right, and a new measurement of the apparent resistivity is made. The process is subsequently repeated until a profile of apparent resistivity data is recorded all along the survey line.

To increase the depth of investigation, the AB separation is increased, and an apparent resistivity profile at a larger depth is obtained (Reynolds, 1997; Furman *et al*., 2003). This is shown in the bottom two images of Figure 2.18 where only two measurements at different positions and pseudo-depths are displayed as examples. By repeating this process for multiple AB separations, a 2D section of the apparent resistivities plotted at pseudo-depths is obtained. This section is referred to as a pseudo-section (Loke, 2011; Milsom and Ericksen, 2011). The pseudo-sections can again be inverted through inversions algorithms to find 2D resistivity models that give responses similar to the responses recorded in the field (Loke, 2011).

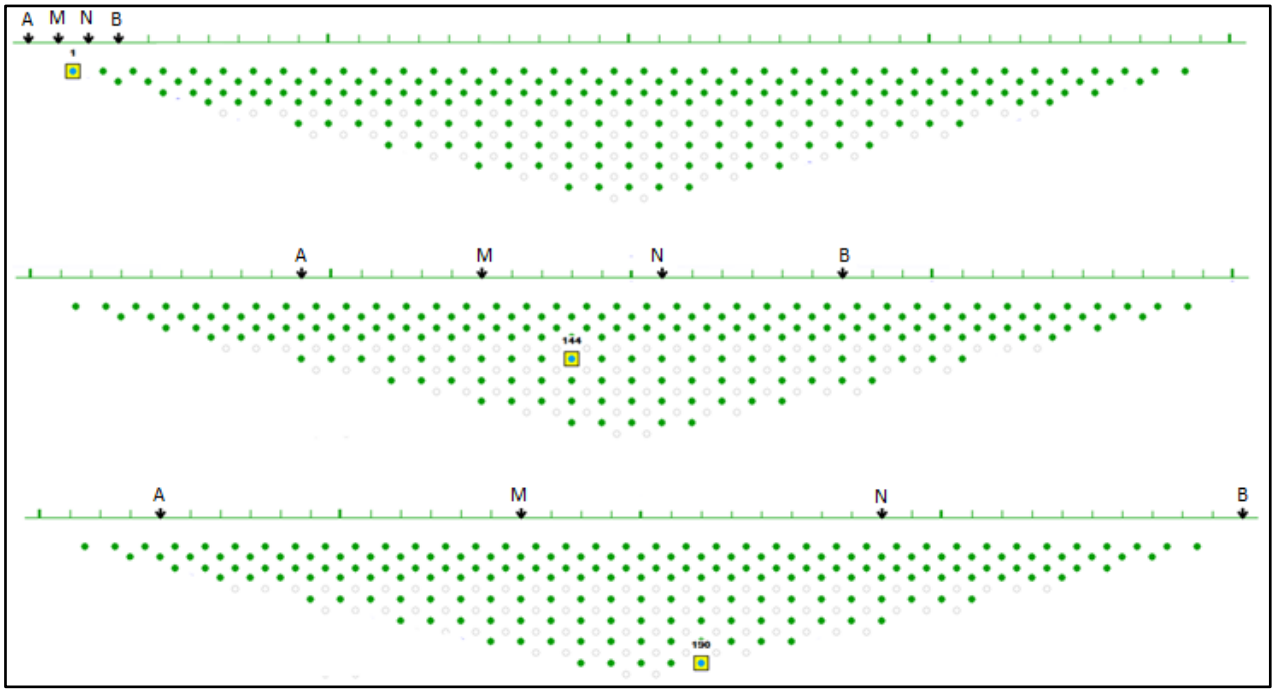


**Figure 2.18: Measurements taken during 2D ERT surveys**

As with all electrical surveying, ERT is very sensitive to materials at shallow depths but the sensitivity decreases with depth (Furman *et al*., 2003).

### 2.8.5 Depth of investigation

It is important to have an understanding of the depth of investigation for resistivity surveys employing the different electrode geometries. The depth of investigation (DOI) in this study refers to the depth to which the data are sensitive to the physical properties of the earth. The DOI is mainly controlled by the separation between the current (AB) electrodes, but also by the distance between the current electrode pair and the potential electrode pair (Bernard, 2003). In general, larger AB separations lead to greater depths of investigation.

Different authors have defined the DOI differently. According to Chandra (2015) in electrical resistivity measurements, the potential difference measured is the sum of contributions from different depths, and contribution from different depths are not the same. Therefore, Chandra (2015) defined the DOI as the depth at which a thin horizontal layer contributes maximum to the total signal measured at the ground surface. This definition is quite similar to the one used by Roy and Apparao (1971) in which they defined the Normalized Depth of Investigation Characteristic (NDIC) as the Depth of Investigation Characteristics (DIC) divided by the total response of the half-space. According to Roy and Apparao (1971) for a particular electrode array, the depth of the thin layer at which DIC curve response is at its maximum is what it is called the DOI for that particular array. For the Wenner and Schlumberger arrays, the DOI is respectively 0.11AB and 0.125AB.

Edwards (1977) proposed another definition of the DOI, wherein he neglected the use of the maximum response and used the median of the DIC function which he referred to as the effective DOI. The median depth is defined as the depth at which the integral of the DIC function from the surface to that depth is equal to the integral from that depth to infinity (Chandra, 2015). According to this definition the DOI for the Wenner array it is 0.17AB, and 0.19AB for the Schlumberger array. The DOI calculated by Roy and Apparao (1971) is thus seen to be smaller than the DOI calculated by Edwards (1977). The definition of Edwards (1977) seems more appropriate since it considers all electrical current flow at different depths in the subsurface, and not only the depth at which maximum current flow takes place.

The above definitions of the DOI were developed by assuming a homogeneous earth. In layered or inhomogeneous media the true DOI will differ from the calculated values, since it will be affected by the resistivities and thicknesses of the subsurface materials. The DOI is furthermore related to the vertical resolution; vertical resolution decreases with an increase in DOI.

Following the methodologies of Roy and Apparao (1971) and Edwards (1977), the DOI may be calculated from the sensitivity function, given by the Fréchet derivative, of the array. This is explained in Section 3.3 of Chapter 3 where the impact of angled survey lines on the DOI is investigated.

### 2.8.6 The resistivities of earth materials

ERT surveys give insight into the subsurface resistivity distribution. However, the apparent resistivity data recorded during ERT surveys still need to be processed and interpreted in terms of the subsurface geological conditions. To do this, knowledge on the general geological conditions of the study area and of the resistivity values of different earth materials is required. Loke (2004) and Dafalla and AlFouzan (2012) listed some of the factors that influence electrical resistivities of material, namely: porosity, saturation, texture of material, pore fluids and the degree of solid phase, fracturing and the percentage of fractures filled with groundwater. The age of the rock also affects the resistivity of material for example; quaternary volcanic rock may have resistivity in the range of 10-200 Ωm, while that equivalent rock but of Precambrian in age may have higher resistivities (Reynolds, 1997). This is caused by the fact that older rocks had more opportunity to be exposed to secondary mineralisation.

Subsurface materials are characterised by a wide range of resistivity values, as listed in Table 2.1. From this table, igneous rocks are seen to exhibit the highest resistivities, while sedimentary rocks tend to be more conductive due to higher porosities and fluid content (Chandra, 2015). Metamorphic rocks tend to have intermediate resistivities.

The resistivity of the subsurface material does not only change from formation to formation but can also change within a formation (Dafalla and AlFouzan, 2012). Resistivity tends to increase with grain

size and the maximum values are commonly associated with coarse grains. The degree of compaction also plays an important role in resistivity of the subsurface material. The resistivity of material decreases with an increase in clay content, and fractures filled with water usually lead to lower resistivities.

**Table 2.1: Resistivity values generally associated with common rocks, minerals and chemicals (Loke, 1999)**

| Material | Resistivity (Ω.m) | Conductivity (S/m) |
|---|---|---|
| **Igneous and metamorphic rocks** | | |
| Granite | $5\times10^{3} - 10^{6}$ | $10^{-6} - 2\times10^{-4}$ |
| Basalt | $10^{3} - 10^{6}$ | $10^{-6} - 10^{-3}$ |
| Slate | $6\times10^{2} - 4\times10^{7}$ | $2.5\times10^{-8} - 1.7\times10^{-3}$ |
| Marble | $10^{2} - 2.5\times10^{8}$ | $4\times10^{-9} - 10^{-2}$ |
| Quartzite | $10^{2} - 2\times10^{8}$ | $5\times10^{-9} - 10^{-2}$ |
| **Sedimentary rocks** | | |
| Sandstone | $8 - 4\times10^{3}$ | $2.5\times10^{-4} - 0.125$ |
| Shale | $20 - 2\times10^{3}$ | $5\times10^{-4} - 0.05$ |
| Limestone | $50 - 4\times10^{2}$ | $2.5\times10^{-3} - 0.02$ |
| **Solids and waters** | | |
| Clay | 1 – 100 | 0.01 – 1 |
| Alluvium | 10 – 800 | $1.25\times10^{-3} - 0.1$ |
| Groundwater (fresh) | 10 – 100 | 0.01 – 0.1 |
| Sea water | 0.2 | 5 |

### 2.8.7 Data processing

The purpose of electrical resistivity surveys is to determine the subsurface resistivity distribution and to correlate changes in the subsurface resistivities to the geological and geohydrological conditions of the subsurface. Interpretation of the resistivity data needs knowledge and consideration of the geological features that might cause resistivity changes.

During field surveys, only apparent resistivities are recorded. Furthermore, the recorded apparent resistivities are associated with pseudo-depths. These depths are dependent on the electrode separations and are commonly given by the DOI, as defined in Section 2.8.5. The pseudo-depths are not the true depths of investigation, but are used as a convenient way of displaying the apparent resistivity data so that changes in the apparent resistivities can be visualised.

To convert the recorded apparent resistivity data into a model of the true subsurface resistivity distribution, the data has to be processed. This is achieved through a mathematical process known as inversion. During the process of inversion, a model of the resistivity distribution of the subsurface is

iteratively adjusted in such a way that the difference between measured and calculated apparent resistivities is minimised. The iterative adjustments are often continued until the calculated difference reaches an acceptable lower threshold. The inversion process is described schematically in Figure 2.19.

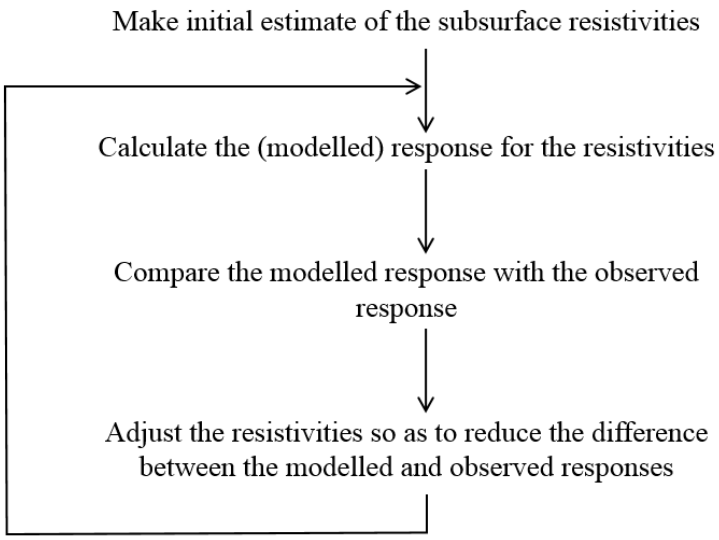


**Figure 2.19: Algorithm for the inversion of apparent resistivity data (Fourie, 2010)**

After inverting the recorded apparent resistivity data the obtained inverted resistivity models are then used during the interpretation process (Fourie, 2010). The number of iterations used depends on the quality of recorded data for every model. For example, a high number of iterations can be used to model good quality data recorded with small errors to obtain a well-defined inverse model. However, when using high number of iterations on poor quality data, the inversion algorithm will model the errors in the data, which will introduce artefacts to the inverse model.

## 2.9 THE EFFECTS OF ELECTRODE MISPLACEMENT ON ELECTRICAL RESISTIVITY SURVEYS

Two-dimensional ERT systems use multi-core cables with fixed electrode spacings. The assumption is made that survey lines are straight and that the electrodes are collinear. However, it often happens that surface obstacles cause some part of the cable to deviate from a straight line. It is therefore important to evaluate the effects of electrode misplacement on electrical resistivity imaging. Electrode misplacement can be categorised into non-systematic and systematic misplacement. Non-systematic electrode misplacement is when individual electrodes are misplaced from their assumed positions, while systematic electrode misplacement is when several electrodes are shifted from their assumed (straight line) positions, such as when an angle occurs in the survey line. The effects of both non-systematic and systematic electrode misplacement are discussed below.

### 2.9.1 Non-systematic electrode misplacement

Zhou and Dahlin (2003) presented an investigation into the electrode spacing error on 2D resistivity imaging surveys wherein they considered the effects of errors at individual electrodes as off-line and in-line electrode spacing errors. Spacing errors of an individual electrode may affect the apparent resistivity data and results obtained, because the erroneous electrodes or misplaced electrode may show different radiating patterns compared to the other electrodes arranged in a straight line. Electrode spacing error caused by potential electrodes may produce an offset in apparent resistivity data as a result of lateral inhomogeneity.

Several researchers have investigated the non-systematic errors that are caused by electrodes misplacement in the resistivity data. Oldenborger *et al*. (2005), Wilkinson *et al*. (2008) and EPA (2016) considered the effects of errors caused by individual electrodes. Oldenborger *et al*. (2005) studied the effects of electrode position errors on the ERT data using dipole-dipole and pole-pole arrays. From the results using a statistical distribution of electrode misplacement, the authors concluded that when electrodes are misplaced, statistical distributions can show a significant depart from a normal distribution. Wilkinson *et al*. (2008) studied the sensitivity to the geometric error of any inter-borehole four-electrode ERT configuration and concluded that geometric errors occur because of uncertainties in the position of an individual electrode. The potential difference and current flow cross-hole configuration was found to be insensitive to the geometric errors. However, the in-hole configuration was found to be extremely sensitive to the geometric errors for any borehole separation.

EPA (2016) explained the theoretically allowed method of displacing one electrode from the collinear array, under the circumstance where it is necessary to displace individual electrodes away from the survey line due to rough terrain, boulders or vegetation. The correct condition of changing the position of one electrode is when the geometric factor $K$ remains the same. For example, the current electrode $A$ can be placed in a new position to give $A'$ such that:

$$\frac{1}{AM} - \frac{1}{AN} = \frac{1}{A'M} - \frac{1}{A'N} \qquad 16$$

This can be achieved by shifting the electrode on a line perpendicular to the array. Furthermore, electrodes cannot be moved more than 45$^o$ off the line, but can only be moved along an arc centred on the nearest potential electrode, as long as it does not exceed 45$^o$ (EPA, 2016).

The above studies were focused on the effects of errors at individual electrodes. However, the main focus in the present study is to investigate the errors caused by the systematic shift of electrodes from a straight survey line when angles are introduced to the survey line.

### 2.9.2 Systematic electrode misplacement

Systematic electrode misplacement occurs when ERT survey lines are angled or curved to avoid some surface obstacle. Since the electrodes are no longer collinear, the fundamental assumption of straight survey lines breaks down. Since the distances between the different electrodes are affected by such systematic misplacements, the geometric factors and calculated apparent resistivities are also affected. Furthermore, since the depth of investigation (DOI) also depends on the distances between the different electrodes, systematic electrode displacement will affect the DOI. Lastly, systematic electrode misplacement will cause a different subsurface volume to be sampled during an ERT survey, since the current flow in the subsurface will take place along flow paths that differ from the flow paths that would have occurred for a straight line.

Since both the apparent resistivities and the DOI may be affected by systematic electrode misplacements, it is to be expected that the inverse resistivity models obtained from the affected data sets will also be affected. In Chapter 3 the effects of systematic electrode misplacement on the apparent resistivities, DOI and volume sampled are investigated, while the effects of such affected data on the inverse resistivity models are studied in Chapter 4.

# CHAPTER 3
# THE INFLUENCE OF ANGLED SURVEY LINES ON ERT DATA RECORDED WITH THE WENNER (α) ARRAY

## 3.1 INTRODUCTION

Two-dimensional (2D) ERT surveys are based on the assumption that all the electrodes are collinear (survey lines are straight) and that the electrode spacing is constant. If this assumption breaks down, the survey will be affected in three ways (Fourie, 2009a):

1) Some of the true (field) geometric factors will differ from the assumed geometric factors and thus affect the calculated apparent resistivities,

2) Since the true distances between some of the electrodes will differ from the assumed distances, the depth of investigation will be affected, and,

3) Since the current and potential electrodes are not collinear for all measurement positions on the survey line, the recorded apparent resistivities may be representative of the subsurface conditions at positions laterally displaced from the survey line.

Because inverse resistivity models are found by applying inversion algorithms to the recorded apparent resistivity data associated with assumed pseudo-depths, errors in the apparent resistivities and pseudo-depths due to angles in the survey lines will lead to errors in the inverted resistivity sections. These errors will be propagated from iteration to iteration during the inversion process (Fourie, 2009b). In this chapter, the impacts of angles in the survey lines on the ERT data recorded using the Wenner (α) geometry are examined. The effects of the errors in the recorded data on the inverted resistivity sections are studied in Chapter 4.

## 3.2 THE INFLUENCE OF ANGLED SURVEY LINES ON THE GEOMETRIC FACTORS AND CALCULATED APPARENT RESISTIVITIES

Consider an ERT survey on an angled survey line with the angle $(\theta)$ at the centre of the survey line, as shown in Figure 3.1. The position vector of the $i^{th}$ electrode on the line is given by:

$$\mathbf{r_i} = s(i-1)\,\hat{\mathbf{x}} \qquad 0 \le i \le (m+1)/2 \qquad 17$$

$$\mathbf{r_i} = s\left[\left(\frac{m-1}{2}\right) + \left(\frac{2i-m-1}{2}\right)\cos\theta\right]\hat{\mathbf{x}} + s\left(\frac{2i-m-1}{2}\right)\sin\theta\,\hat{\mathbf{y}} \qquad (m+1)/2 < i \le m \qquad 18$$

where $m$ is the total number of electrodes and $s$ is the distance between adjacent electrode positions (the standard electrode spacing). The distance between any two electrodes ($i$ and $j$) is given by:

$$r_{ij} = |\mathbf{r}_i - \mathbf{r}_j| \qquad 19$$

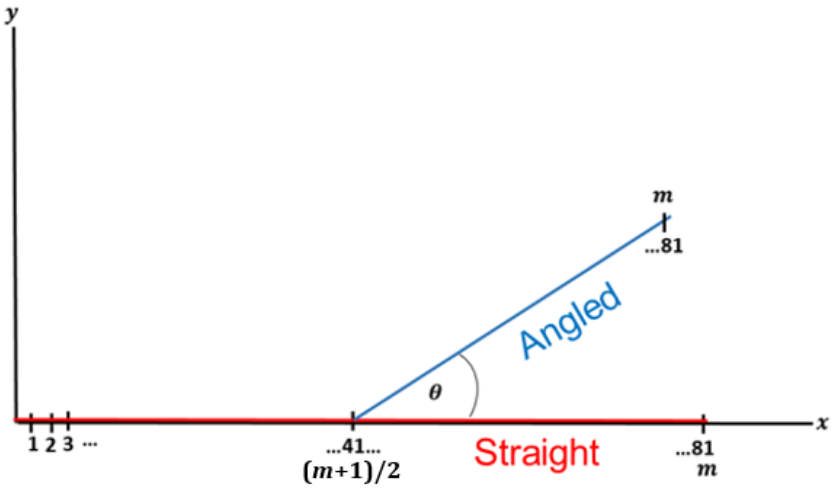


**Figure 3.1: Electrode positions along an angled survey line with 81 electrode positions**

Equations 17, 18 and 19 can now be used to calculate the true geometric factors for the ERT survey along the angled line. Once the true geometric factors ($K_{true}$) are known, they can be compared to the assumed (straight line) geometric factors ($K_{true}$) to evaluate the effects of the angled survey line on the calculated apparent resistivities. In Figure 3.2 and Figure 3.3, the percentage error using the assumed geometric factors is shown for survey lines with angles of 22.5° and 45°, respectively. These angles were chosen to represent small and large angles in the survey line, respectively. In these figures, the values of $[100 \times (K_{ass} - K_{true})]/K_{true}$ are plotted. The values on the horizontal ($x$-) axes indicate the electrode positions along the survey line (the total number of electrodes equals 81, similar to the system used during the field surveys discussed in Chapter 5). The values on the vertical ($z$-) axes are the $n$-factors which give the number of standard electrode spacings between the active electrodes.

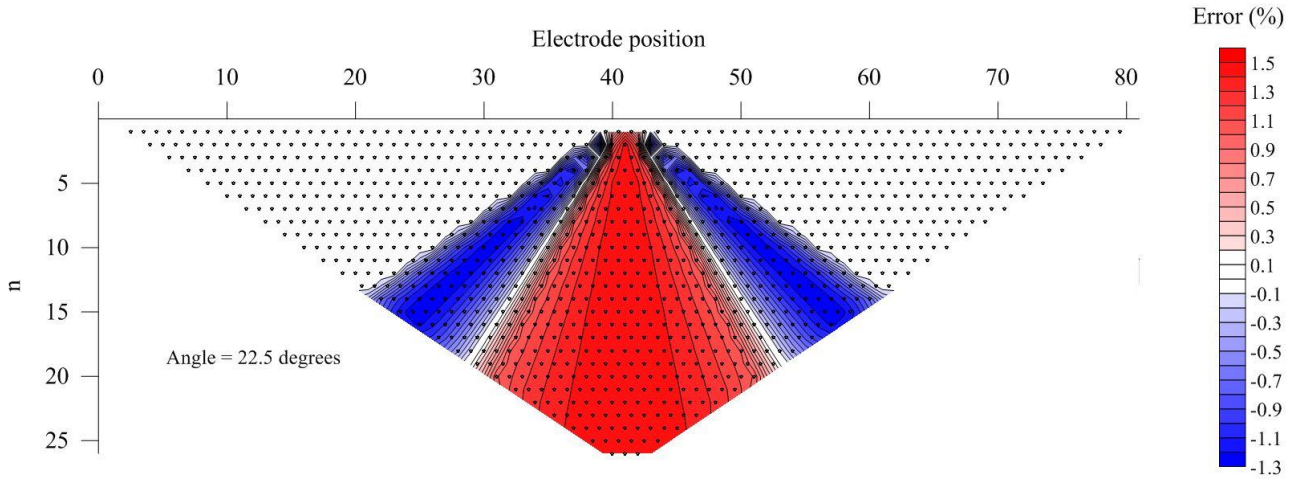


**Figure 3.2: Percentage error in the assumed geometric factors and calculated apparent resistivities for a survey line with an angle of 22.5°**

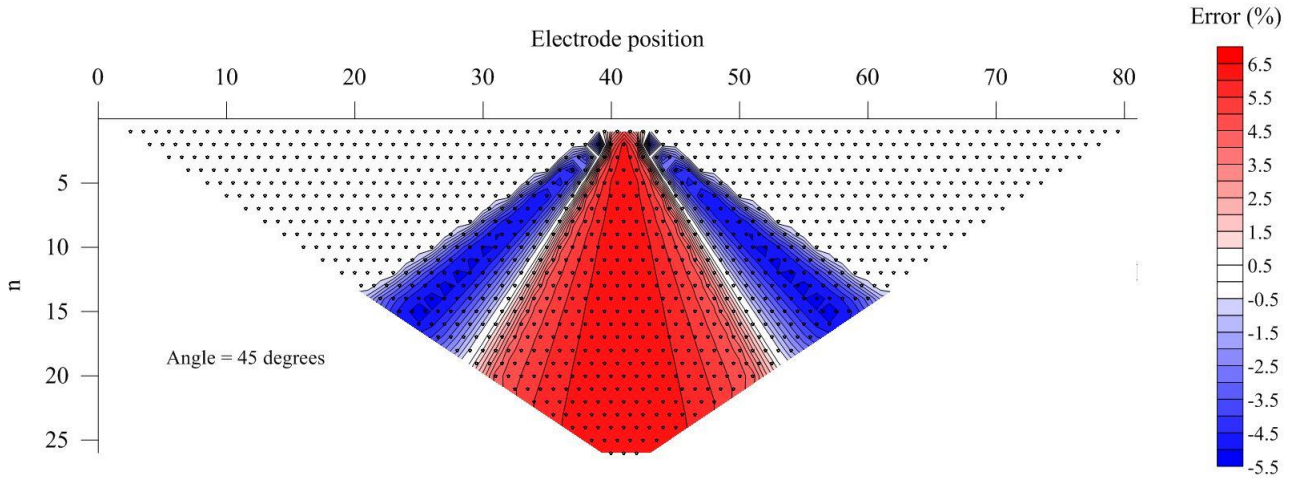


**Figure 3.3: Percentage error in the assumed geometric factors and calculated apparent resistivities for a survey line with an angle of 45º**

From Figure 3.2 and Figure 3.3 it is seen that the geometric factors and apparent resistivities are overestimated in a fan-shaped zone centred at the angle in the survey line. On either side of this zone, two zones occur in which the geometric factor and apparent resistivities are underestimated. It is further seen that the percentage errors in the assumed geometric factors and apparent resistivities are quite small (<1.5% for the 22.5° angle and <6.5% for the 45°angle). As expected, the error is larger for larger the larger angle in the survey line.

## 3.3 THE INFLUENCE OF ANGLED SURVEY LINES ON THE DEPTH OF INVESTIGATION

Following the methodologies of Roy and Apparao (1971) and Edwards (1977), the depth investigation characteristic ($DIC$) for any four-electrode array (including the Wenner (α) array) can be calculated for the following vector positions of the current electrodes (A and B) and potential electrodes (M and N) at the surface of the Earth (where $z = 0$):

$$\mathbf{A} = (x_A, y_A, 0)$$

$$\mathbf{B} = (x_B, y_B, 0)$$

$$\mathbf{M} = (x_M, y_M, 0)$$

$$\mathbf{N} = (x_N, y_N, 0)$$

The electric potential at any point in the ground due to current injection (+$I$) at the one current electrode and current removal (-$I$) at the other current electrode is given by:

$$V_D = \frac{\rho I}{2\pi}\left[\{(x-x_M)^2 + (y-y_M)^2 + z^2\}^{-0.5} - \{(x-x_B)^2 + (y-y_B)^2 + z^2\}^{-0.5}\right] \qquad 20$$

or:

$$V_D = \frac{\rho I}{2\pi}\left[{r_A}^{-1} - {r_B}^{-1}\right] \quad (21)$$

where $r_A$ and $r_B$ are the distances from the measurement position to the current electrodes. The electrical potential difference between the potential electrodes due to the current flow at the subsurface position $(x, y, z)$ is:

$$dV_{MN} = \frac{\rho I}{4\pi^2}\left[F_{AM} - F_{AN} - F_{BM} + F_{BN}\right] dx\, dy\, dz \quad (22)$$

where:

$$F_{AM} = \frac{(x - x_A)(x - x_M) + (y - y_A)(y - y_M) + z^2}{{r_A}^3\, {r_M}^3} \quad (23)$$

with similar expressions for $F_{AN}$, $F_{BM}$ and $F_{BN}$. In these expressions $r_M$ and $r_N$ are the distances from the measurement position to the potential electrodes. The *DIC* is found by integrating over the horizontal distances $x$ and $y$ from $-\infty$ to $+\infty$. This requires double integration with respect to these variables for each of the four expressions in Equation 22, that is:

$$\begin{aligned} DIC &= \iint_{-\infty}^{+\infty} dV_{MN}\, dx\, dy\, dz \\ &= \frac{\rho I}{4\pi^2}\left[\iint_{-\infty}^{+\infty} F_{AM}\, dx\, dy - \iint_{-\infty}^{+\infty} F_{AN}\, dx\, dy - \iint_{-\infty}^{+\infty} F_{BM}\, dx\, dy \right. \\ &\quad \left. + \iint_{-\infty}^{+\infty} F_{BN}\, dx\, dy\right] dz \end{aligned} \quad (24)$$

First, consider the double integration over $F_{AM}$. The integral can be written as:

$$\begin{aligned} \iint_{-\infty}^{+\infty} F_{AM}\, dx\, dy &= \iint_{-\infty}^{+\infty} \frac{(x - x_A)(x - x_M)}{{r_A}^3\, {r_M}^3} dx\, dy + \iint_{-\infty}^{+\infty} \frac{(y - y_A)(y - y_M)}{{r_A}^3\, {r_M}^3} dx\, dy \\ &\quad + \iint_{-\infty}^{+\infty} \frac{z^2}{{r_A}^3\, {r_M}^3}\, dx\, dy \end{aligned} \quad (25)$$

By making the substitutions:

$$x^* = x - x_A$$

$${x_M}^* = x_M - x_A$$

$$y^* = y - y_A$$

$${y_M}^* = y_M - y_A$$

Equation 23 becomes:

$$\iint_{-\infty}^{+\infty} F_{AM}\,dx\,dy = \iint_{-\infty}^{+\infty} \frac{x^*(x^* - {x_M}^*)}{(x^{*2} + y^{*2} + z^2)^{1.5}\,\{(x^* - {x_M}^*)^2 + (y^* - {y_M}^*)^2 + z^2\}^{1.5}}\,dx^*\,dy^*$$
$$+ \iint_{-\infty}^{+\infty} \frac{y^*(y^* - {y_M}^*)}{(x^{*2} + y^{*2} + z^2)^{1.5}\,\{(x^* - {x_M}^*)^2 + (y^* - {y_M}^*)^2 + z^2\}^{1.5}}\,dx^*\,dy^* \qquad 26$$
$$+ \iint_{-\infty}^{+\infty} \frac{z^2}{(x^{*2} + y^{*2} + z^2)^{1.5}\,\{(x^* - {x_M}^*)^2 + (y^* - {y_M}^*)^2 + z^2\}^{1.5}}\,dx^*\,dy^*$$

These integrals may be solved using Fourier transform pairs, as shown by Roy and Apparao (1971). One then finds that:

$$\iint_{-\infty}^{+\infty} F_{ij}\,dx\,dy = \frac{8\pi z}{\left[\left(x_j - x_i\right)^2 + \left(y_j - y_i\right)^2 + 4z^2\right]^{1.5}} \qquad 27$$

with $i$ and $j$ representing the current electrodes (A and B) and the potential electrodes (M and N), respectively. We thus have:

$$DIC = \frac{2\rho I z}{\pi}[f_{AM} - f_{AN} - f_{BM} + f_{BN}]\,dz \qquad 28$$

where:

$$f_{ij} = \left[\left(x_j - x_i\right)^2 + \left(y_j - y_i\right)^2 + 4z^2\right]^{-1.5} \qquad 29$$

The total half-space response ($HSR$) is found by integrating Equation 28 over $z$ from 0 to $+\infty$:

$$HSR = \int_0^{+\infty} DIC = \frac{\rho I}{2\pi}\,[{r_{AM}}^{-1} - {r_{AN}}^{-1} - {r_{BM}}^{-1} + {r_{BN}}^{-1}] = \frac{\rho I}{K} \qquad 30$$

where:

$${r_{ij}}^2 = \left(x_j - x_i\right)^2 + \left(y_j - y_i\right)^2 \qquad 31$$

and $K$ is the geometric factor of the general four-electrode array (refer to Equation 11). The normalised depth of investigation characteristic ($NDIC$) is then found by dividing the $DIC$ by the $HSR$ to give:

$$NDIC = \frac{2zK}{\pi}[f_{AM} - f_{AN} - f_{BM} + f_{BN}]\,dz \qquad 32$$

To determine the median depth ($z_{med}$) the following equation must be solved:

$$\int_0^{z_{med}} NDIC = \frac{1}{2} \qquad 33$$

or:

$$\frac{K}{\pi}\left[-(r_{AM}+4z_{med}{}^2)^{-0.5}+r_{AM}{}^{-0.5}+(r_{AN}+4z_{med}{}^2)^{-0.5}-r_{AN}{}^{-0.5}+(r_{BM}+4z_{med}{}^2)^{-0.5}\right.$$
$$\left.-r_{BM}{}^{-0.5}-(r_{BN}+4z_{med}{}^2)^{-0.5}+r_{BN}{}^{-0.5}\right]=1 \qquad 34$$

Equation 34 can be solved numerically for the different electrode positions employed during ERT surveys. In Figure 3.4 and Figure 3.5, the percentage error in the assumed median depth for surveys lines making angles of 22.5° and 45° at their centres, respectively, are shown for the Wenner (α) array. The pseudo-depth is seen to be underestimated in a fan-shaped zone centred at the angle in the survey line. The errors in the pseudo-depth for angled survey lines are observed to be quite small (<1.1% for a 22.5° angle and <3.8% for a 45° angle).

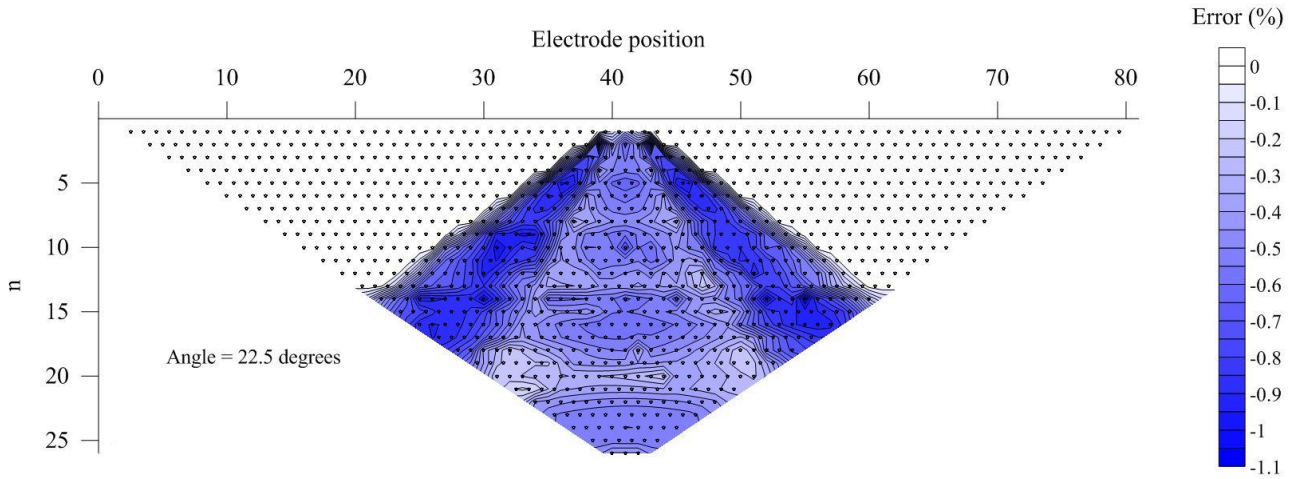


**Figure 3.4: Percentage error in the median depth ($z_{med}$) for a survey line with an angle of 22.5°**

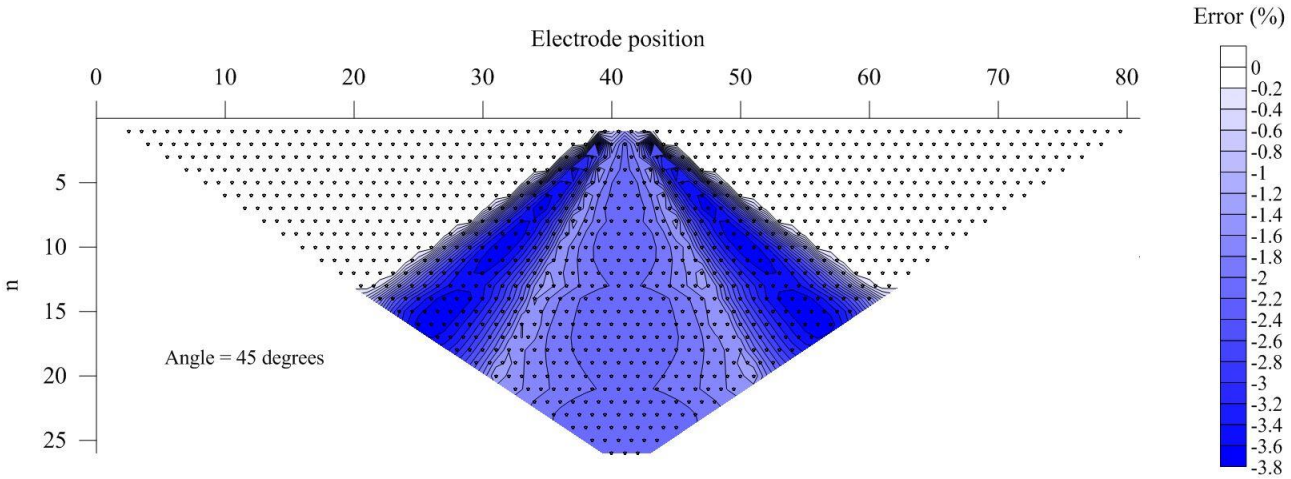


**Figure 3.5: Percentage error in the median depth ($z_{med}$) for a survey line with an angle of 45°**

## 3.4 THE SUBSURFACE VOLUME INVESTIGATED ALONG ANGLED SURVEY LINES

The influence of angled survey lines on the subsurface volume investigated can be determined from the sensitivity function of an electrode array to the changes in the subsurface resistivities. The sensitivity function may be calculated from the three-dimensional Fréchet derivative (Oldenburg 1978; Loke 2004). The three-dimensional Fréchet derivative ($F_{3D}$) is given by:

$$F_{3D}(\mathbf{r}) = \nabla\varphi_A \cdot \nabla\varphi_M - \nabla\varphi_A \cdot \nabla\varphi_N - \nabla\varphi_B \cdot \nabla\varphi_M + \nabla\varphi_B \cdot \nabla\varphi_N \qquad 35$$

where $\varphi_l$ is the electric potential at position **r** due to a unit current source at the position of electrodes ($l = A, B$ for the current electrodes; $l = M, N$ for the potential electrodes).

Fourie (2009a) studied the influence of curved and angled survey lines on the lateral position of measurement, wherein the 3D Fréchet derivative was used to create a 3D sensitivity map. The (*xy*-) sections of the sensitivity to resistivity changes in the subsurface are shown in Figure 3.6. In this figure, the depth of the sections increases from top to bottom. Comparison of the sensitivity for the straight survey line to the sensitivity for the angled survey line shows that, for an angled survey line, the array is sensitive to resistivity changes at position laterally displaced from the survey line. Hence, the maximum sensitivity does not lie along the survey line. The displacement is larger for large AB spacings and affects the deeper measurements more severely.

Fourie (2009a) concluded that lateral displacement of the measurement position directly results from the survey geometry and cannot be compensated for. The author noted that this fact should be taken into account when interpreting the models obtained from 2D ERT surveys along curved/angled survey lines.

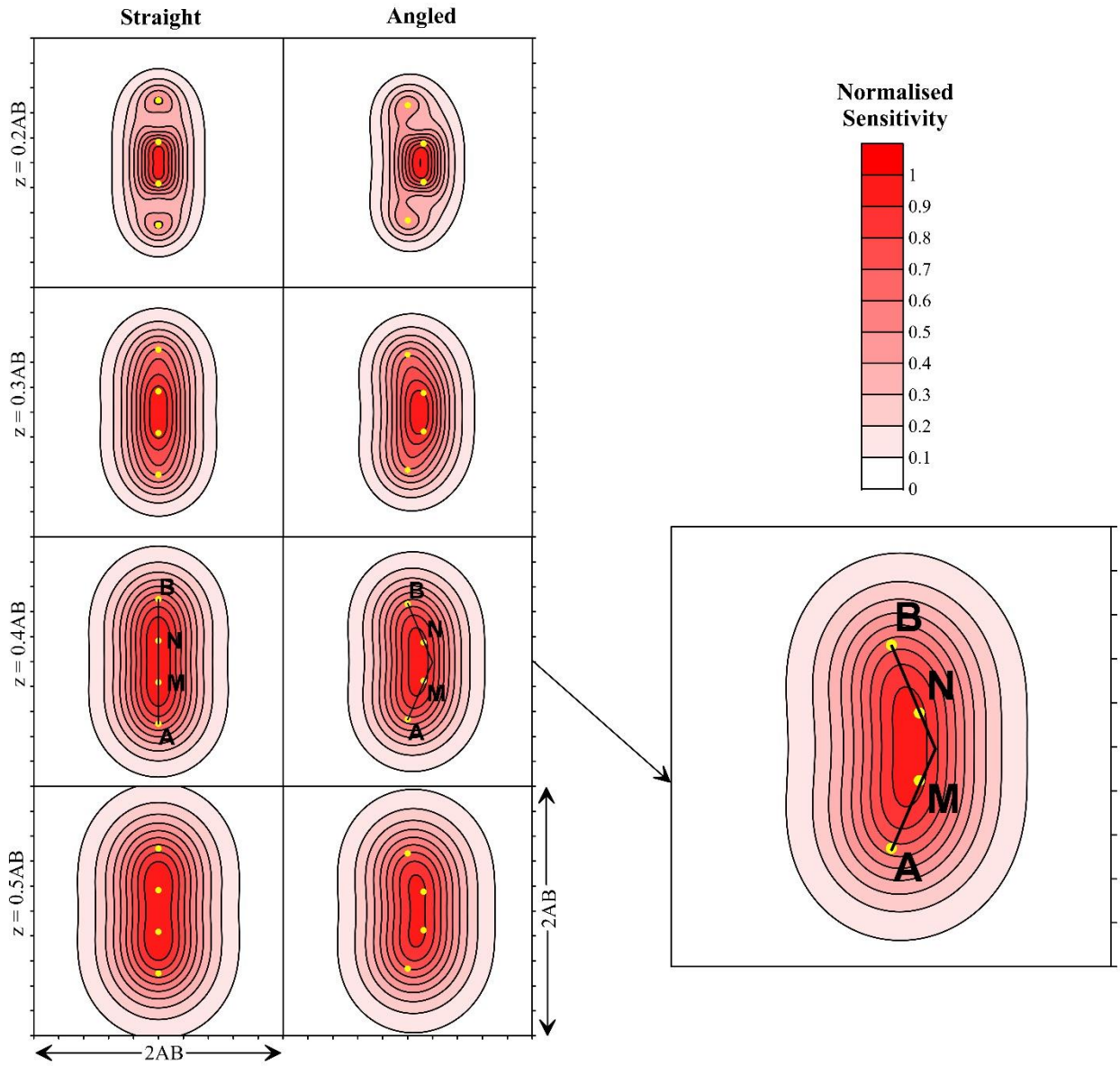


**Figure 3.6: The sensitivity of the Wenner (α) array to changes in the subsurface resistivities for straight and angled survey lines at different depths (adapted from Fourie, 2009a)**

## 3.5 DISCUSSION

In this chapter the effects of introducing angles on ERT survey lines were investigated by considering how the geometric factors, apparent resistivities, depths of investigation and the subsurface volumes surveyed are affected by angles in the survey lines. Two angles in the survey line were considered during the investigation: 22.5°, representing small angles, and 45°, representing large angles.

The results showed that errors introduced on the geometric factors and apparent resistivities are small (<1.5% for 22.5° and <6.5% for 45°) and are located at the position of the angle in the survey line extending outwards with depth. Within this zone the geometric factors and apparent resistivities are underestimated in some regions and overestimated in others. Similarly, the errors in the median depths (used as pseudo-depths for display and during inversion) caused by angles in the survey line

are small (<1.1% for 22.5° and <3.8% for 45°) and also occur near the centre of the survey line. Both the errors in the geometric factors and the median depth can be seen to increase with an increase in angle. Furthermore, angles in the survey line cause the subsurface volume investigated to differ from the volume investigated using a straight survey line. The volume of the subsurface investigated is laterally displaced from the survey line. This is seen to be more severe for larger current electrode spacings (larger depths of investigation).

Although the errors for the apparent resistivities and median depths introduced by angles in the survey line are small, these errors may lead to distorted inverse resistivity models. During each iteration of the inversion algorithm, the errors may be propagated, affecting larger parts of the model and also increasing in magnitude. The impact of such errors on the inverted resistivity models is investigated in Chapter 4.

# CHAPTER 4: MODELLING THE IMPACT OF ANGLED SURVEY LINES ON ERT SURVEYS ACROSS GEOLOGICAL STRUCTURES IN KAROO ROCKS

## 4.1 INTRODUCTION

In recent years, the two-dimensional (2D) ERT method has been widely used for different investigations in Karoo formations. Numerical modelling of the expected ERT response is often done before carrying out field measurements, to simulate the effect of real geological conditions and to study the effectiveness of the method applied for the investigation (Danielsen and Dahlin, 2010).

In Chapter 3 the influence of angles in ERT survey lines on the geometric factors, apparent resistivities, depths of investigations and measurement positions were studied. Since angles in the survey lines were seen to affect the apparent resistivity data set, it follows that the inverse resistivity models will also be affected by such angles. This chapter studies the influence of angled survey lines on the inverse resistivity models by considering models of geological conditions typically encountered in the Karoo rocks. Eight models were created which correspond to the geological conditions often encountered in the Karoo rocks. These models include: horizontal and vertical contacts, vertical and inclined dolerite dykes, dolerite sills, and weathered zones. The number of electrodes used for each model was 81, and the spacing between the electrodes was set to 5 m, giving a survey line length of 400 m. These settings were chosen to correspond to the equipment used for the measurements taken during the field survey (Chapter 5).

## 4.2 DESCRIPTION OF FORWARD AND INVERSE NUMERICAL MODELLING SOFTWARE

Numerical modelling is an inexpensive and effective process to assist in planning and designing field surveys. It can also be used to test the success and limitations of the technique used before conducting a field survey. According to Hassan *et al*. (2015), ERT numerical modelling is a two-step procedure that involves:

- Creating a synthetic data set (pseudo-section) of apparent resistivities based on the existing information and assumptions (forward modelling), and,
- Finding a model of the subsurface resistivity distribution that corresponds to the measured apparent resistivity data set (inverse modelling).

In this study, simulations of different geological conditions associated with groundwater encountered in the Karoo formations were completed using forward and inverse modelling software. The forward

and inverse modelling were done by respectively using the RES2DMOD and RES2DINV software packages created by Loke (2004). These software packages are briefly described below.

### 4.2.1 RES2DMOD

The software package RES2DMOD was used for forward modelling. This software allows the user to create different models of the subsurface by using a text editor to modify the input files. The software calculates the apparent resistivity distribution for a 2D survey carried out with a chosen electrodes geometry (Loke, 2002). The calculated apparent resistivities are presented in the form of pseudo-sections with the apparent resistivities plotted at pseudo-depths corresponding to the separations and positions of the electrodes during each modelled measurement.

In this study, forward modelling was done for the Wenner (α) array using input models representing different geological structures associated with groundwater occurrence in Karoo rocks.

### 4.2.2 RES2DINV

The software package used for inverse modelling was RES2DINV, also developed by (Loke, 2002). RES2DINV is used to generate models of the true subsurface resistivity distribution using the apparent resistivities and pseudo-depths as inputs. In the current study, inverse models were created for both straight and angled data sets.

The inversion algorithm used during the current investigations is the widely used regularised least square or *robust inversion* method. Robust inversion (also known as the L1-norm) produces models with sharp boundaries between the materials with different resistivity values. It assumes that the resistivity values within each region are approximately constant. Considering the fact that the Karoo Supergroup is characterized by the presence of dolerite intrusions, faults and contact zones with sharp boundaries, robust inversion is the appropriate choice of inversion algorithm, and is used for all the inverse modelling conducted as part of the current study.

## 4.3 MODELLING APPROACH

To investigate the influence of angled survey lines on the ERT data recorded across various geological structures, the following steps were taken during the forward and inverse modelling (shown schematically in Figure 4.1):

- A model of the subsurface resistivity distribution for a particular geological feature (contact zone, dyke, sill, weathered zone) was created. This model was used as input to the forward modelling software (RES2DMOD).

- Using the forward modelling software, pseudo-sections of the apparent resistivity values corresponding to the different models were obtained. These pseudo-sections represent the measurements taken along straight survey lines.
- The modelled pseudo-sections were adjusted to correspond to the measurements that would have been taken along angled survey lines. This was done by calculating the true geometric factors for measurements along the angled survey lines, and by adjusting the apparent resistivity values accordingly. Survey lines with two angles at the centres of the lines were considered for the calculations: 22.5$^{o}$, representing small angles, and 45$^{o}$, representing large angles.
- The three pseudo-sections thus generated for each model (straight, 22.5$^{o}$ angle and 45$^{o}$ angle) were then inverted to obtain models of the subsurface resistivity distribution. The software package RES2DINV was used for inversion. These inverse models were compared to the input model and to each other to evaluate the impact of angled survey lines on the obtained resistivity models.

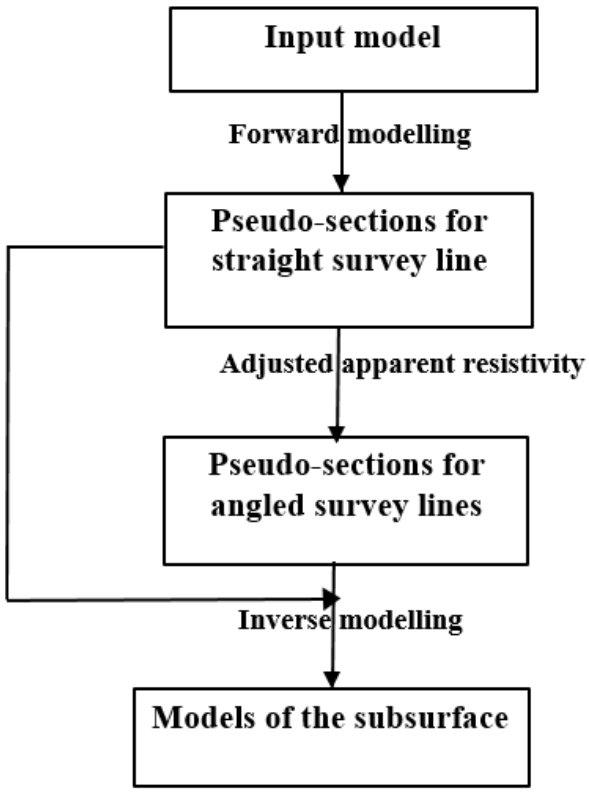


**Figure 4.1: Illustration of steps followed to complete the subsurface modelling investigation**

### 4.3.1 Modelling contact zones

A contact zone can be defined as a surface along which separate or different geologic formations touch each other. The contact zone may either be in an area where there was an intrusion, where the contact is formed between intrusive rocks and the country rocks, or in faulted formations. It can also

be found in beds with different geological characteristics. Therefore, contact zones can either be vertical, inclined or horizontal.

In Karoo rocks, it is not always possible to identify or visually observe contact zones. Contact zones can only be visually observed in mountainous areas with road cuts, or in stream beds. In flat-lying areas, contact zones can only be detected by geophysical techniques or invasive studies of the subsurface lithology. In Karoo rocks, contact zones may control groundwater occurrence, groundwater movement, and aquifer yield. In this study, horizontal and vertical contact zones are investigated and the results are presented in Sections 4.4 and 4.5, respectively.

### 4.3.2 Modelling dolerite dykes

The Karoo Supergroup is characterised by an abundance of dolerite dyke intrusions. Dykes can be visually identified by the presence of dense or green vegetation and slight changes in topography in some areas, whereas in other areas dykes are not visible at surface but can be well exposed in stream beds. Furthermore, dolerite dyke intrusions are often impermeable themselves and cause damming of groundwater because they form barriers to groundwater flow. The effectiveness of a dyke to act as a barrier depends on the degree of fracturing and the thickness of the dyke. As explained earlier, dolerite dykes are regarded as the main targets for groundwater exploration in Karoo rocks (Botha *et al*., 1998).

Dolerite dykes encountered in the Karoo Supergroup are of different sizes and they can either be vertical or inclined. In the upcoming sections (Sections 4.6 to 4.9), four different models are developed to simulate thick and thin vertical dykes, and thick and thin inclined dykes.

### 4.3.3 Modelling weathered zones

Weathering cause changes in the properties of rocks, this includes changes in the conductivity and permeability of the rocks. Permeability is the capability of a rock mass to allow fluid to pass through. It is dependent on the shape, cementation and packing of the grains, connectivity and the size of the pore spaces. Therefore, weathering increases permeability while decreasing the resistivity of the rocks. This is the reason why weathered zone in the constructed model in Section 4.11 is assigned lower resistivity value than the country-rock.

## 4.4 MODELLING A HORIZONTAL CONTACT

### 4.4.1 Forward modelling

For the horizontal contact model, the contact was assumed to be between two layers (L1 and L2) with different resistivity values (bottom image of Figure 4.2). The top layer (L1) was constructed with a

thickness of 30 m and the rock type was assumed to have a resistivity value of 50 Ωm. The bottom layer (L2) was constructed as the host rock with the resistivity value of 500 Ωm. These resistivity values represent values typically encountered in the Karoo rocks. The top layer was given a lower resistivity value because it is prone to weathering (Chandra, 2015). The bottom layer was assigned a higher resistivity because it is protected from weathering by the overlying layer (L1).

The pseudo-section found through forward modelling is shown in the top image of Figure 4.2. The pseudo-section displays resistivity values that are constant in a lateral sense but gradually increase with depth. It is not possible to identify the depth of the contact from the pseudo-section.

### 4.4.1 Inverse modelling

The inverse resistivity models obtained for the horizontal contact are shown in Figure 4.3 for a straight survey line (top) and angled survey lines with angles of 22.5$^o$ (centre) and 45$^o$ (bottom). The inverse resistivity model for a straight survey line gives a fairly good representation of the input model (the depth of the contact is shown as a horizontal black line). However, the transition zone between the high and low resistivity layers is gradual and the sharp boundary is not well defined. This failure to accurately image the boundary is the combined result of the limitations of the inversion process and the smearing caused during contouring. In addition, the modelled resistivities of both the shallow and deep layer display variations, both laterally and vertically, unlike the input model which consisted of two layers of homogeneous resistivities. Despite these imperfections, the inverse resistivity model for the straight line yields a reasonably accurate representation of the input model.

The inverse resistivity model of the 22.5° survey line also gives a reasonably accurate depiction of the horizontal boundary. However, a slight distortion of the boundary is observed near the centre of the line where the angle occurs. The modelled resistivities of the upper and lower layers are also seen to be affected by the angle in the survey line, and differ more from the input model values than for the straight survey line.

For the 45° angled survey line, the horizontal contact between the two layers is completely distorted. Near the centre of the survey line, the depth to the interface is underestimated by the inverse model. Furthermore, the modelled resistivities of the deep layer exhibit large lateral variations, overestimating the resistivity near the centre and underestimating it towards the sides of the modelled section. This creates the impression that a near-vertical resistive body occurs near the centre of the modelled section. Such a feature could be misinterpreted as a thick vertical dyke.

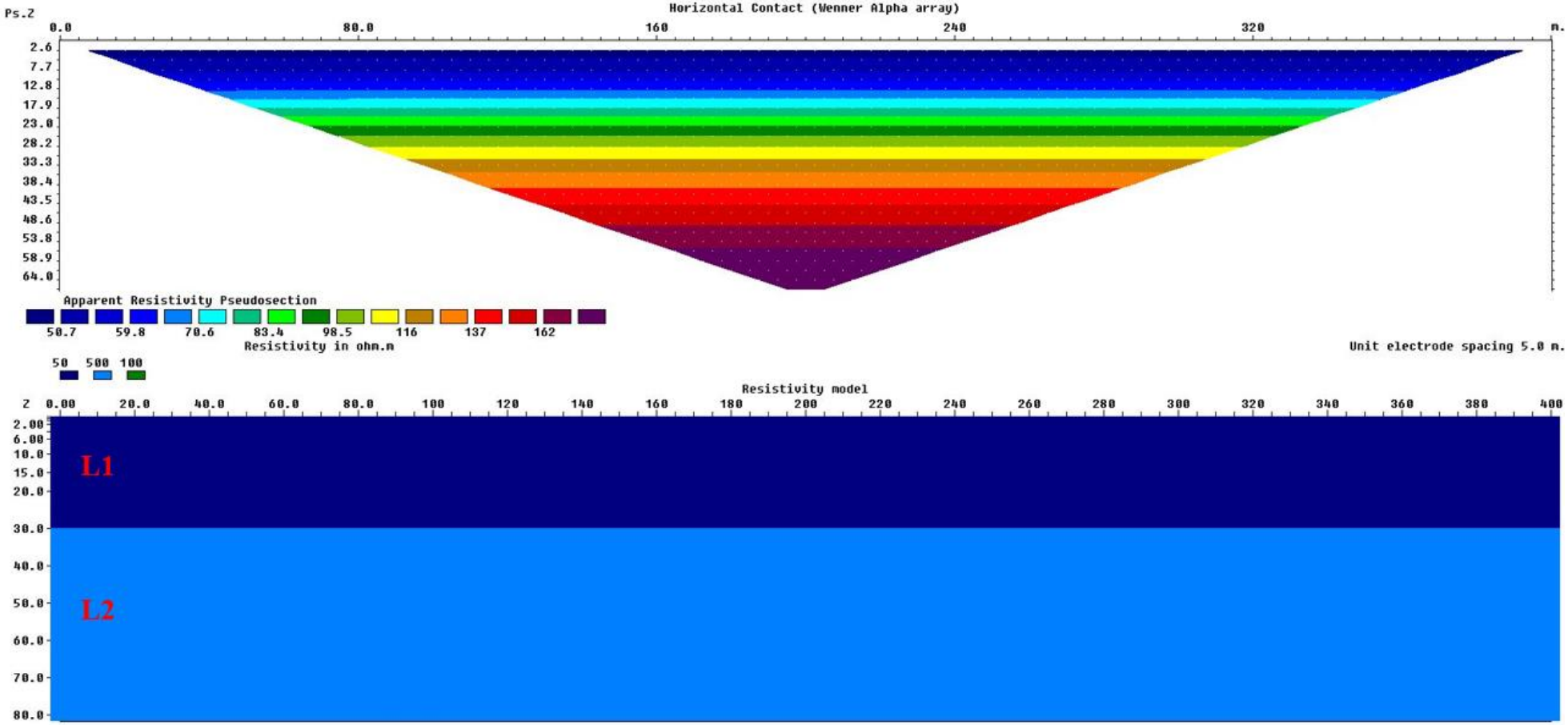


**Figure 4.2. Input model (bottom) and calculated pseudo-section (top) for the model representing a horizontal contact**

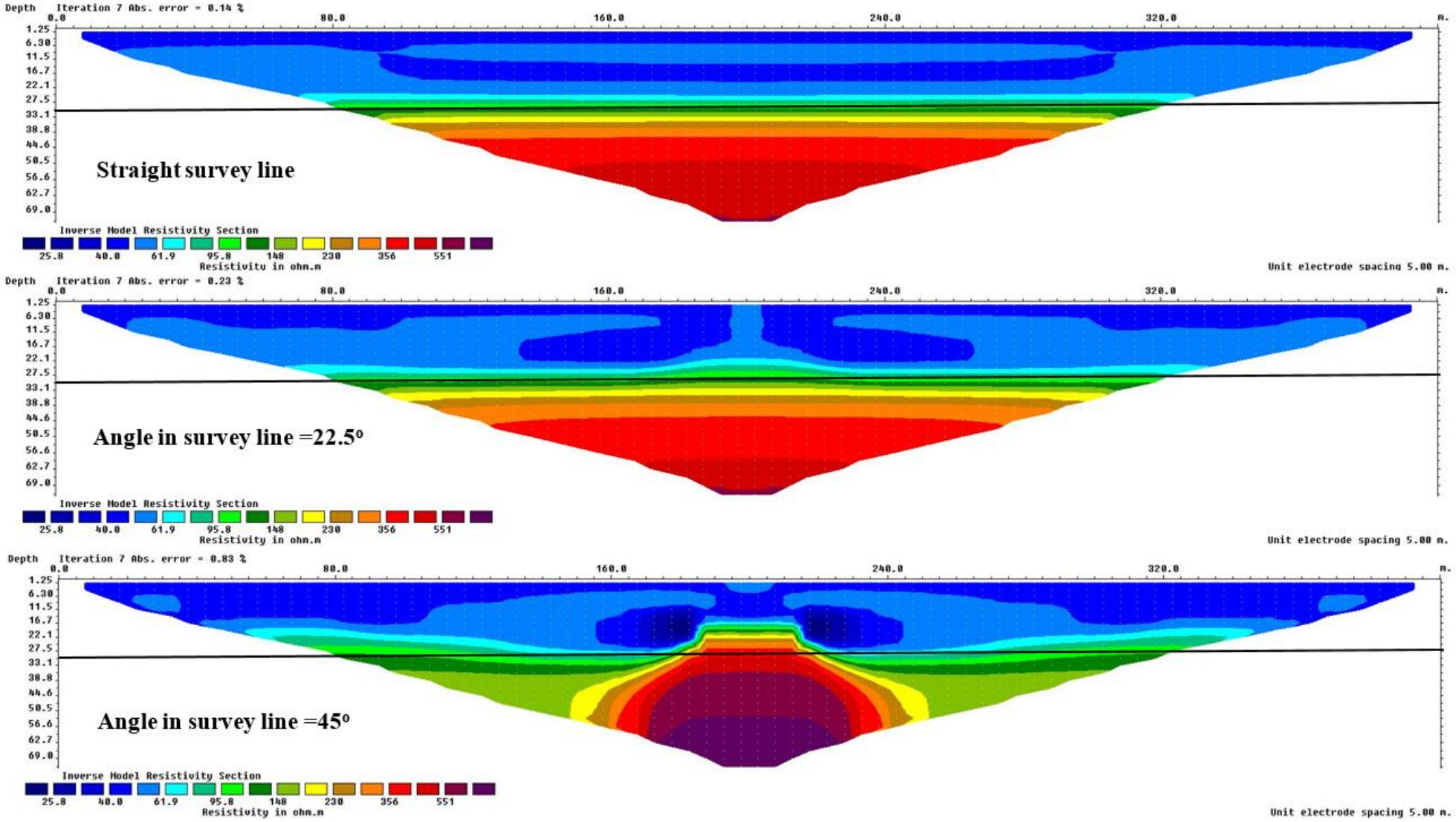


**Figure 4.3. Inverse models obtained for the horizontal contact for a straight survey line (top), a survey line with a 22.5º angle (middle) and a survey line with a 45º angle (bottom). The depth of the contact in the input model is shown as horizontal black lines**

### 4.4.2 Modelling errors introduced by angled survey lines

The differences between the modelled resistivity values for the angled survey lines and the straight survey line may be calculated from:

$$\text{Difference} = \rho_{angled} - \rho_{straight} \qquad 36$$

In Figure 4.4 the differences are shown for a survey lines with a 22.5° angle (top) and a 45° angle (bottom). For a 22.5° angled survey line, a local maximum in the difference is observed near the centre of the survey line at a depth of approximately 25 m. Below a depth of approximately 30 m, the difference is consistently negative, showing that the model of the angled line underestimates the resistivities of the deep layer. The difference ranges between -70 Ωm to 70 Ωm.

For the 45° survey line, much larger differences are observed, ranging from -300 Ωm to 350 Ωm. A zone of large positive differences occurs near the centre of the section, showing that the inverse model for the angled line overestimates the resistivities in this region. To the sides of this zone, the resistivities of the deep layer are underestimated.

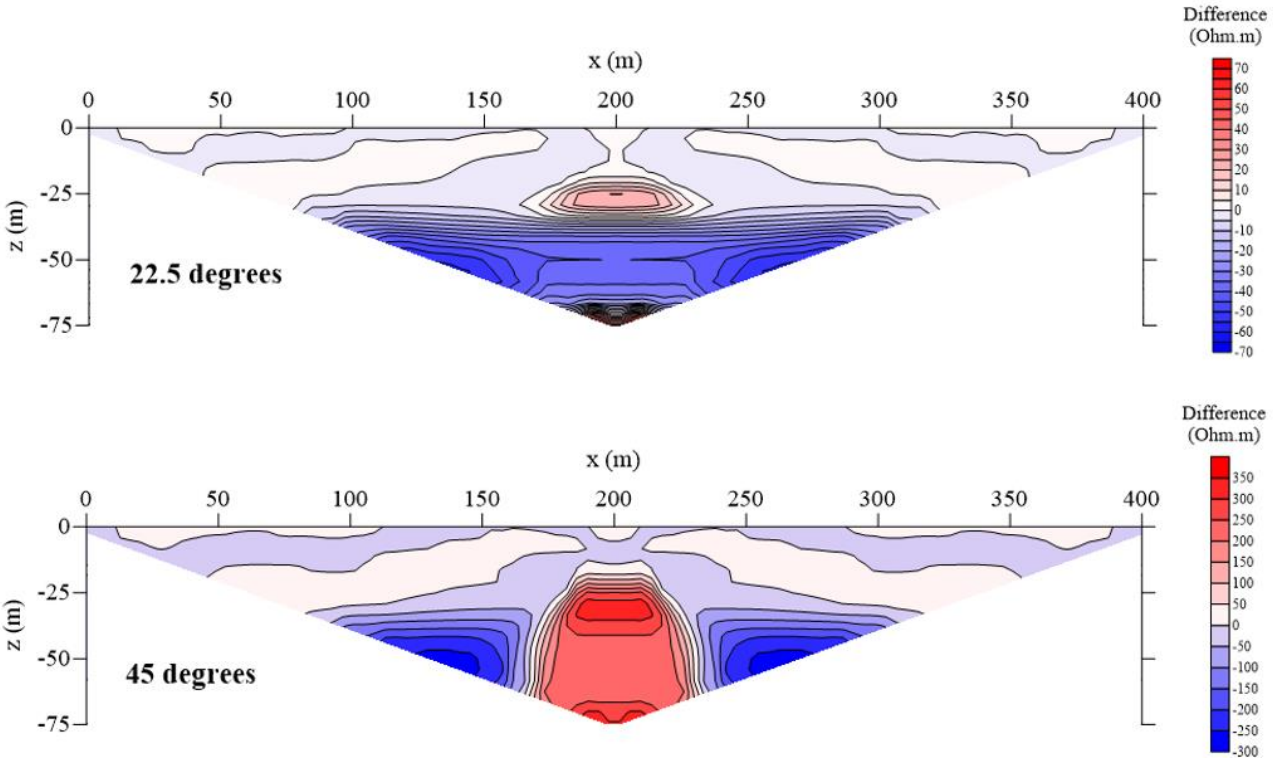


**Figure 4.4: Differences between the modelled resistivity values recorded on the angled survey lines (22.5º and 45°) and the resistivity values recorded on a straight survey line for horizontal contact**

The absolute error made by the inverse resistivity models in retrieving the resistivity values of the input model may be calculated from:

$$\text{error} = \rho_{modelled} - \rho_{input} \quad 37$$

In Figure 4.5 the errors made by the straight (top), 22° (centre) and 45° (bottom) survey lines are presented. For the straight line, the largest errors occur in the vicinity of the boundary at a depth of 30 m. This shows that the inversion process was not able to accurately locate the contact. The inverse model also underestimates the resistivity of the deep layer, except for the deepest positions below the centre of the survey line. The error ranges from -500 Ωm near the contact to +100 Ωm at the deepest positions.

Similar errors are made by the inverse model of the 22.5° survey line. However, the large errors in the vicinity of the contact extend to greater depths than for the straight line and the error for the deepest measurements is larger. The error ranges from -450 Ωm near the contact to +150 Ωm at the deepest positions.

The errors for the 45° survey line are very prominent, especially directly below the angle in the survey line where errors approach +450 Ωm. The resistivity of the deep layer is greatly underestimate, with large negative errors extending all the way from the depth of the contact to the bottom of the section.

### 4.4.3 Estimating the depth of the contact by 1D inversion of sounding data

To investigate the influence of angles in survey lines on the depth of investigation, the apparent resistivity data were extracted for three sounding centres (stations 100, 150 and 200) on each of the survey lines (straight, 22.5° and 45°). The data were then subjected to 1D inversion to determine the depth of the contact and the resistivities of the two layers. The software package IPI2WIN (Bobatchev *et al*., 2001) was used for the inverse modelling.

Modelling was done in two ways:

1) Unconstrained modelling, to find a subsurface model that gives the best fit (lowest error) between the input data and the modelled data, and,

2) Constrained modelling, to find the depth of the contact while keeping the resistivity values of the two layers constant at their true values (50 Ωm and 500 Ωm for the top layer and bottom layers, respectively).

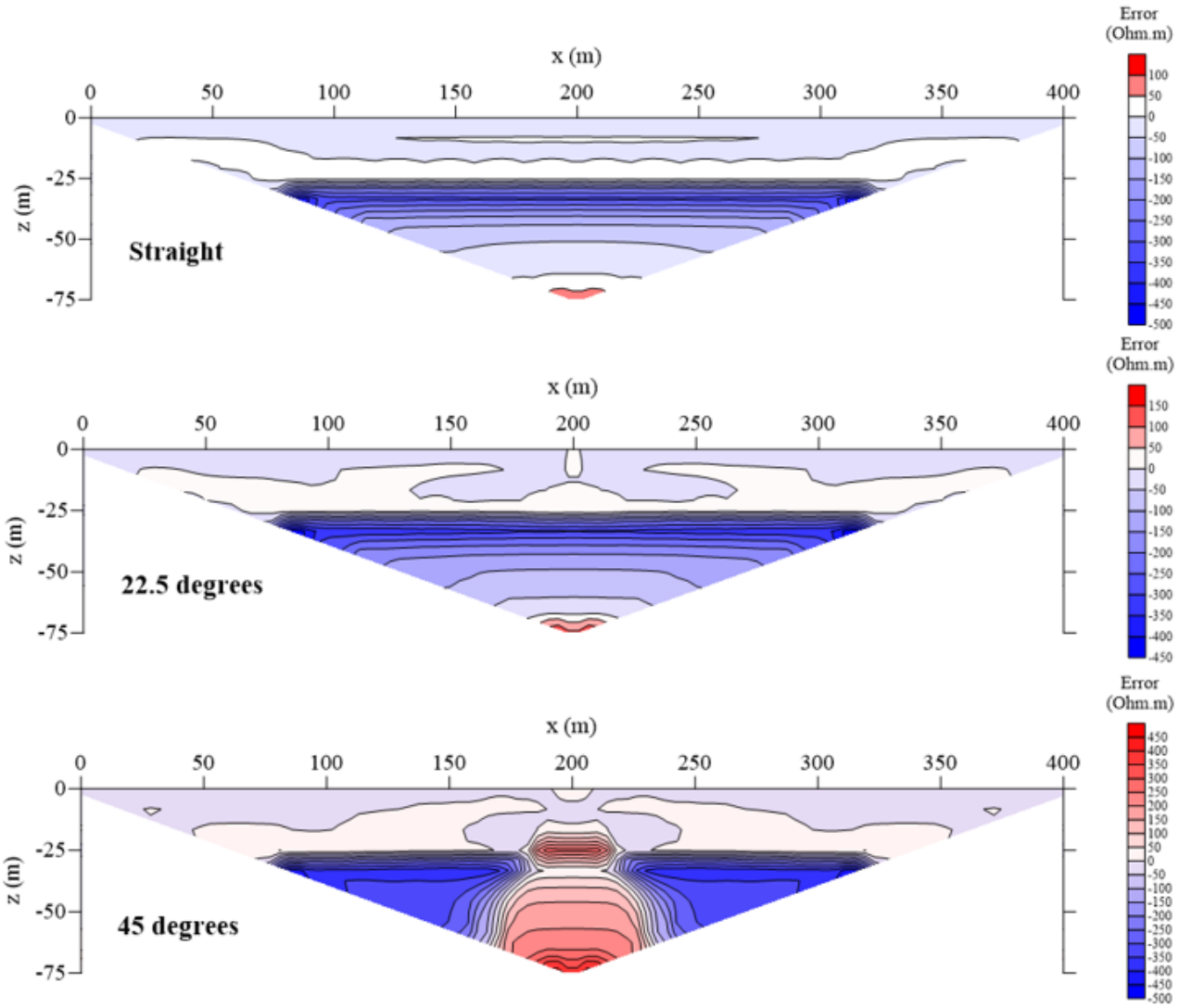


**Figure 4.5: Errors in the modelled resistivity values for the straight survey line (top), and angled survey lines (middle: 22.5º; bottom: 45º) for a horizontal contact**

An example of the 1D inversion results is shown in Figure 4.6 where the results for station 100 on the 45º survey line are shown for both the unconstrained (Figure 4.6a) and constrained (Figure 4.6b) inversions. In this example, both the unconstrained and constrained inversions found the same depth for the contact (28.87 m, compared to the true value of 30 m), and similar values for the resistivity of the shallow layer (50.02 Ωm and 49.87 Ωm, compared to the true value of 50 Ωm), but the resistivity of the deep layer was significantly underestimated in the unconstrained model (437.1 Ωm, compared to the true value of 500 Ωm).

In Table 4.1 the modelled depths of the contact and layer resistivities are shown for the straight and angled survey lines, while the percentage error in the modelled parameter values are listed in Table 4.2.

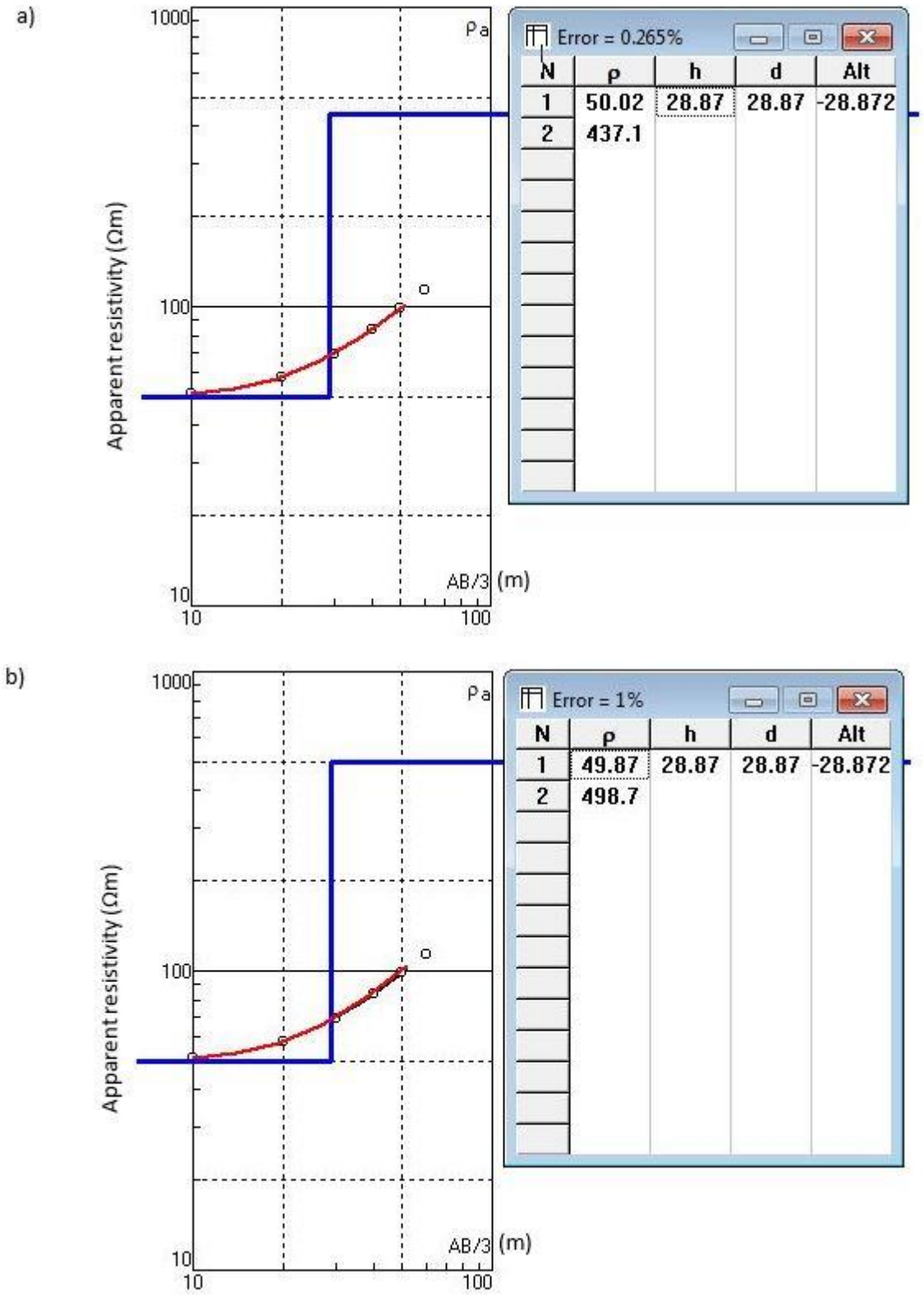


**Figure 4.6: Example of the modelled values for the thickness of the top layer and the resistivities of the two layers for a) the best fit inversion, and b) an inversion in which the resistivities are constrained to their true values (sounding centre = 100; angle = 45º)**

**Table 4.1: Modelled parameter values and RMS errors for 1D inversions of the sounding data recorded at sounding centres 100, 150 and 200**

| Modelled parameters | | | | | | | |
|---|---|---|---|---|---|---|---|
| Parameter | Sounding Centre | Straight | | 22.5° | | 45° | |
| | | Best Fit | Constrained | Best Fit | Constrained | Best Fit | Constrained |
| $h_1$ (30 m) | 100 | 28.92 | 28.92 | 28.93 | 29.31 | 28.87 | 28.87 |
| | 150 | 29.56 | 29.56 | 30.51 | 29.68 | 35.26 | 30.10 |
| | 200 | 29.80 | 29.80 | 29.78 | 28.58 | 29.80 | 26.20 |
| $\rho_1$ (50 Ωm) | 100 | 50.02 | 49.87 | 50.03 | 49.87 | 50.02 | 49.87 |
| | 150 | 50.13 | 49.87 | 50.35 | 49.87 | 51.32 | 49.90 |
| | 200 | 50.19 | 49.87 | 50.93 | 49.87 | 54.20 | 49.90 |
| $\rho_2$ (500 Ωm) | 100 | 440.0 | 498.7 | 440.9 | 498.7 | 437.1 | 498.7 |
| | 150 | 492.0 | 498.7 | 542.0 | 498.7 | 1 097.0 | 499.0 |
| | 200 | 507.2 | 498.7 | 514.0 | 498.7 | 548.0 | 499.0 |
| RMSE (%) | 100 | 0.266 | 0.938 | 0.266 | 0.483 | 0.265 | 1.000 |
| | 150 | 0.297 | 0.472 | 0.613 | 0.813 | 2.090 | 3.170 |
| | 200 | 0.321 | 0.854 | 0.315 | 1.010 | 0.321 | 3.500 |

**Table 4.2: Percentage error in the modelled parameter values for 1D inversions of the sounding data recorded at sounding centres 100, 150 and 200**

| %Error in the modelled parameters | | | | | | | |
|---|---|---|---|---|---|---|---|
| Parameter | Sounding Centre | Straight | | 22.5° | | 45° | |
| | | Best Fit | Constrained | Best Fit | Constrained | Best Fit | Constrained |
| $h_1$ | 100 | -3.60 | -3.60 | -3.57 | -2.30 | -3.77 | -3.77 |
| | 150 | -1.47 | -1.47 | 1.70 | -1.07 | 17.5 | 0.33 |
| | 200 | -0.67 | -0.67 | -0.73 | -4.73 | -0.67 | -12.7 |
| $\rho_1$ | 100 | 0.04 | -0.26 | 0.06 | -0.26 | 0.04 | -0.26 |
| | 150 | 0.26 | -0.26 | 0.70 | -0.26 | 2.64 | -0.20 |
| | 200 | 0.38 | -0.26 | 1.86 | -0.26 | 8.40 | -0.20 |
| $\rho_2$ | 100 | -12.0 | -0.26 | -11.8 | -0.26 | -12.6 | -0.26 |
| | 150 | -1.60 | -0.26 | 8.40 | -0.26 | 119.4 | -0.20 |
| | 200 | 1.44 | -0.26 | 2.80 | -0.26 | 9.60 | -0.20 |

For the unconstrained (best fit) modelling, the depth of the contact is accurately retrieved (error <5%) for all three sounding centres on all lines. A notable exception is for sounding centre 150 on the 45° survey line where the depth is overestimated by 17.5%. For the constrained modelling, the errors are similarly small, except for sounding centre 200 on the 45° survey line where the depth is underestimated by 12.7%. For unconstrained modelling, the resistivity of the top layer is accurately retrieved (error <3%) for all sounding centres on all lines, except for sounding centre 200 on the 45° line where the resistivity is overestimated by 8.40%. Unconstrained modelling also lead to large errors in the resistivity values of the deep layer, exceeding 12% on the straight line and 119% on the 45° line.

The data listed in Table 4.1 and Table 4.2 show that the depth to the contact may be significantly overestimated or underestimated when angles are introduced to a survey line. As expected, a larger angle is seen to affect the depth estimation more severely.

## 4.5 MODELLING A VERTICAL CONTACT

### 4.5.1 Forward modelling

The input model used to model the subsurface resistivity response from a vertical contact is shown in Figure 4.7 (bottom). The model consists of two geological units of different resistivity values, separated by a vertical contact. The unit on the left side was assigned a resistivity value of 50 Ωm while the unit on the right side was given a value of 500 Ωm. The vertical contact occurs in the centre of the survey lines at a distance of 200 m from the start of the line.

The calculated pseudo-section for the vertical contact model is shown in Figure 4.7 (top). Although the surface position of the contact can be established from the pseudo-section, it is not clear from the pseudo-section that the contact is vertical.

### 4.5.2 Inverse modelling

The inverse resistivity models for the vertical contact are displayed in Figure 4.8 for a straight survey line (top) and for angled survey lines with an angle of 22.5° (middle) and 45° (bottom). The exact positions of the vertical contacts are shown as black lines running from top to the bottom of the inverse models at centre of the survey line (at the 200 m station). From Figure 4.8 it is clear that the model for the straight survey line retrieved the position of the vertical contact very well, especially for shallow depths (<30 m). The resistivities of the two units in contact were also recovered well, although some variations in the resistivity values are observed.

The inverse model for the 22.5$^{o}$ survey line looks very similar to the model for the straight line. The vertical contact is again well imaged at shallow depths, with some distortion at greater depths. The most prominent difference between the two models is the shallow localised zone of low resistivity in the 50 Ωm unit near the contact.

For the survey line with the 45° angle, the resistivity model is severely distorted. Although the position of the contact can still be identified, artefacts created by the angle cause localised zones of high and low resistivities. The distortions is particularly severe in the low resistivity (50 Ωm) unit, although the high resistivity (500 Ωm) unit is also affected.

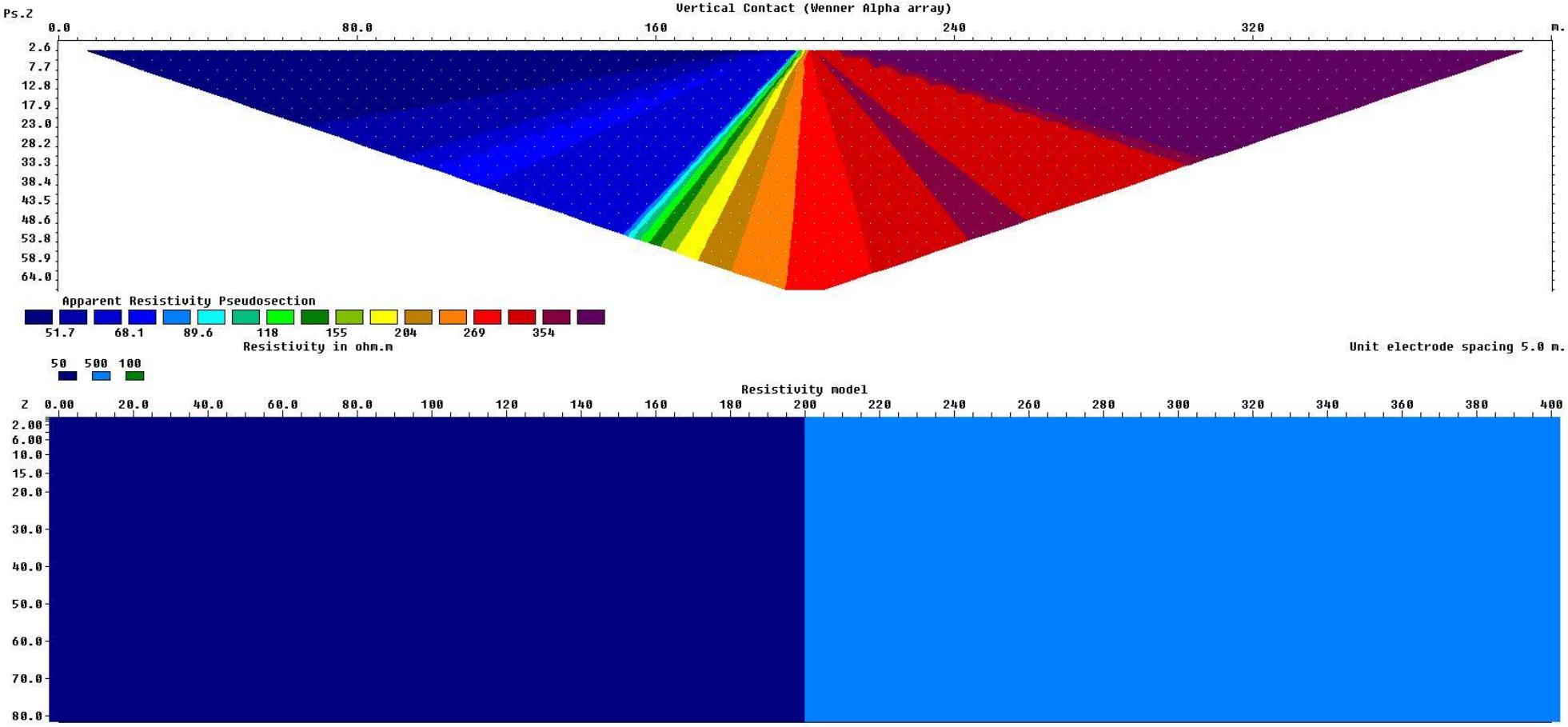


**Figure 4.7. Input model (bottom) and calculated pseudo-section (top) for the model representing a vertical contact**

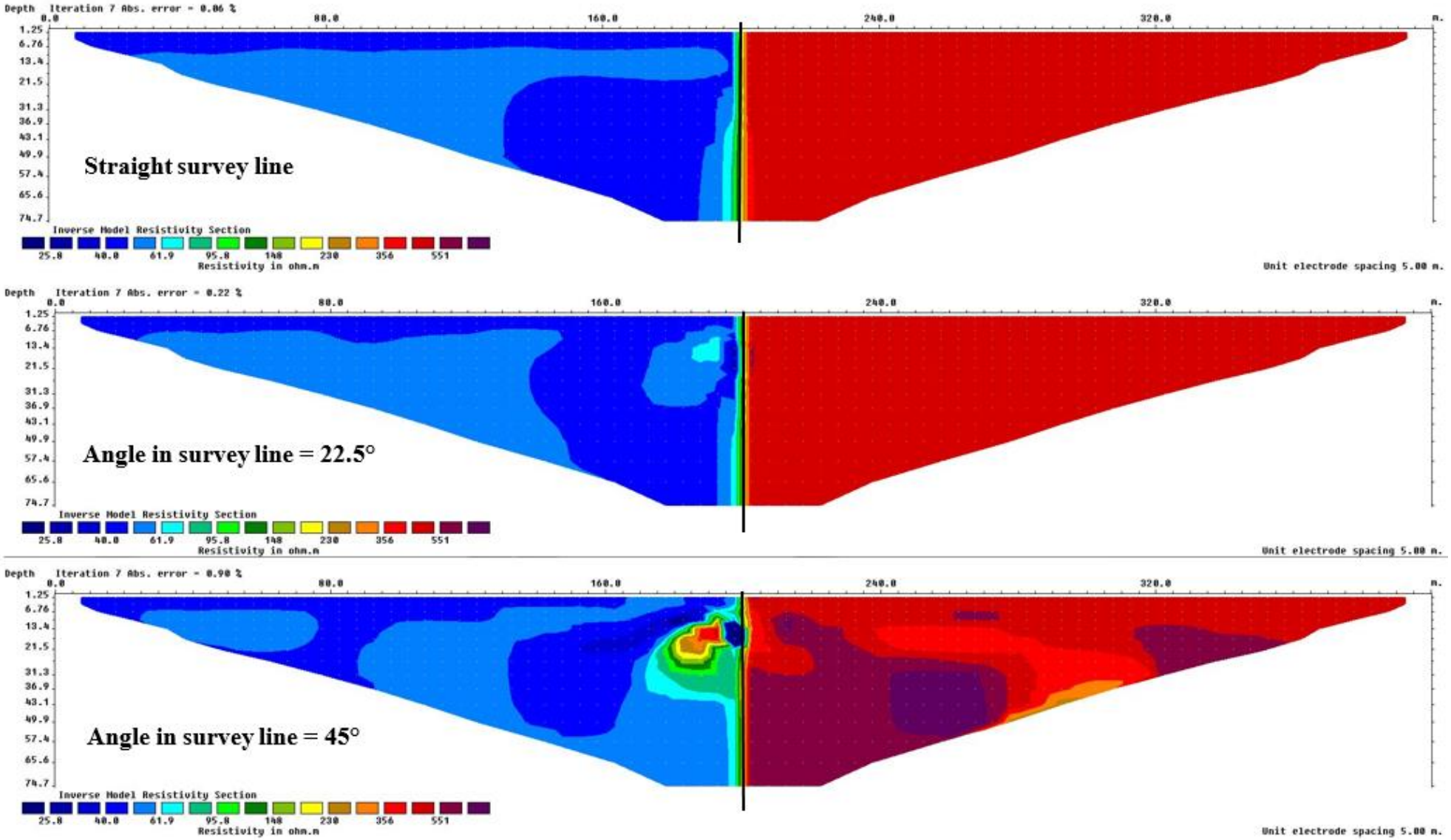


**Figure 4.8. Inverse models obtained for the vertical contact for a straight survey line (top), a survey line with a 22.5º angle (middle) and a survey line with a 45º angle (bottom). The input model contact zone is shown as black vertical lines**

### 4.5.3 Modelling errors introduced by angled survey lines

The differences between the modelled resistivity values for a straight survey line and the modelled resistivity for angled survey lines are shown in Figure 4.9 (top: 22.5°; bottom: 45°). It is clear that large differences between the models of the straight and 22.5° lines occur near the contact. Furthermore, large differences occur within the high resistivity unit (on the right). The differences range from a value of -50 Ωm to +60 Ωm.

For the 45° line, the differences between the models are much larger, ranging from -300 Ωm to +400 Ωm. The localised zones of where large differences are observed, are also more prominent for the 45° line.

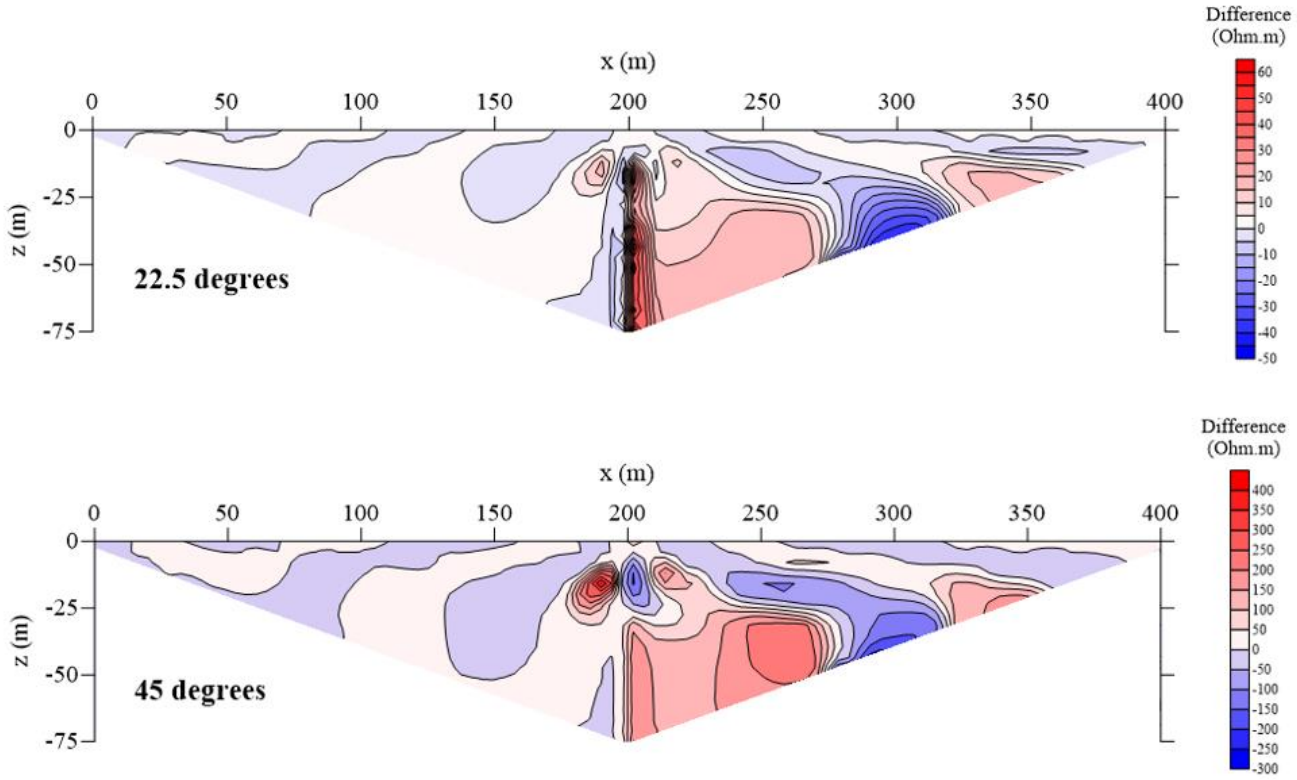


**Figure 4.9: Differences between the modelled resistivity values for the angled survey lines (22.5° and 45°) and the modelled resistivity values for a straight survey line for a vertical contact.**

The absolute error made by the inverse resistivity models in retrieving the resistivity values of the input model are shown in Figure 4.10. For the straight survey line, the largest errors occur in the vicinity of the vertical contact. The vertical zone of negative errors shows that the resistivities are underestimated in the unit of high resistivity (right-hand side). The resistivity of this unit is also underestimated in the shallow subsurface.

The inverse model of the 22.5° survey line both overestimates and underestimates the resistivities of the two geological units at different positions. Again, the largest errors occur in the high resistivity unit. These errors range from -50 Ωm to +50 Ωm. For the 45° line, a similar pattern of errors is seen as for the 22.5° line, but the errors are much larger, ranging of -420 Ωm to +260 Ωm.

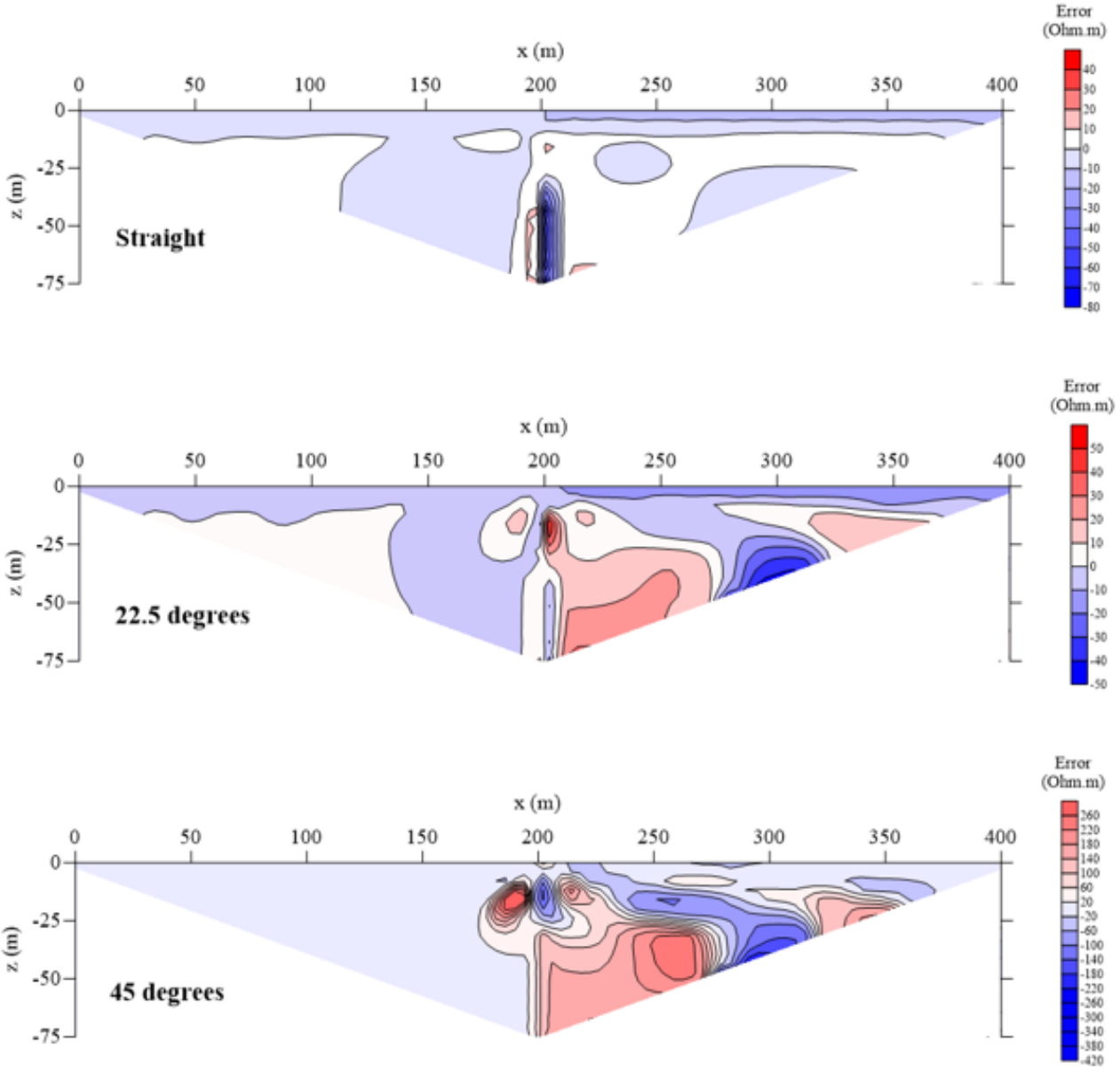


**Figure 4.10: Errors in the modelled resistivity values for the straight survey line (top), and angled survey lines (middle: 22.5º; bottom: 45º) for a vertical contact.**

## 4.6 MODELLING A THIN VERTICAL DYKE

### 4.6.1 Forward modelling

The input resistivity model for a thin vertical dyke is shown in Figure 4.11 (bottom). The dyke was assigned a width of 15 m, and was located at the centre of the survey line. The host rock was assumed

to have a resistivity value of 50 Ωm while the dolerite dyke intrusion was assigned a resistivity value of 500 Ωm.

The pseudo-section calculated for the input model is shown in the top graphic of Figure 4.11. It is clear that the presence of the dyke affects the apparent resistivities at positions laterally removed from the dyke.

### 4.6.2 Inverse modelling

Figure 4.12 shows the inverse resistivity models obtained from the pseudo-sections found for the straight and angled survey lines across the thin vertical dyke. The inverse resistivity model of the straight line manages to image the dyke well in the shallow subsurface, but fails to do so below depths of approximately 25 m. The modelled dyke thickens with depth and becomes less resistive. The inverse resistivity model of the 22.5° line is very similar to the model of the straight line, and also fails to map the dyke boundaries accurately in the deeper parts of the model.

The inverse resistivity model of the 45° line gives a much more distorted image of the dyke. The dyke only resembles a dyke-like structure in the shallow subsurface, and thickens with depth. Many artefacts are introduced to the model by the large angle in the survey line.

### 4.6.3 Modelling errors introduced by angled survey lines

The differences between modelled resistivity values for the angled survey lines and the resistivity values for the straight survey line are shown in Figure 4.13 (top: 22.5°; bottom: 45°). For the 22.5° line large differences (both negative and positive) occur near the centre of the model where the dyke is located. Large positive differences are also observed in the deepest part of the section. The differences range from -100 Ωm to +100 Ωm.

Larger differences (-200 Ωm to +1 000 Ωm) are observed for the 45° line. The highest positive difference also occurs at the centre of the survey line where dolerite dyke was positioned in the input model. The larger angle in the survey line also affects the modelled resistivities of the host rock more severely than for the 25° line.

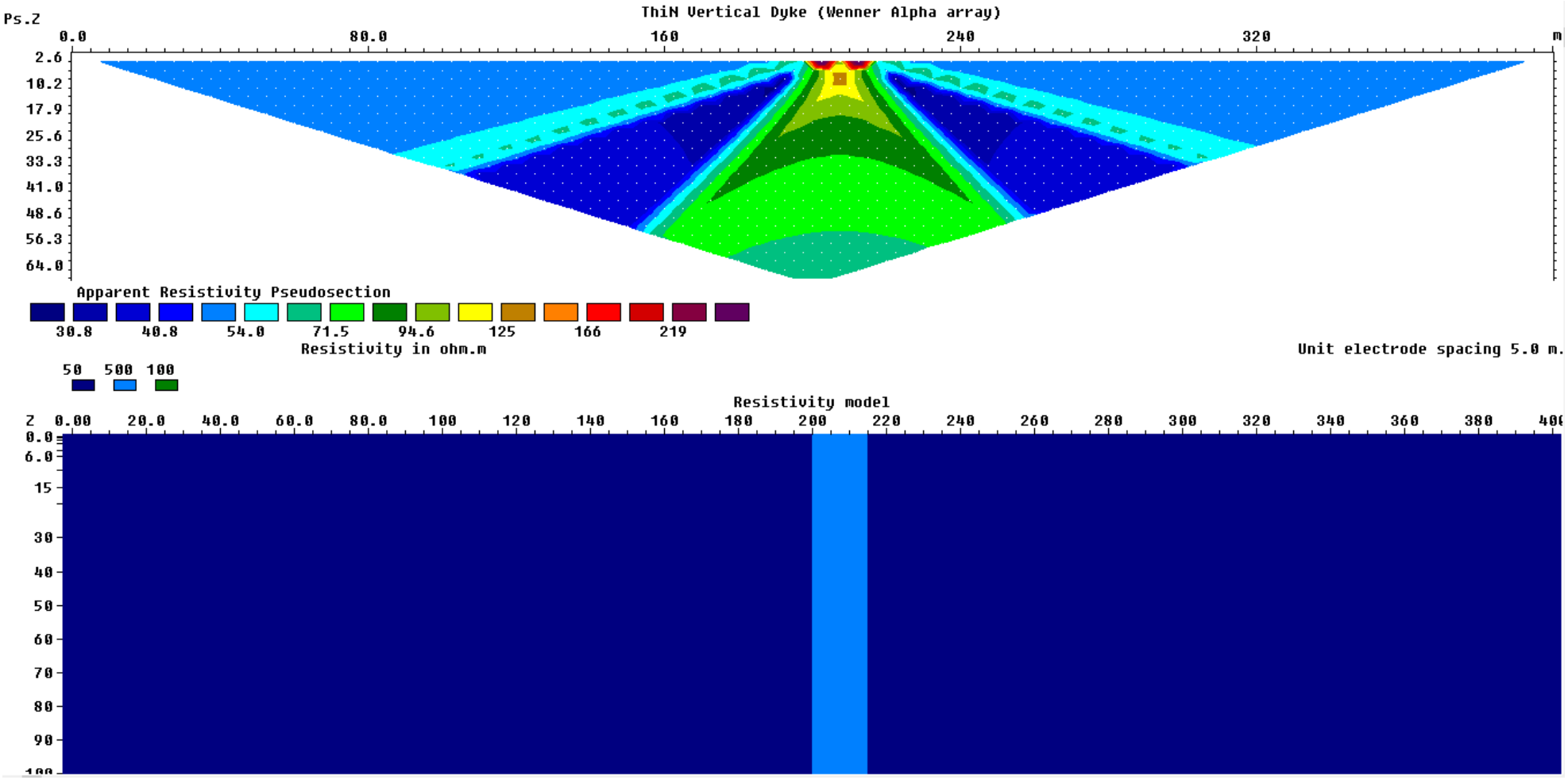


**Figure 4.11. Input model (bottom) and calculated pseudo-section (top) for the model representing a thin vertical dyke**

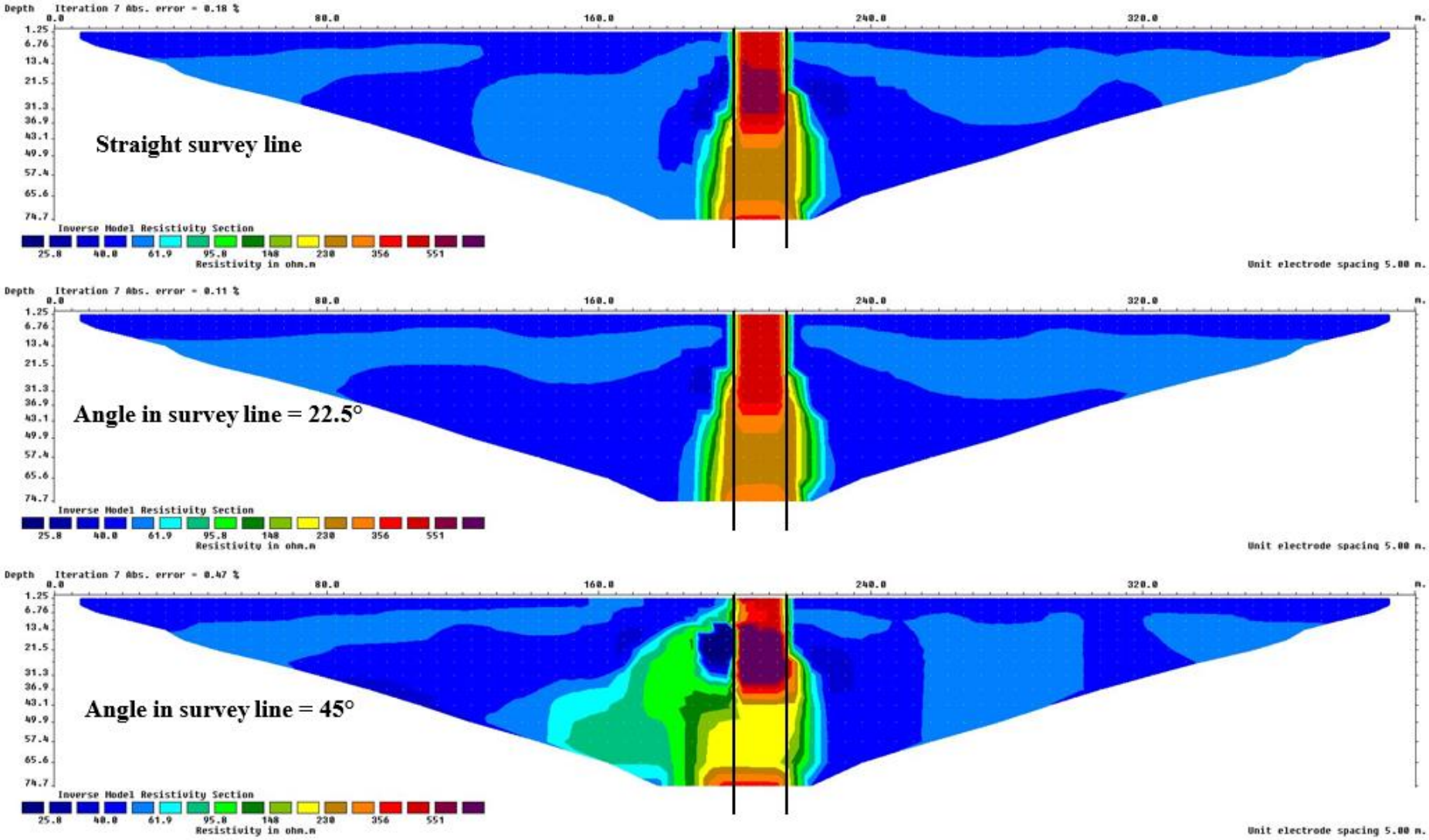


**Figure 4.12. Inverse models obtained for thin vertical dyke for a straight survey line (top), a survey line with a 22.5º angle (middle) and a survey line with a 45º angle (bottom). The input model contact of the dyke is shown as parallel vertical black lines**

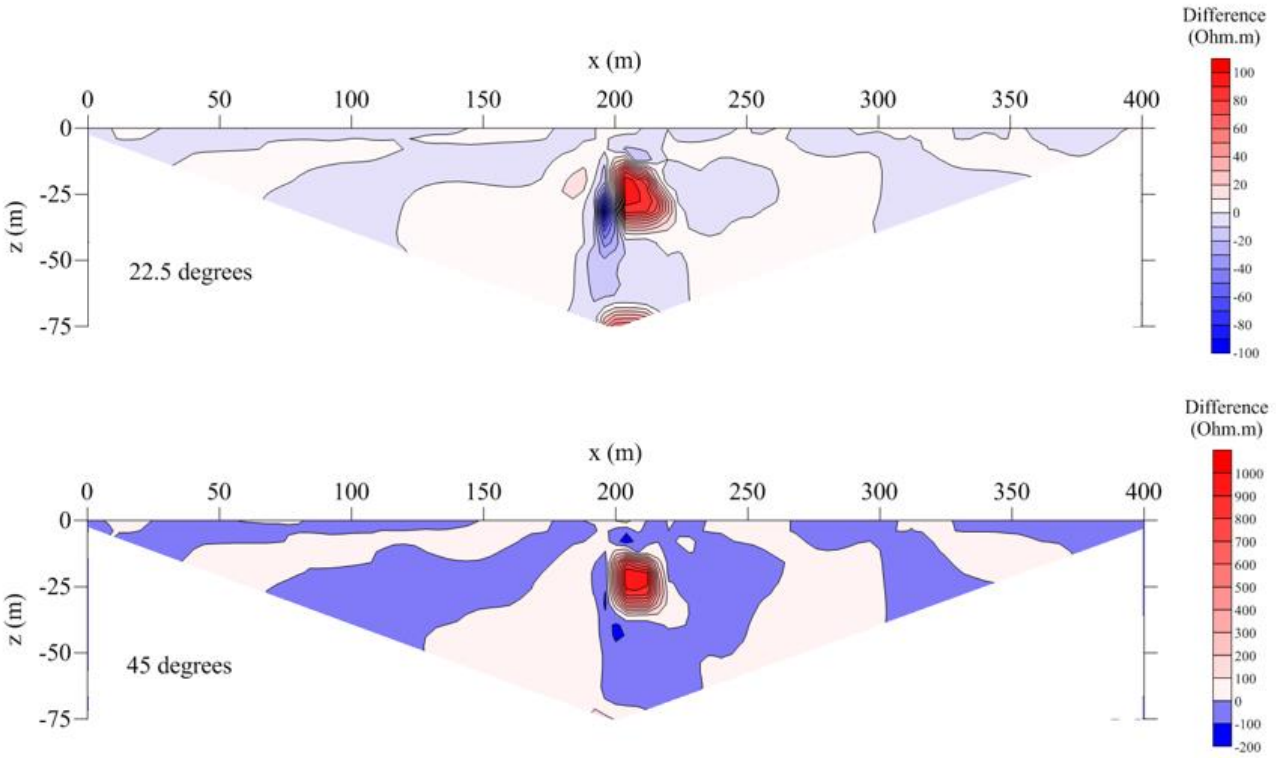


**Figure 4.13: Differences between the modelled resistivity values for the angled survey lines (22.5º and 45º) and the modelled resistivity values for a straight survey line for the thin vertical dyke.**

The resistivity errors for the straight and angled survey lines are shown in Figure 4.14. Below a depth of approximately 25 m, the inverse resistivity model of the straight line displays large errors at the position of the dyke. Both positive and negative errors occur within this zone. The inverse resistivity model of the 22.5º line has a very similar error pattern to that of the straight line, although the large errors at the position of the dyke extend to shallower depths. The errors range between -180 Ωm to +220 Ωm.

The inverse resistivity model of the 45º line has much larger errors, ranging from -300 Ωm to +1 000 Ωm. This high positive error corresponds to an error percentage of 200%. It is thus seen that the large angle in the survey line resulted in a huge overestimation of the dyke resistivity at a position approximately 25 m below surface.

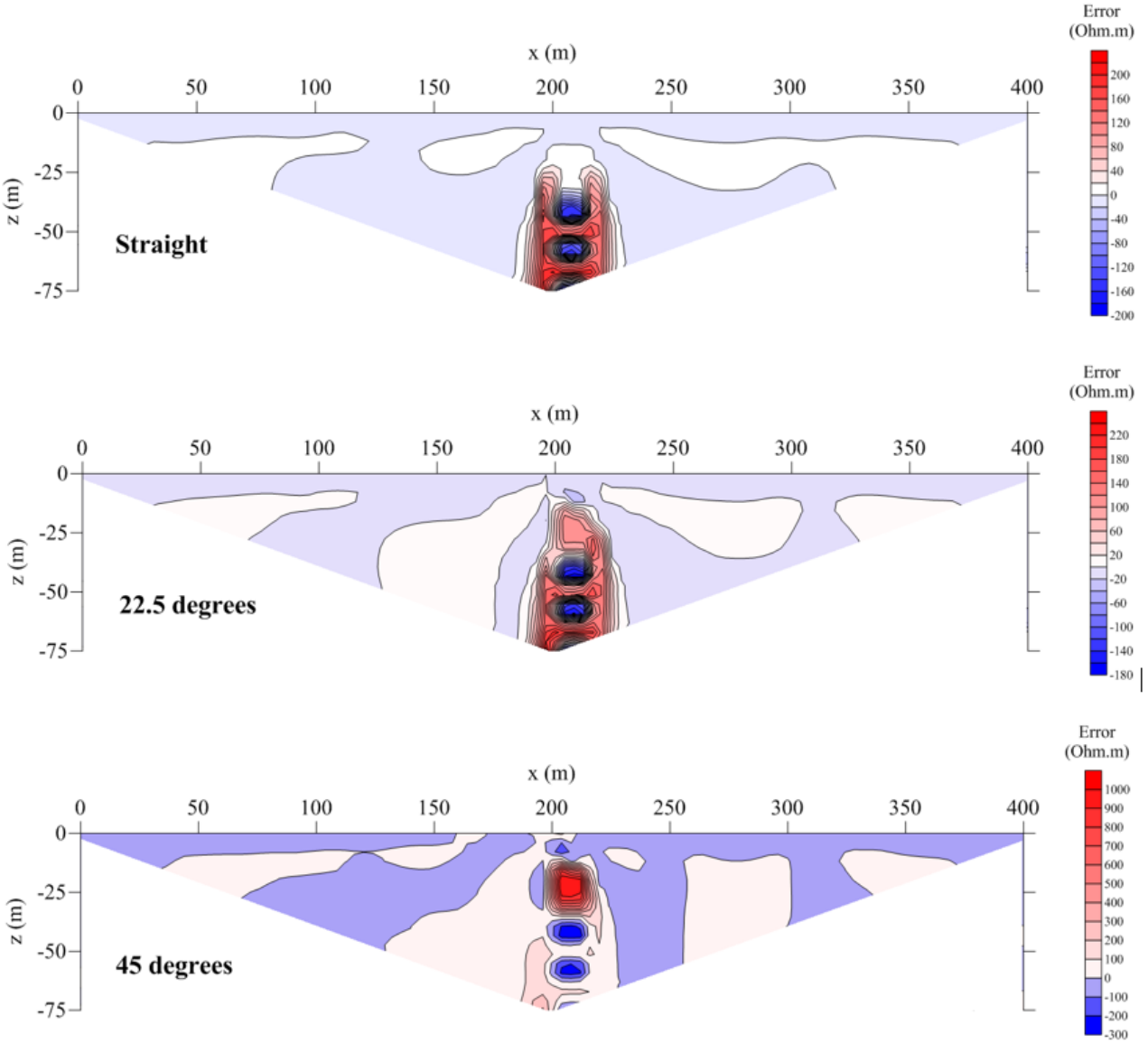


**Figure 4.14: Errors in the modelled resistivity values for the straight survey line (top), and angled survey lines (middle: 22.5º; bottom: 45º) for the thin vertical dyke.**

## 4.7 MODELLING A THIN INCLINED DYKE

### 4.7.1 Forward modelling

The resistivity model of a thin inclined dyke is shown in Figure 4.15 (bottom). This dyke has a thickness of 15 m, dipping to the right at an angle of 60°, and is positioned so that its top occurs at the centre of the line. The host rock was assigned a resistivity value of 50 Ωm, while dolerite dyke intrusion was assumed to have a resistivity value of 500 Ωm. Dolerite dykes can act as a barrier or pathway of groundwater depending on the degree of fracturing, and the orientation of the dyke. Holland (2012) also emphasised that the orientation of dolerite dykes have an influence on the occurrence of groundwater. It is therefore important to be able to determine the dip direction and dip angle from ERT surveys.

The pseudo-section calculated for the thin inclined dyke is shown in Figure 4.15 (top). The asymmetry in the pseudo-section is due to the dip of the dyke.

### 4.7.2 Inverse modelling

Figure 4.16 shows the inverse resistivity models obtained for the straight survey line (top), as well as for the angled survey lines (middle: 22.5°; bottom: 45°). It is clear that even the model for the straight survey line was not very successful in imaging the inclined dyke. Neither the top or bottom interfaces of the dyke is well defined. At larger depths, the dip of the dyke seems to decrease, while the resistivity of the dyke is also lower in the deeper parts of the model. Furthermore, the width of the dyke appears to increase with depth. Localised artefacts in the host rock are also observed.

The inverse model of the 22.5° line is very similar to the model of the straight line, but the variations in the host rock resistivity are more pronounced. The inverse model of the 45° line completely fails to recover the dyke at depth. The modelled resistivities of the host rock show large variations and artefacts are created which could lead to incorrect interpretations.

### 4.7.3 Modelling errors introduced by angled survey lines

The differences between the modelled resistivity values for the angled survey lines and the modelled resistivity values for the straight survey line are shown in Figure 4.17 (top: 22.5°; bottom: 45°). The differences for the 22.5° survey line show several localised zones of positive and negative differences. These zones generally occur in the vicinity of the inclined dyke, and the differences within these zones range between -90 Ωm and +80 Ωm.

The differences for the model of the 45° survey line display fewer zones of large differences, but with higher magnitude. The differences now range between -250 Ωm and +550 Ωm. The modelled resistivities of the host rock also show larger differences with the modelled resistivities found for the straight line.

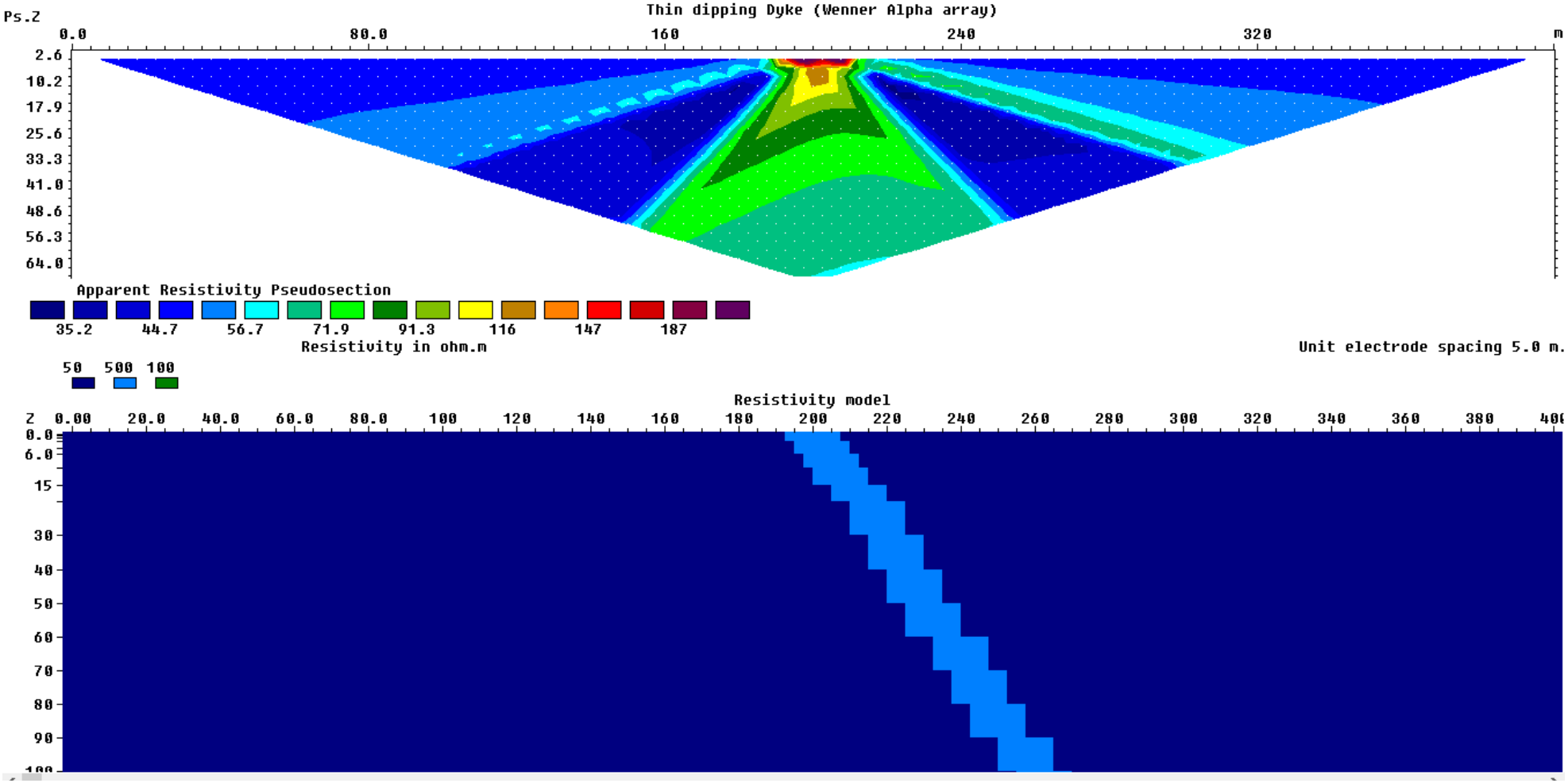


**Figure 4.15. Input model (bottom) and calculated pseudo-section (top) for the model representing a thin inclined dyke**

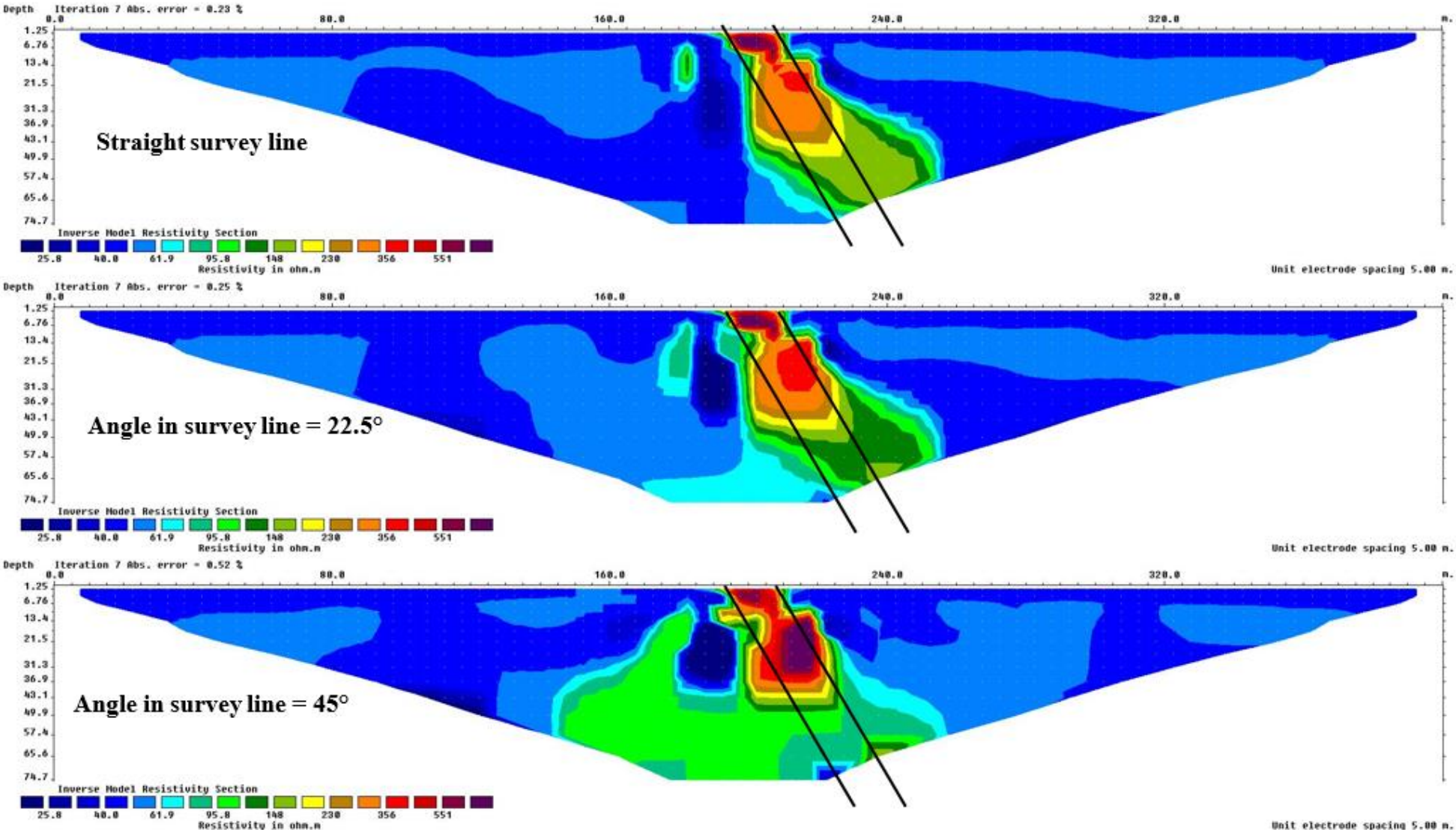


**Figure 4.16. Inverse models obtained for the thin inclined dyke for a straight survey line (top), a survey line with a 22.5º angle (middle) and a survey line with a 45º angle (bottom). The input model contact of the dyke is shown by parallel diagonal black lines**

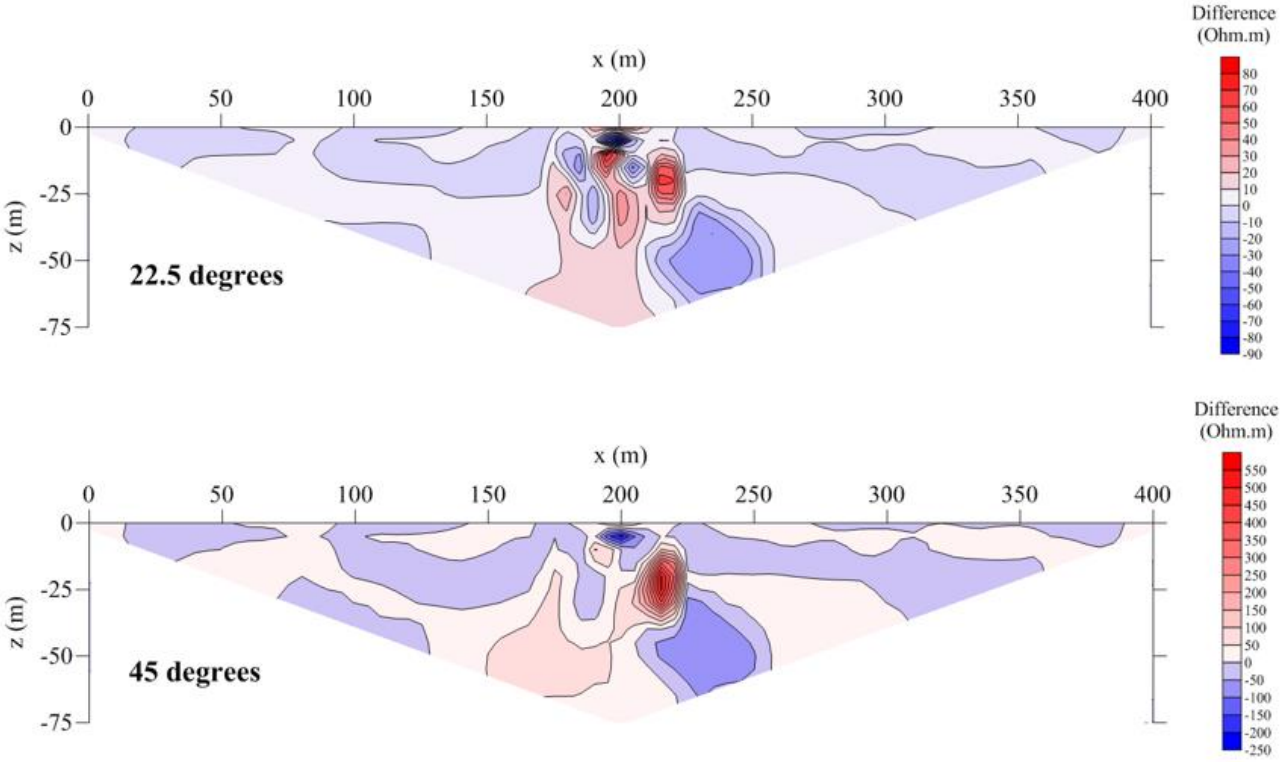


**Figure 4.17: Differences between the modelled resistivity values for the angled survey lines (22.5º and 45°) and the modelled resistivity values for a straight survey line for the thin inclined dyke.**

The errors for the modelled resistivity values for the straight survey line, and angled survey lines are shown in Figure 4.18. For the straight survey line, a zone negative errors occur at approximately the position of the inclined dyke. On both sides of this zone, zones of high positive errors are seen. The magnitude of the errors ranges between -350 Ωm to +300 Ωm. The error pattern for the 22.5° survey line strongly resembles that of the straight line, although the magnitude of the errors are larger, now varying between -400 Ωm and +350 Ωm.

For the 45° survey line, the error pattern again consists of a zone of large negative errors corresponding to the position of the dyke. However, a localised zone of positive errors now causes the zone of negative errors to be discontinuous at a depth of approximately 25 m. The magnitude of the errors ranges between -450 Ωm to +650 Ωm, showing that the large angle in the survey line had a strong detrimental effect on the accuracy of the model.

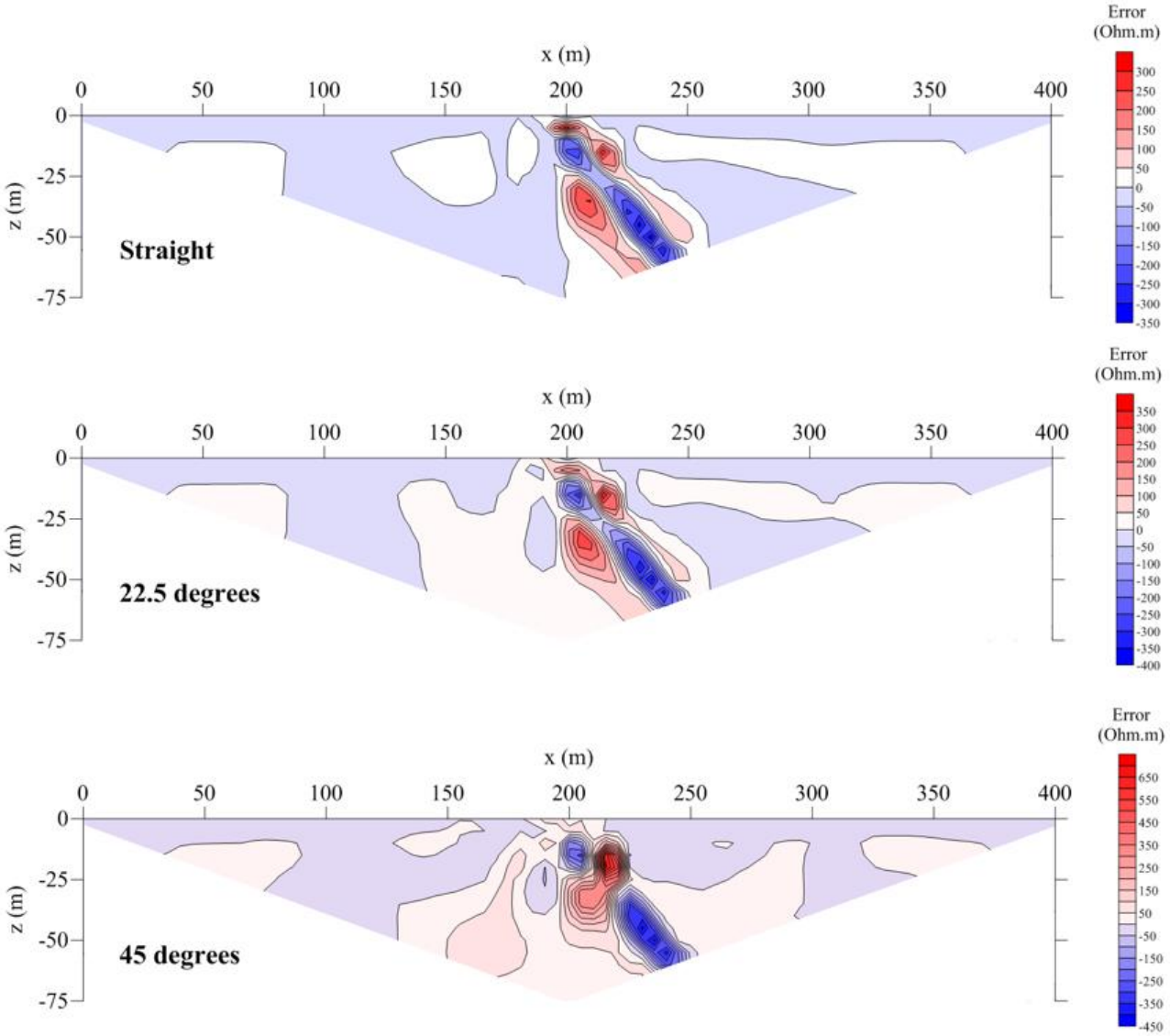


**Figure 4.18: Errors in the modelled resistivity values for the straight survey line (top), and angled survey lines (middle: 22.5º; bottom: 45º) for the thin inclined dyke.**

## 4.8 MODELLING A THICK VERTICAL DYKE

### 4.8.1 Forward modelling

The input resistivity model for the thick vertical dyke is shown in Figure 4.19 (bottom). The dyke was located at the centre of the line and was assigned a thickness of 37.5m. The host rock was assigned a resistivity value of 50 Ωm, while the dolerite dyke intrusion was given a resistivity value of 500 Ωm. The pseudo-section calculated for this model is shown in Figure 4.19 (top). The symmetry of the pseudo-section reflects the vertical orientation of the dyke.

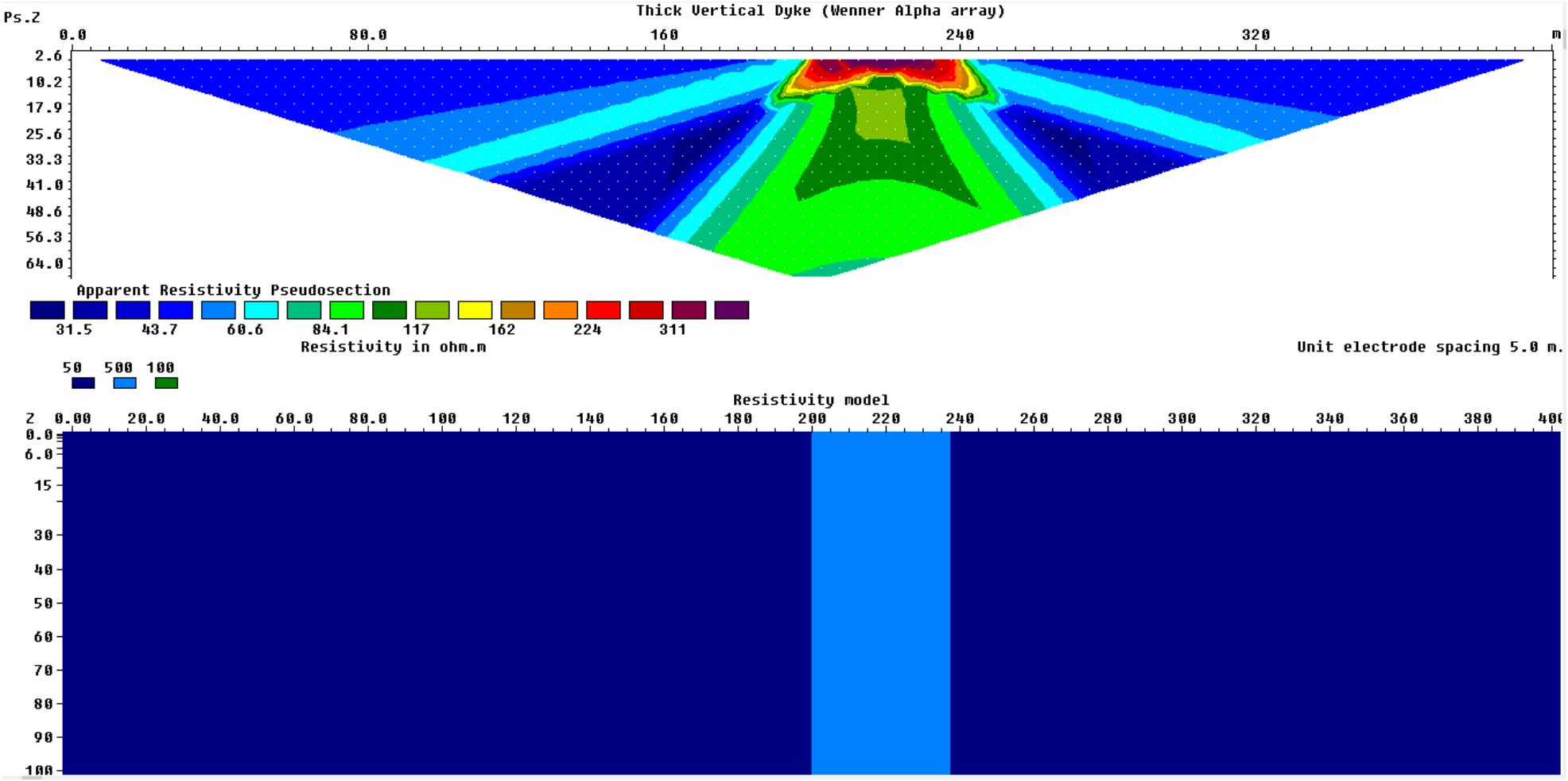


**Figure 4.19. Input model (bottom) and calculated pseudo-section (top) for the model representing a thick vertical dyke**

### 4.8.2 Inverse modelling

The inverse resistivity models for the straight and angled survey lines are shown in Figure 4.20 (top: straight; middle: 22.5°; bottom: 45°). The resistivity model for the straight line is fairly successful in retrieving the dyke, although the dyke boundaries become increasingly smeared with depth, particularly on the right-hand side of the dyke. Artefacts are also observed to the right of the dyke.

The resistivity model for the 22.5° line looks very similar to the model for the straight line, but the smearing of the dyke contacts with depth is more pronounced, and additional artefacts are introduced to the host rock to the left of the dyke. For the 45° survey line, the inverse resistivity model displays numerous artefacts on both sides of the dyke. At depth, the thickness of the modelled dyke is greater than the actual (input) thickness. The resistivity of the dyke material also varies significantly through the body.

### 4.8.3 Modelling errors introduced by angled survey lines

The differences between the modelled resistivity values for the angled and straight survey lines are shown in Figure 4.21 (top: 22.5°; bottom: 45°). The most significant difference between the models of the 22.5° line and the straight line occurs at the deepest parts of the models where a large positive difference (~300 Ωm) occurs within the boundaries of the dyke. A zone of negative differences is also observed immediately above this zone. The differences range between -40 Ωm and +300 Ωm.

For the model of the 45° survey line, the differences are significantly higher, ranging from -200 Ωm and 650 Ωm. The largest resistivity differences occur within the boundaries of the thick vertical dyke.

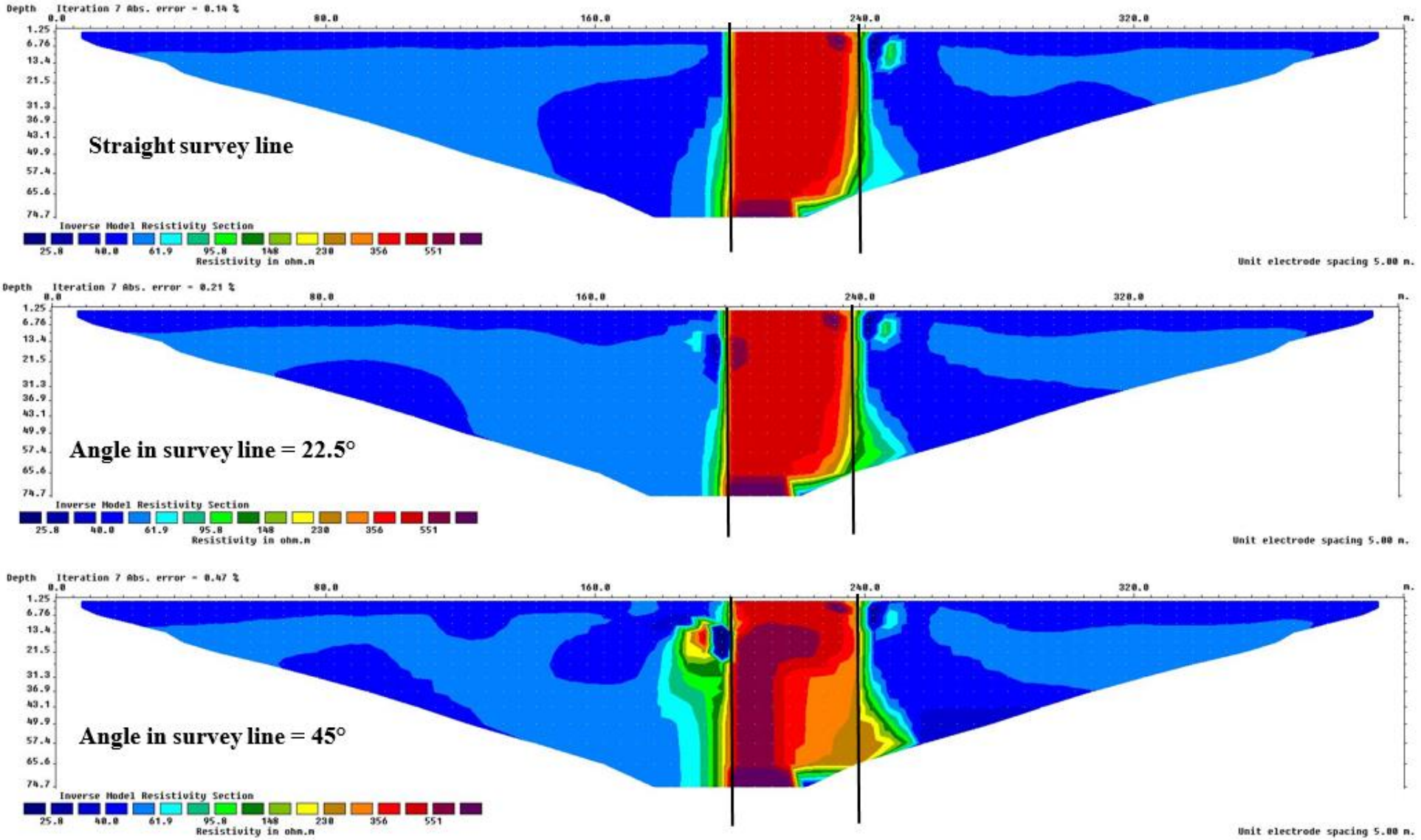


**Figure 4.20. Inverse models obtained for thick vertical dyke for a straight survey line (top), a survey line with a 22.5º angle (middle) and a survey line with a 45º angle (bottom). The input model contact of the dyke is shown as a parallel vertical black line**

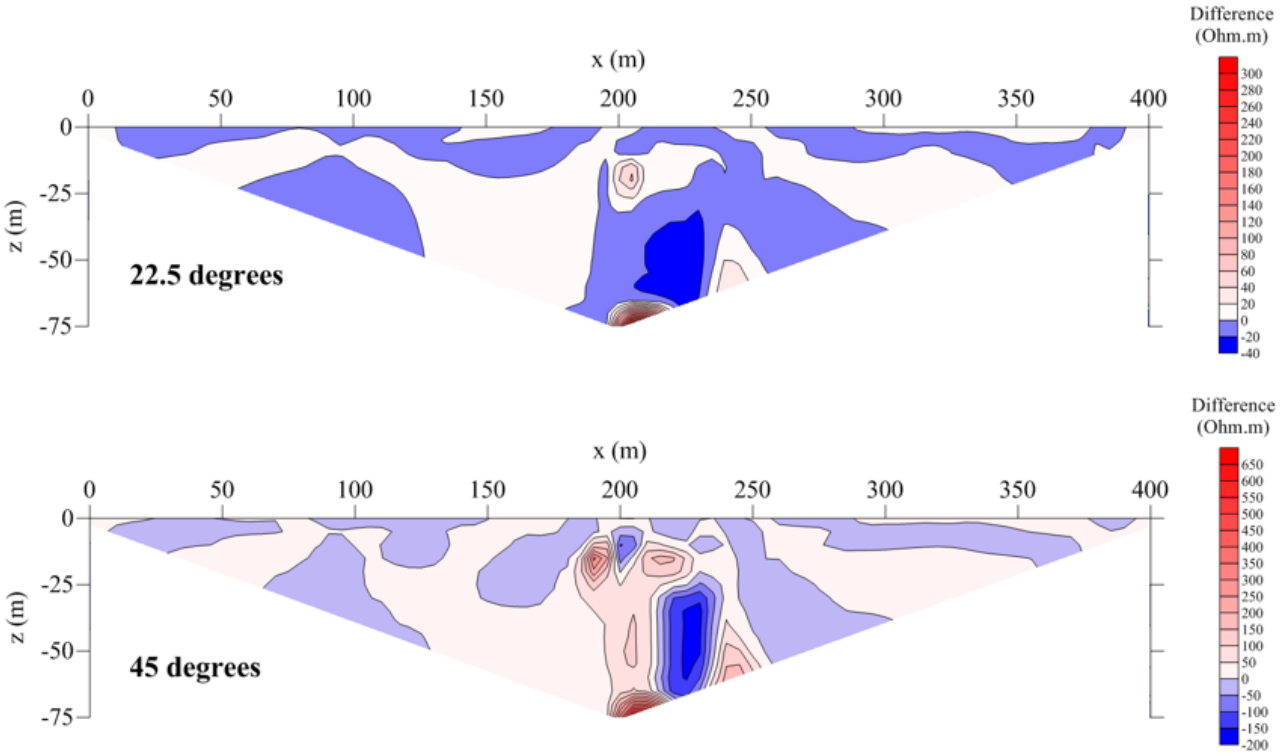


**Figure 4.21: Differences between the modelled resistivity values for the angled survey lines (22.5º and 45°) and the modelled resistivity values for a straight survey line for the thick vertical dyke.**

The errors of the resistivity models in retrieving the input model are shown in Figure 4.22 (top: straight; middle: 22.5º; bottom: 45º). The error patterns for the straight and 22.5º lines are very similar, with the largest errors occurring along the right-hand boundary of the thick dyke. This shows that this particular boundary was not recovered well during inverse modelling. The maximum positive errors occur at the deepest parts of the models within the boundaries of the thick dyke. For the straight line, the errors range from -450 Ωm to +250 Ωm, while for the 22.5º survey line these error range between -450 Ωm and +550 Ωm.

Introducing an angle of 45° to the survey line leads to much larger positive errors, with the errors now ranging from -500 Ωm to +900 Ωm. More localised zones of positive and negative errors are also seen. These errors are observed to be greatest within the boundaries of the thick vertical dyke.

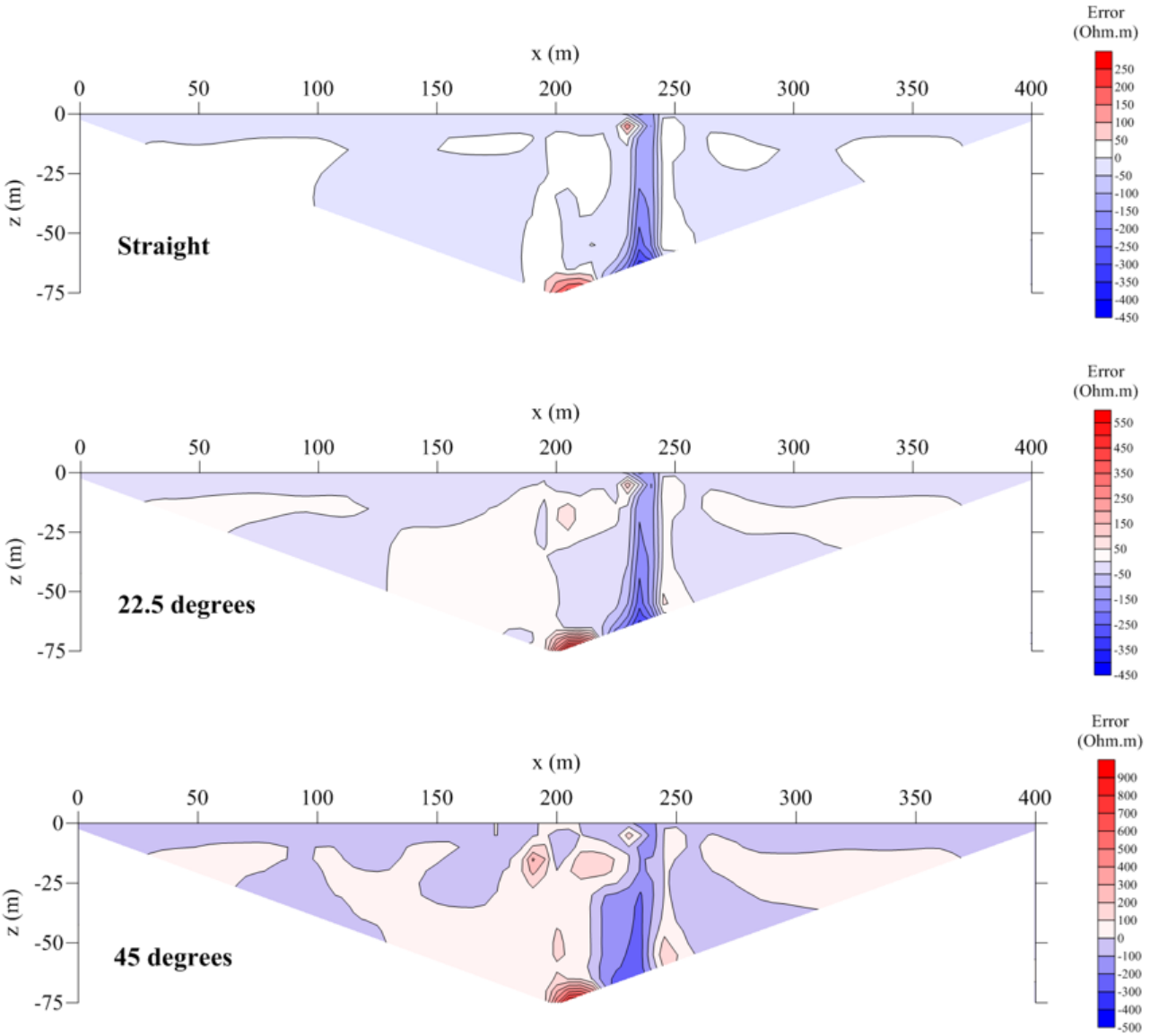


**Figure 4.22: Errors in the modelled resistivity values for the straight survey line (top), and angled survey lines (middle: 22.5º; bottom: 45º) for the thick vertical dyke.**

## 4.9 MODELLING A THICK INCLINED DYKE

### 4.9.1 Forward modelling

Figure 4.23 (bottom) shows the input resistivity model for a 35 m-thick inclined dyke, dipping to the right at an angle of 60°. The host rock was assigned a resistivity value of 50 Ωm, while dolerite dyke intrusion was assumed to have a resistivity value of 500 Ωm. The calculated pseudo-section corresponding to this input model is shown in Figure 4.23 (top). Although the asymmetric apparent resistivity pattern of the pseudo-section reflects the asymmetry of the input model, it is not possible to determine the dip of the dyke from the pseudo-section.

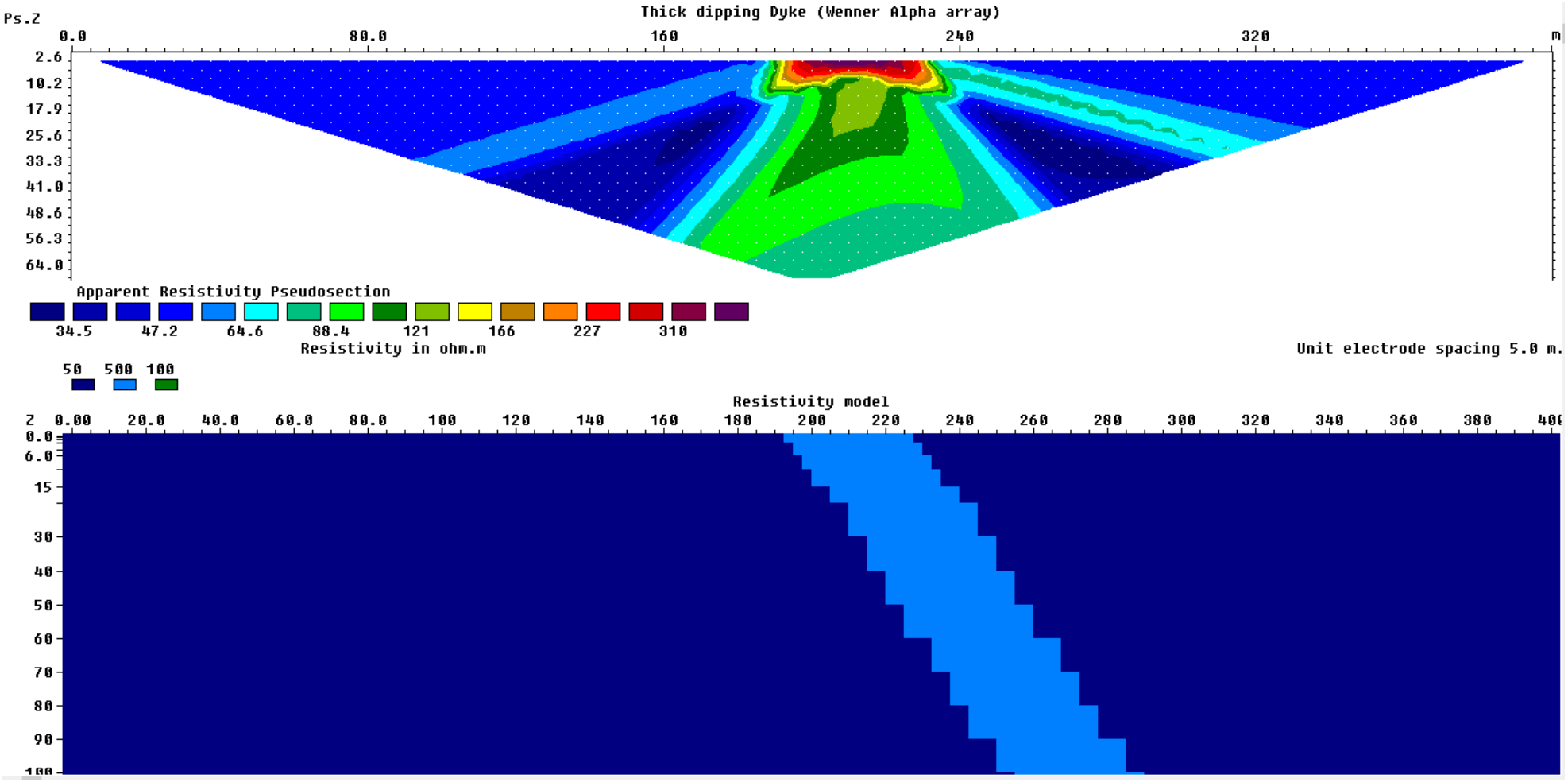


**Figure 4.23. Input model (bottom) and calculated pseudo-section (top) for the model representing a thick inclined dyke**

### 4.9.2 Inverse modelling

The inverse resistivity models for the straight and angled survey lines are displayed in Figure 4.24 (top: straight; middle: 22.5°; bottom: 45°). Although the model for the straight survey line does show the dyke in its correct position with the correct dip, both the up-dip and down-dip boundaries have an undulating character that differs from the input model. The thickness of the dyke is also overestimated in the deeper parts of the model. In addition, localised resistivity artefacts are observed.

The model of the 22.5° survey lines looks very similar to the model of the straight line, although the artefacts now affect the model more severely. There is also a greater variation in the modelled resistivity of the dyke. For the 45° survey line, the inverse model succeeds in retrieving the down-dip boundary of the dyke, but the up-dip boundary is severely distorted with the dyke even appearing to dip in the opposite direction in the deeper parts of the model. The dyke thickness is also greatly overestimated at depth. The artefacts introduced to the model by the larger angle in the survey line are also more prominent.

### 4.9.3 Modelling errors introduced by angled survey lines

The differences between the modelled resistivity values for angled survey lines (22.5° and 45°) and the resistivity value of a straight survey line are shown in Figure 4.25. For the 22.5° survey line, both localised negative and positive differences are observed within and in the vicinity of the inclined dyke. These differences range from -80 Ωm to +80 Ωm. The 45° survey line displays similar localised differences within and adjacent to the inclined dyke, but the differences are now much larger, ranging from -200 Ωm to +450 Ωm.

The contoured resistivity differences still show the dolerite dyke intrusion even though it is not clearly visible as it was in the input model. The difference is low for a 22.5° angled survey line with high resistivity values of difference appearing at the position of high resistivity dolerite dyke. For a 45° angle in a survey line, the difference is relatively high ranging from -200 Ωm to +450 Ωm.

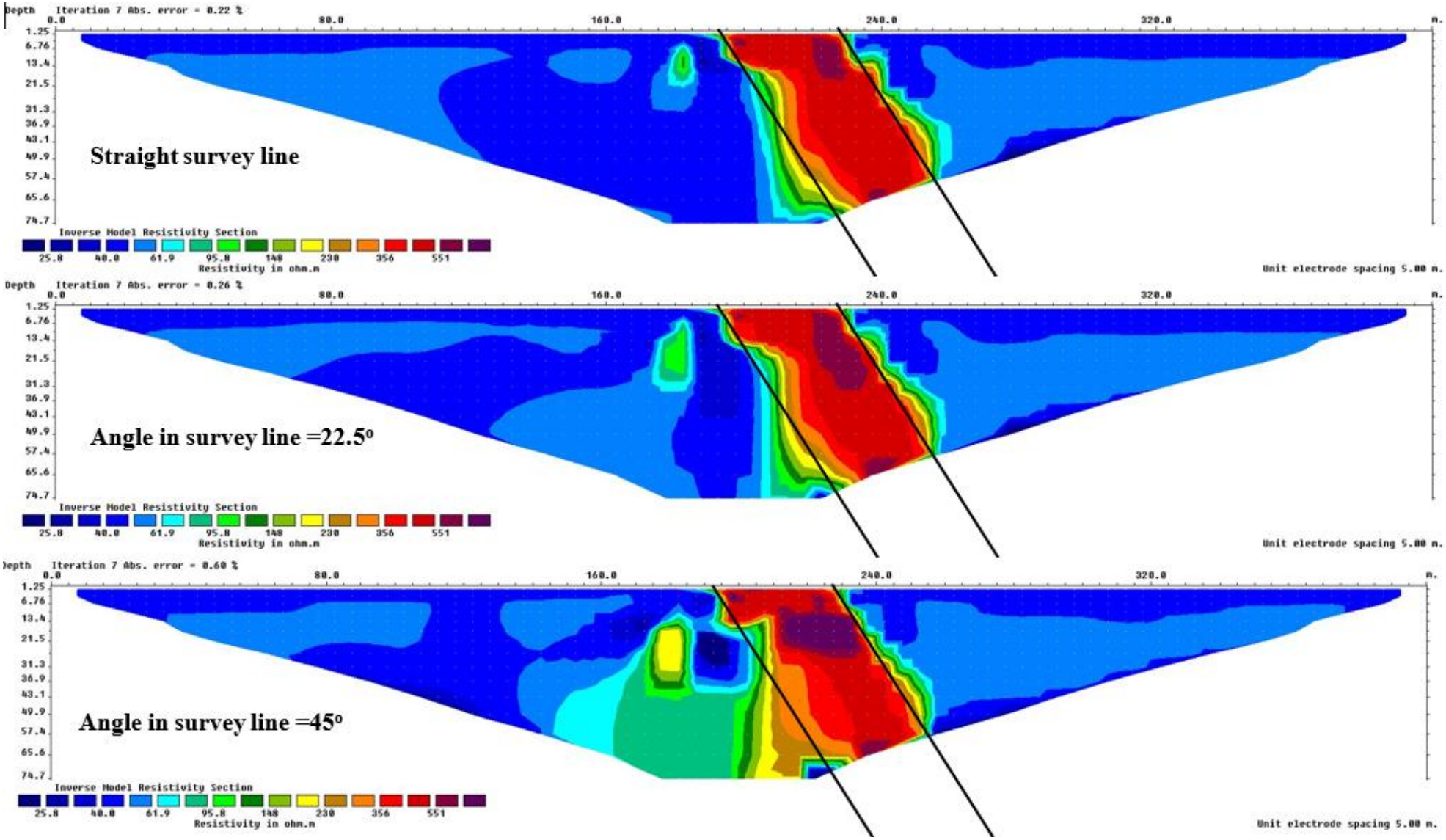


**Figure 4.24. Inverse models obtained for the thick inclined dyke for a straight survey line (top), a survey line with a 22.5º angle (middle) and a survey line with a 45º angle (bottom). The input model contact of the dyke is shown as parallel diagonal black lines**

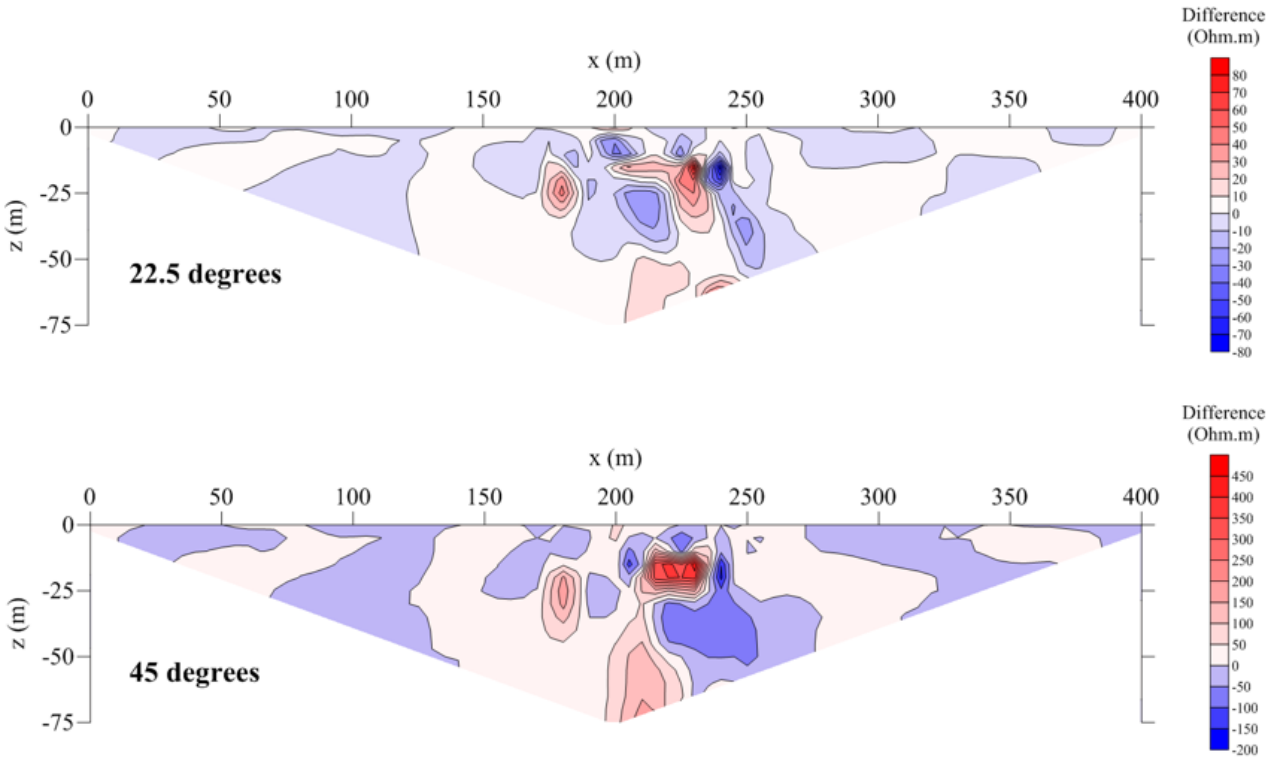


**Figure 4.25: Differences between the modelled resistivity values for the angled survey lines (22.5º and 45°) and the modelled resistivity values for a straight survey line for the thick inclined dyke.**

The errors in retrieving the input model are shown in Figure 4.26 for the modelled resistivity values for straight survey line (top), as well as the 22.5° and 45° survey lines (middle and bottom). For both the straight survey line and 22.5° line, localised errors with magnitudes ranging from -350 Ωm to +350 Ωm are seen within and adjacent to the position of the inclined dyke. The magnitude of these errors increases significantly for the 45° survey line, now ranging between -400 Ωm and +600 Ωm.

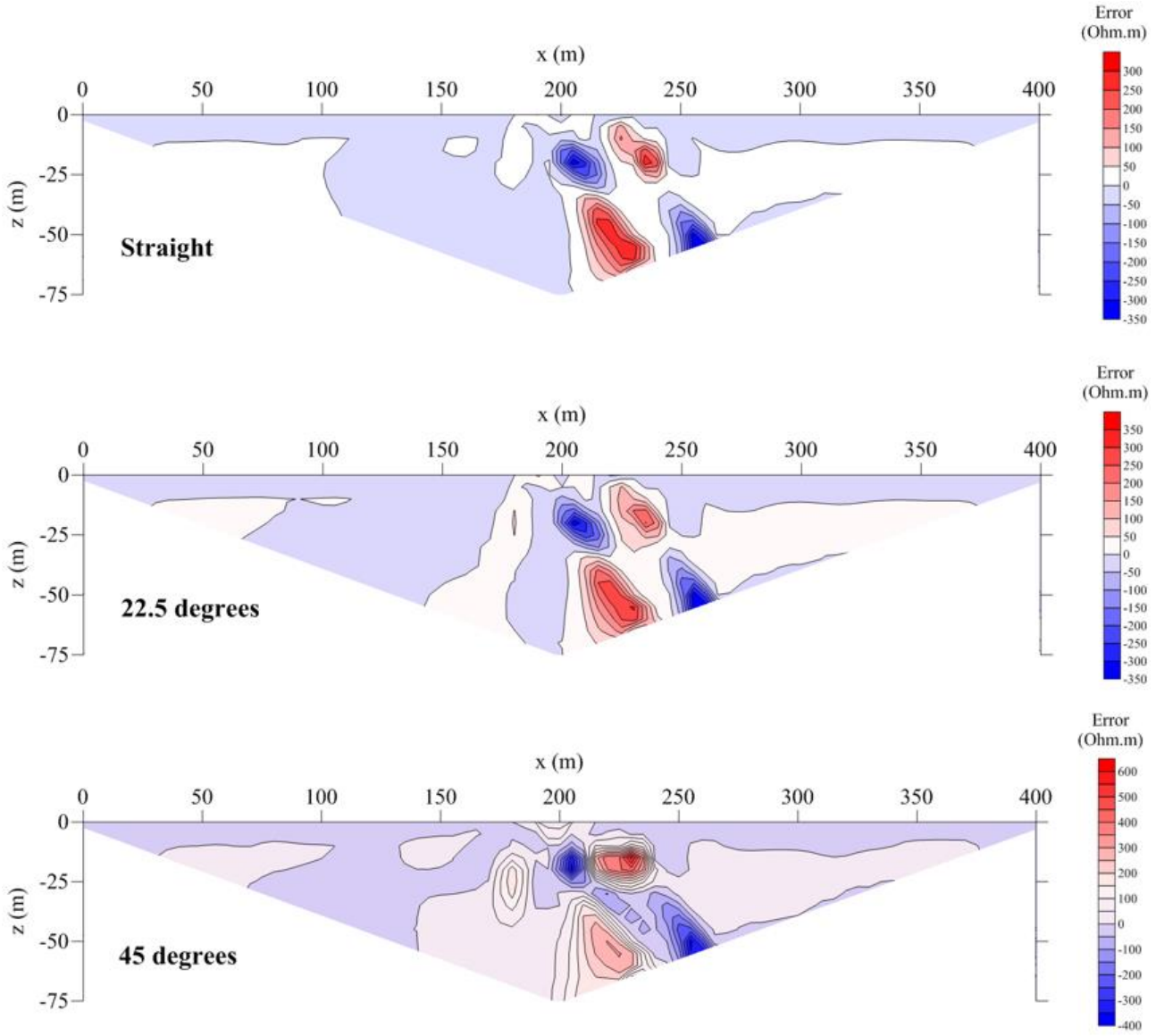


**Figure 4.26: Errors in the modelled resistivity values for the straight survey line (top), and angled survey lines (middle: 22.5º; bottom: 45º) for the thick inclined dyke.**

## 4.10 MODELLING A DOLERITE SILL

### 4.10.1 Forward modelling

The forward model of the dolerite sill is shown in Figure 4.27 (bottom). The sill was assumed to be outcropping, 30 m thick and extending to the centre of the model. The host rock was assumed to have a resistivity of 50 Ωm (Figure 4.27).

The pseudo-section calculated for the input model is shown in Figure 4.27 (top). Although the presence of the sill is clearly visible on the left-hand side of the pseudo-section, its thickness cannot be determined from the pseudo-section.

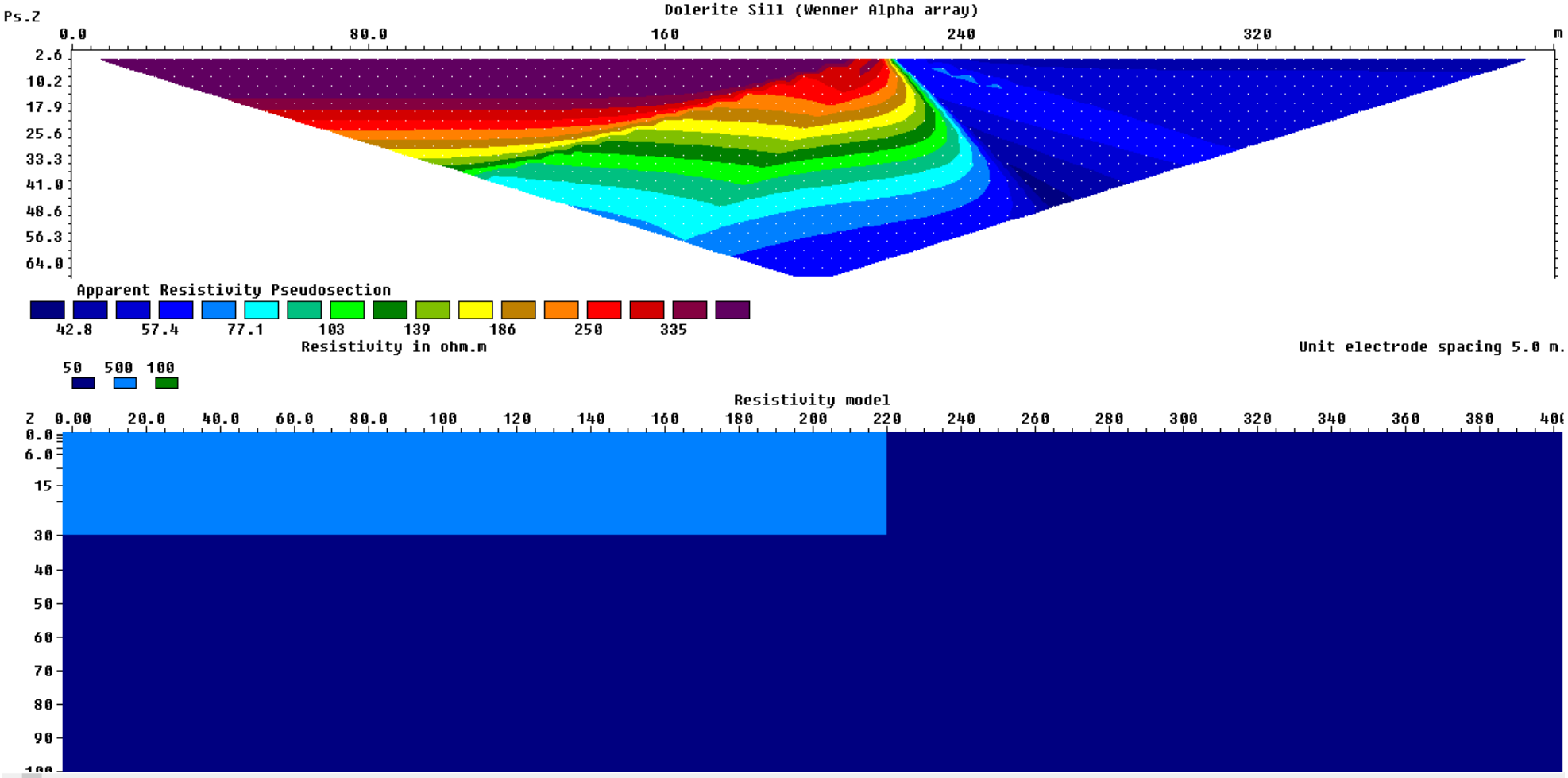


**Figure 4.27. Input model (bottom) and calculated pseudo-section (top) for the model representing a sill**

### 4.10.2 Inverse modelling

Figure 4.28 shows the inverse resistivity models for the dolerite sill for the straight survey line (top), and the 22.5° and 45° survey lines (middle and bottom). Comparison of the inverse models shows that the modelled resistivity section for straight survey line corresponds better with the input resistivity model than the models of the angled survey lines. The vertical contact between the high resistivity dolerite sill (500 Ωm) and the low resistivity host rock (50 Ωm) is well defined, but the bottom contact is not.

The inverse model for the 22.5° survey line is very similar to the model for the straight line, but the bottom contact between the sill and the host rock is even less sharp than for the straight line. The inverse resistivity model section for the 45° survey line completely distorts the shape of the sill. Particularly the bottom contact is poorly defined and has a wave-like appearance. The thickness of the sill is underestimated at some positions and overestimated at others. Localised zone of high resistivities (exceeding 500 Ωm) are also observed within the sill.

### 4.10.3 Modelling errors introduced by angled survey lines

The differences between the modelled resistivities for the angled survey lines and the resistivity values for a straight survey line are shown in Figure 4.29 (top: 22.5°; bottom: 45°). The differences between the resistivity values of the 22.5° line and the straight survey line are relatively low, ranging from -100 Ωm to +140 Ωm. The position of the dolerite sill in the contoured differences can only be identified by a few patches of high resistivity differences occurring near the edge of the model and near the centre of the survey line. For the 45° survey line, larger differences are observed, ranging from -220 Ωm to +330 Ωm. These differences are again located near the bottom contact and corner of the sill.

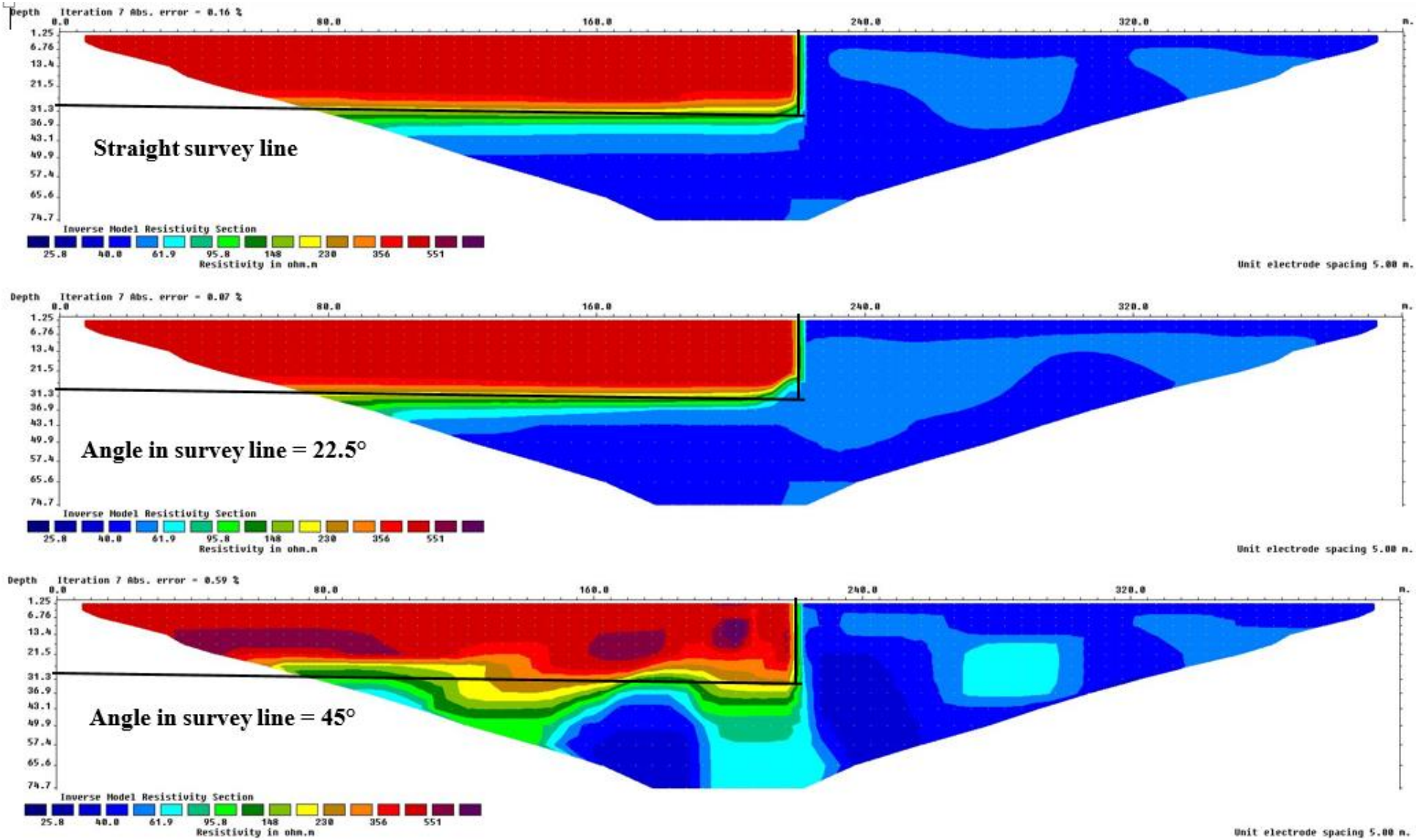


**Figure 4.28. Inverse models obtained for the dolerite sill for a straight survey line (top), a survey line with a 22.5º angle (middle) and a survey line with a 45º angle (bottom). The input model contact of dolerite sill is shown as black lines**

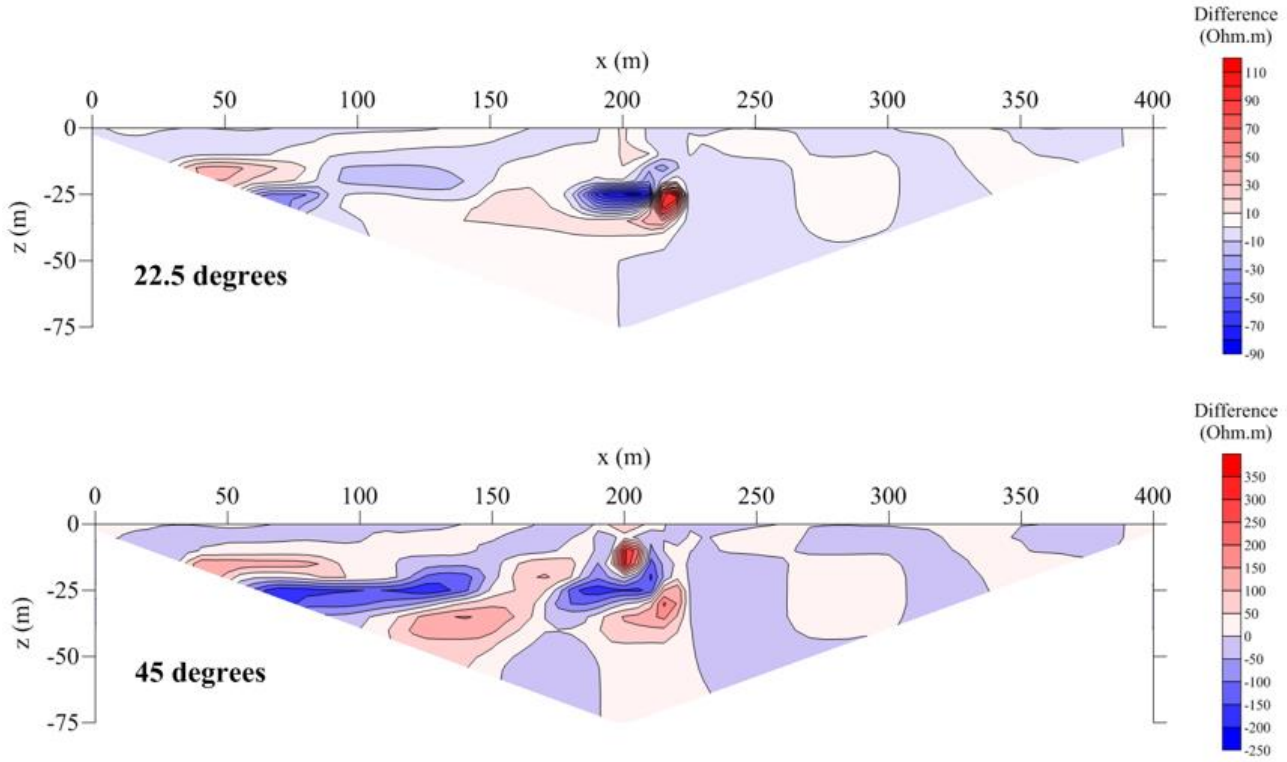


**Figure 4.29: Differences between the modelled resistivity values for the angled survey lines (22.5º and 45°) and the modelled resistivity values for a straight survey line for the dolerite sill.**

The errors in retrieving the input model are shown in Figure 4.30 for straight survey line (top), and the 22.5° (middle) and 45° (bottom) lines. For the straight survey line, the largest errors occur near the bottom contact and corner of the sill, and range between -200 Ωm and 160 Ωm. A similar pattern is observed for the 22.5°, although the errors are now lower, ranging between -140 Ωm and +140 Ωm.

For the 45° survey line, the errors are significantly higher, ranging from -300 Ωm to +350 Ωm. The highest errors again occur near the bottom contact and corner of the sill. Larger errors are also made in retrieving the resistivity of the host rock than for the straight and 22.5° lines.

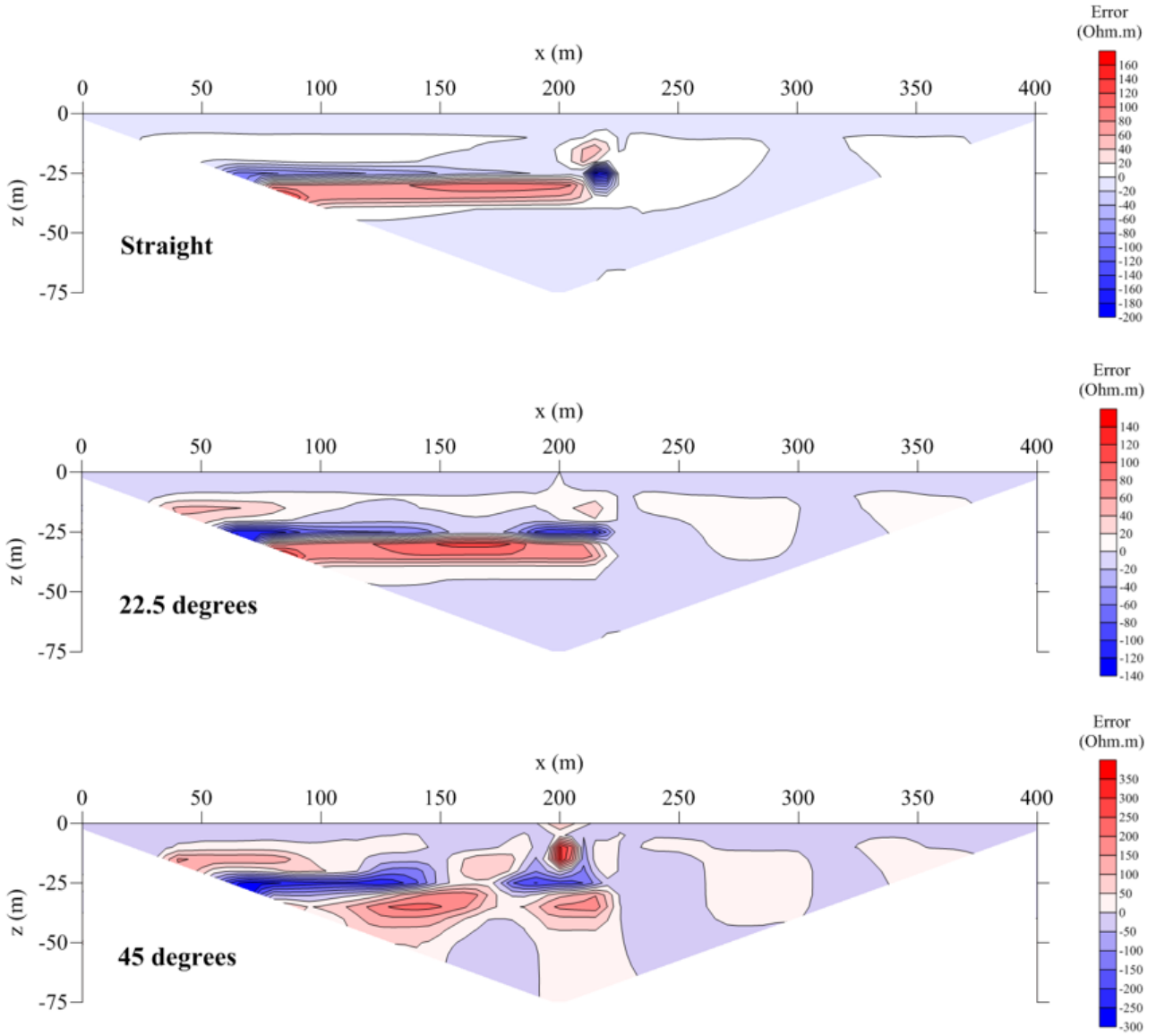


**Figure 4.30: Errors in the modelled resistivity values for the straight survey line (top), and angled survey lines (middle: 22.5º; bottom: 45º) for a dolerite sill.**

## 4.11 MODELLING A WEATHERED ZONE

### 4.11.1 Forward modelling

Figure 4.31 (bottom) shows the input resistivity model for a localised weathered zone. The model consists of a 10-m-thick horizontal layer of weathered material overlying a resistive host rock with a resistivity of +500 Ωm. A localised zone of deeper weathering (to a depth of 30 m) occurs near the centre of the model. This zone of deeper weathering has a lateral extent of 70 m.

The pseudo-section for the model of the weathered layer is shown in Figure 4.31 (top). The apparent resistivity contours are generally flat, but are distorted downwards in the vicinity of the zone of deeper weathering.

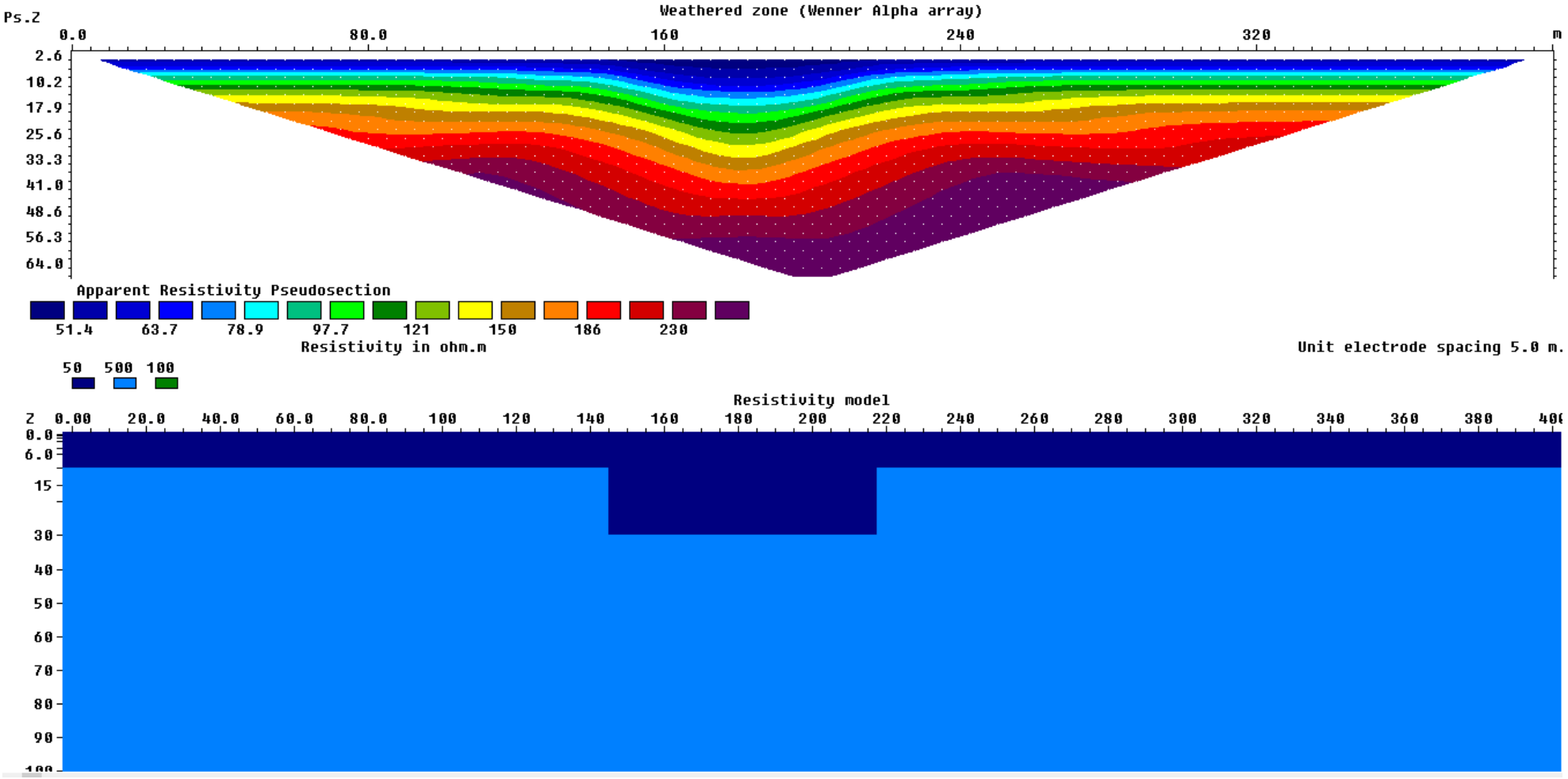


**Figure 4.31. Input model (bottom) and calculated pseudo-section (top) for the model representing a weathered zone**

### 4.11.2 Inverse modelling

Figure 4.32 shows the inverse resistivity models of the weathered zone for the straight survey line, 22.5° and 45° lines (top, middle and bottom, respectively). Comparison of the input resistivity model with the model of straight survey line that the inverse model was largely successful in retrieving the input model. However, the bottom contact of the zone of deeper weathering is not well defined.

The inverse model for the 22.5° line is much more distorted, with large resistivity variations observed within the unweathered material. Below the zone of deeper weathering, the resistivity of the unweathered material is underestimated. The bottom contact of the zone of deeper weathering is also more poorly defined than for the straight survey line.

The model for the 45° line shows a complete distortion compared to the input model. More artefacts are seen in the resistivity of the top layer and the rectangular shape of weathered material in the centre of the survey line is completely destroyed. The weathered zone appears to extend to the bottom of the unweathered material.

### 4.11.3 Modelling errors introduced by angled survey lines

The difference between the modelled resistivity values for the angled survey lines and the resistivity values for straight survey line are shown in Figure 4.33 (top: 22.5°; bottom: 45°). For the 22.5° survey line, the difference is most prominent at positions directly below the zone of deeper weathering. Here the resistivities of the angled survey line display a large zone of negative differences. The differences range between -120 Ωm to +160 Ωm.

Introducing an angle of 45° to the survey line leads much larger differences between the resistivities of the angled and straight lines. The differences now vary between -200 Ωm to +300 Ωm. The largest negative differences occur below the zone of deep weathering, while the largest positive differences occur near the sides of this zone.

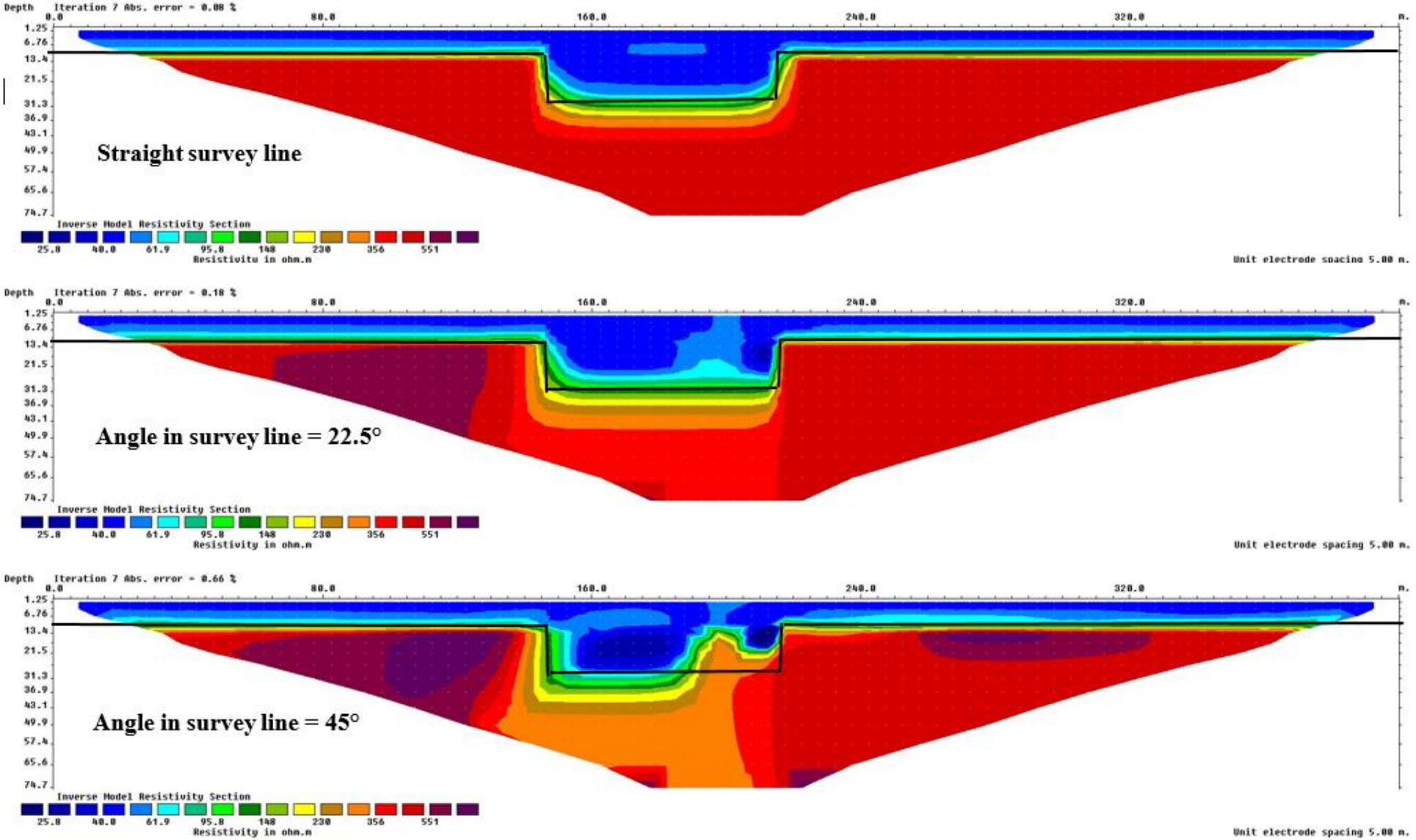


**Figure 4.32. Inverse models obtained for the weathered zone for a straight survey line (top), a survey line with a 22.5º angle (middle) and a survey line with a 45º angle (bottom). The input model weathered zone contact is shown as black lines**

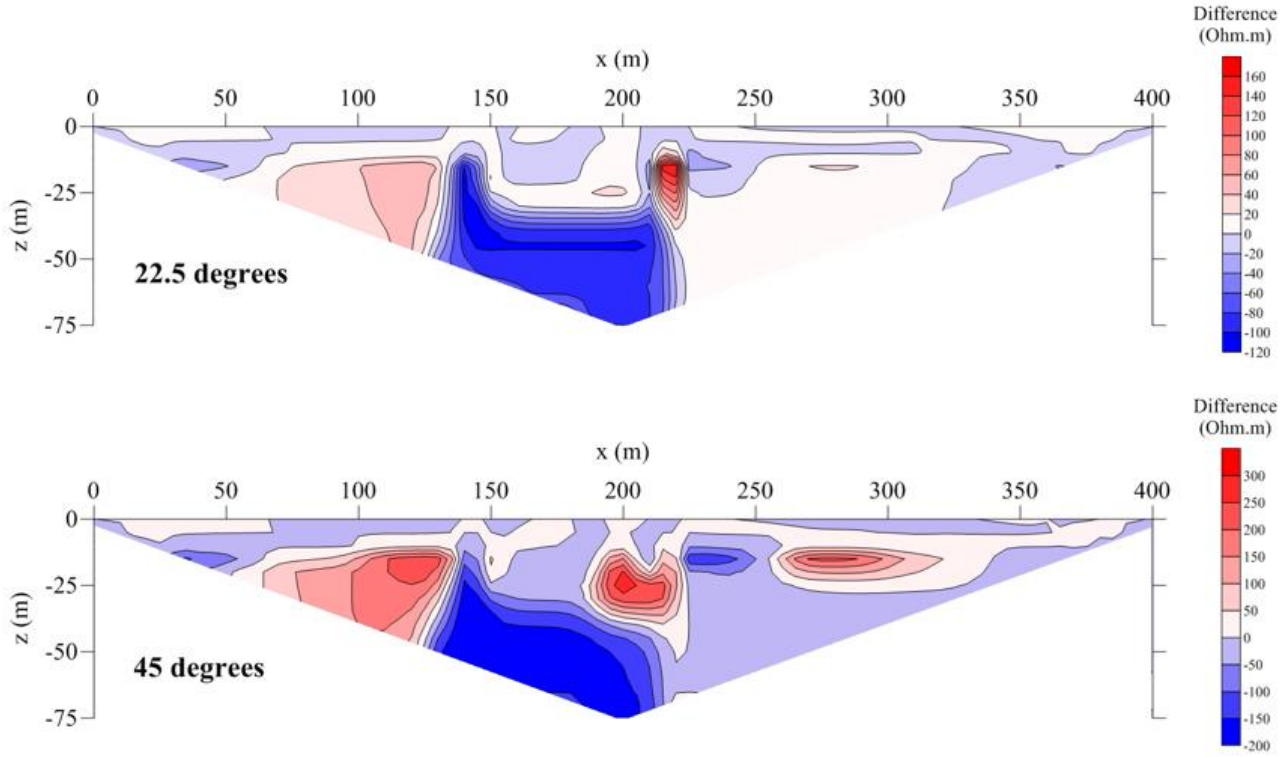


**Figure 4.33: Differences between the modelled resistivity values for the angled survey lines (22.5º and 45°) and the modelled resistivity values for a straight survey line for a weathered zone.**

The errors in retrieving the input model are shown in Figure 4.34 for the straight line, 22.5° and 45° lines (top, middle, and bottom). For the straight survey line, large negative errors occur in the vicinity of the bottom boundary of the zone of deeper weathering, while zones of positive errors are seen to occur in the unweathered material. The errors range between -280 Ωm to +80 Ωm.

For the model of the 22.5° line, the zone of negative errors extends to greater depths below the zone of deeper weathering, and larger positive errors are observed in the unweathered material to the left of the zone of deeper weathering. The errors now vary between -340 Ωm to +60 Ωm.

For the 45° line, the errors increase further to range between -400 Ωm to +300 Ωm. Localised zones of both positive and negative errors are now seen in the unweathered material.

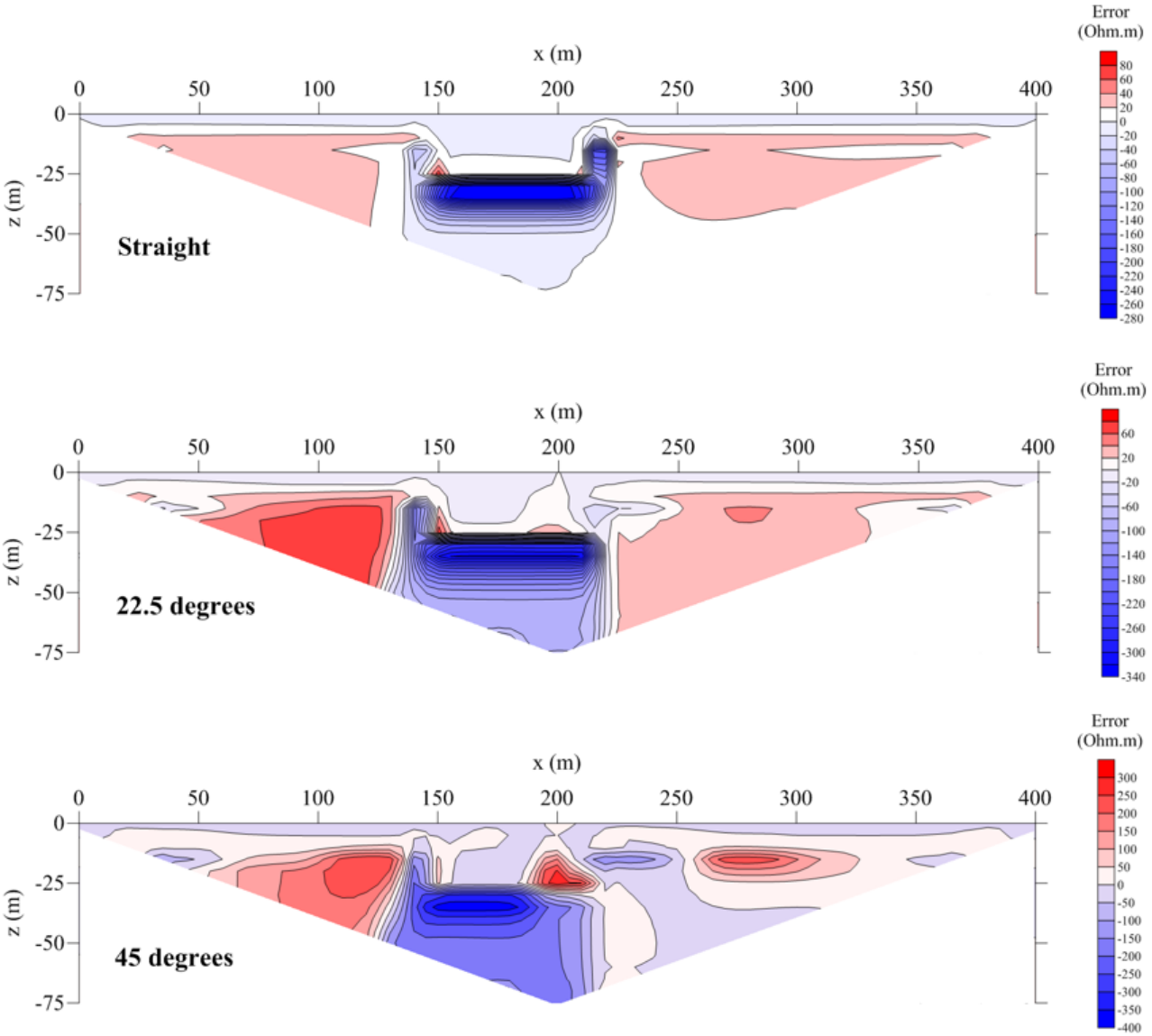


**Figure 4.34: Errors in the modelled resistivity values for the straight survey line (top), and angled survey lines (middle: 22.5º; bottom: 45º) for a weathered zone.**

## 4.12 DISCUSSION

In this chapter, the influence of angled survey lines on the inverse resistivity models was studied by creating eight different models representing structures typically targeted during groundwater exploration programmes in Karoo rocks. Both small (22.5º) and large (45º) angles were considered for the survey lines.

The modelling results showed that the errors introduced to the apparent resistivities when conducting 2D ERT surveys along angled lines may lead to distorted inverse resistivity models. The distortion was particularly severe for the line with the larger angle and it can generally be expected that larger angles will lead to more distortion of the models. In most models the distortion was most severe at

the contacts between the different subsurface materials. The thicknesses of the geological units and the dips of inclined units could thus not be accurately determined from these distorted models.

Since the contacts between different rock units are often the targets during groundwater exploration, the above observation has particular significance since boreholes sited on distorted models may not be positioned optimally to intersect the targeted contacts. It is therefore imperative that apparent resistivity data be corrected to compensate for the errors introduced by angles in the survey line before the data are inverted to obtain resistivity models of the subsurface.

In Chapter 5 the results of real ERT survey along straight and angled survey lines will be presented. It will also be shown how the apparent resistivity data recorded along angled survey lines can be corrected to a degree to improve the accuracy of the inverted resistivity models.

# CHAPTER 5:
# ERT SURVEYS ALONG ANGLED SURVEY LINES – FIELD INVESTIGATIONS

## 5.1 INTRODUCTION

In Chapter 4 models representing the geological conditions that could be encountered in Karoo rocks were studied. These models were idealised representations of the real geological conditions that could potentially be encountered in the field. It is important to augment the numerical modelling with real data obtained from field surveys to allow comparison with the numerical modelling results. This may validate the numerical modelling results or reveal the shortcomings of the numerical models in studying the influence of angled survey lines.

This chapter presents the results of ERT field surveys conducted in three different sites, namely: 1) the Bloemfontein campus of the University of the Free State, 2) a site near the Coca-Cola factory south-west of the Bloemfontein CBD, and the Heelvroeg farm to the north-west of Bloemfontein. These sites were selected because different geological conditions are known to occur at each site.

## 5.2 METHOD OF INVESTIGATION

The Lund Imaging System was used for all the field surveys. This system consists of (Figure 5.1):

- A Terrameter, which records the voltages and currents during each measurement and calculates the corresponding apparent resistivity,
- An Electrode Selector, which switches between the different electrodes used during the survey,
- Four multi-core cables, each with 21 electrode connections, with unit electrode spacings of 5 m, laid out head-to-tail along the survey line,
- Eighty-one steel electrodes inserted at 5 m intervals along the survey lines.

The total line lengths were 400 m (80 × 5 m). The Wenner (α) electrode geometry was used to record apparent resistivity data on all the survey lines. Two protocols were used to take the measurements, namely: the Wenner_L and Wenner_S protocols. The Wenner_L protocol records deeper data at lower resolution using electrodes on all four cables. However, only every second electrode is active during the measurements. The Wenner_S protocol records data at shallow depth with higher resolution using electrodes on the central two cables, and all the electrodes are active during the measurements.

At each site, three surveys were conducted: one along a straight line, and two surveys along angled lines with angles of 22.5º and 45º at the centres of the lines.

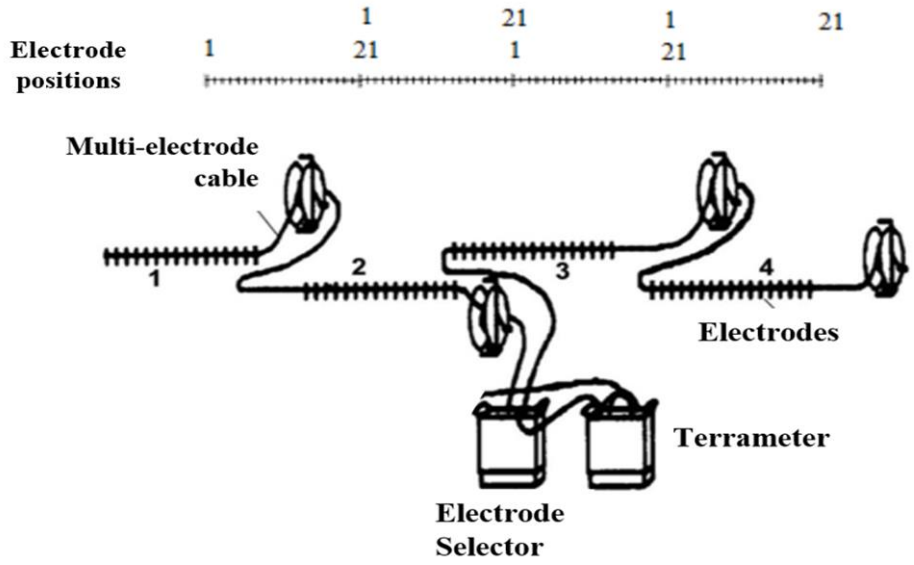


**Figure 5.1: Schematic illustration of Lund Imaging System (Loke, 2004)**

## 5.3 REGIONAL SETTING

The study areas are located in the central part of South Africa on the southern edge of the Highveld bordering on the semi-arid region of the Karoo. Many areas in this region comprise of flat with occasional hills covered by Highveld grassland vegetation. The study areas were chosen at a distance of less than 50 km from the Bloemfontein central business district (CBD) in the Free State province. The map of the regional setting of the three sites at which field surveys were conducted is shown in Figure 5.2.

The University of the Free State (Bloemfontein) campus site is situated on the western side of the UFS campus, and is characterised by a flat area covered by grass with few scattered saplings. The Heelvroeg farm is located approximately 26 km north-west of the Bloemfontein CBD, and can be reached along the R64 leading to the Krugersdrift Dam. The farm is located in a flat-lying area covered by dry grass. The site near the Coca-Cola factory occurs south-east of the Bloemfontein CBD, at a distance of approximately 7 km.

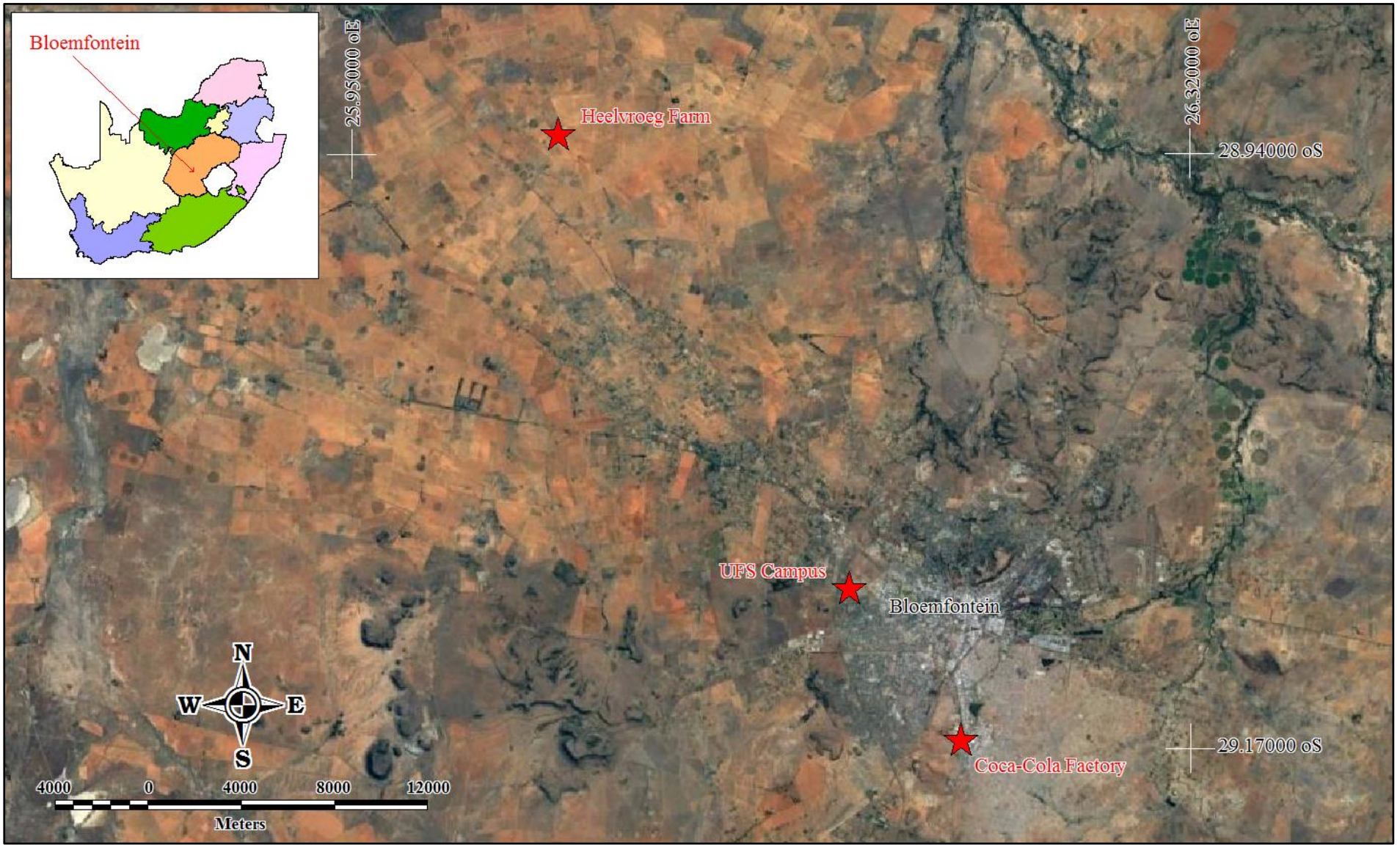


**Figure 5.2. Regional setting of the three sites at which field surveys were conducted**

## 5.4 GEOLOGICAL SETTING

The regional geological setting of the three test sites is shown in Figure 5.3. All three sites are underlain by rocks of the Karoo Supergroup, although recent quaternary deposits in the form of dune sand and calcrete cover large parts of the study area. There is some disagreement in the 1:250 000 geological maps shown in Figure 5.3; the older map covering the south-eastern part of the study area does not connect well with the newer maps to the north and west (all maps were obtained from the Council for Geoscience). The older map includes two of the three test sites, namely the Coca-Cola factory and the UFS campus.

Although the older geological map indicates that the Karoo rocks that occur at surface consist of sandstones, shales and mudstones belonging to the Ecca Group (Lower and Upper Stages), it is known that the Bloemfontein area is generally underlain by the rocks of the Beaufort Group according to the newer nomenclature. Botha *et al*. (1998) indicated that campus test site, located on the north-western corner of the UFS campus, is underlain by sedimentary rocks of the Adelaide Subgroup. These sedimentary rocks consist of fine-grained grey sandstone and coarse arkoses, alternating with green and maroon-coloured mudstone beds. The Coca-Cola factory is similarly located on rocks of the Beaufort Group.

The Heelvroeg farm is located north-west of the Bloemfontein CBD. It occurs in area covered by quaternary deposit consisting of red and grey aeolian dune sand, overlying the Beaufort Group.

Dolerite intrusions in the form of sills, linear dykes and ring-dykes are ubiquitous, although these intrusions are often covered by dune sand in the western parts of the study area.

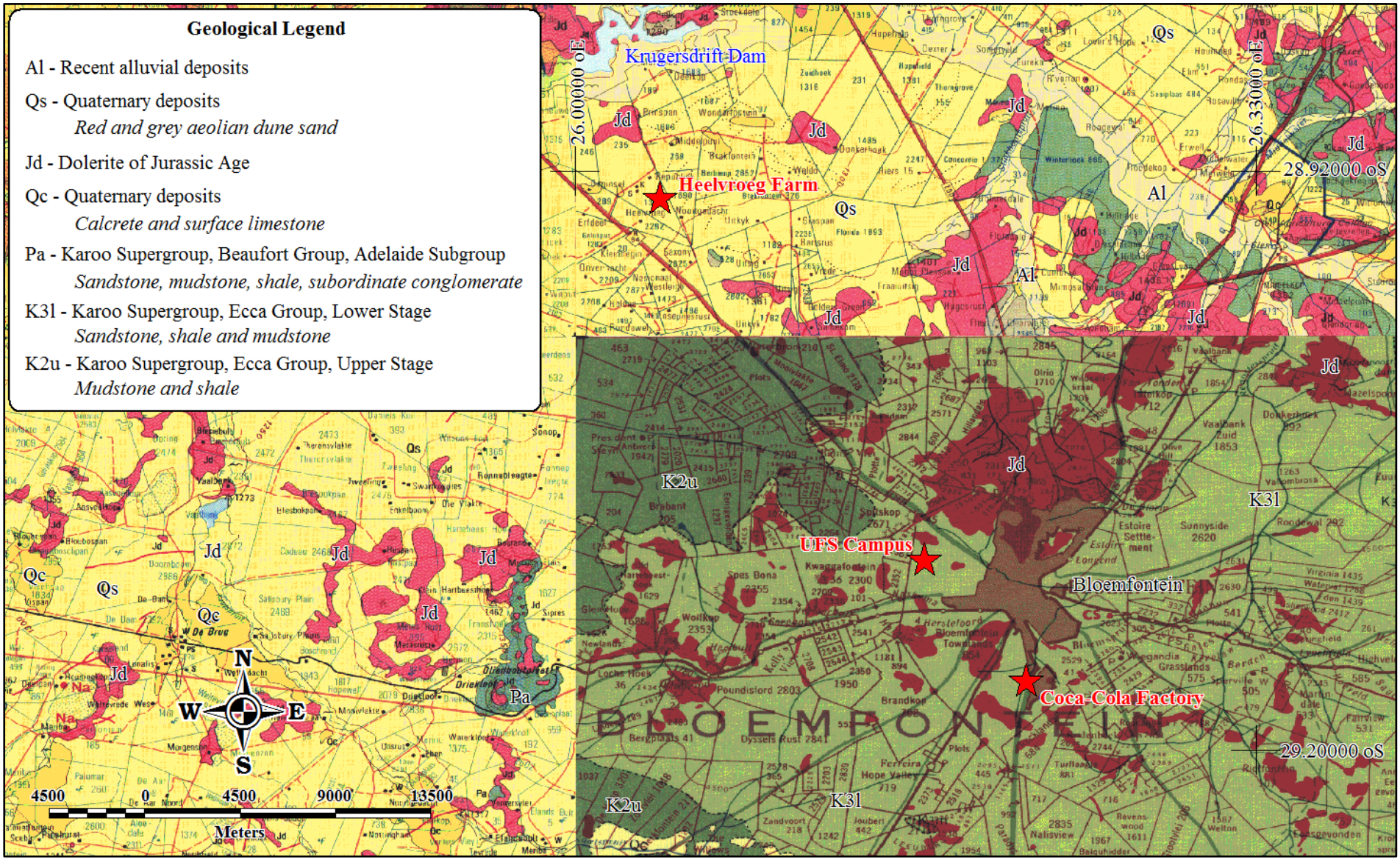


**Figure 5.3. Geological setting of the three sites at which field surveys were conducted**

## 5.5 FIELD SURVEY 1 – THE UFS CAMPUS

The survey on the UFS campus was conducted in an open field with no visible outcrops. The near-surface in the survey area has been disturbed by previous research activities conducted by the Department of Soil, Crop and Climate Sciences. Although little information on the subsurface geology at the site is available, the results of previous drilling exercises on the UFS campus and visual observations in road cuttings suggest that the site is likely underlain by sedimentary rocks of the Karoo Supergroup. The survey in this area was completed with the purpose of evaluating the response of angled ERT survey lines in an area with near-horizontal geological strata.

### 5.5.1 Survey geometry

The ERT surveys were conducted along three 400-m long survey lines, namely: 1) a straight survey line, 2) a survey line making an angle of 22.5° at its centre, and 3) a survey line making an angle of 45° at its centre (Figure 5.4). The coordinates for the three profiles are listed in Table 5.1 at 0 m (S), 200 m (centre point) and 400 m (N) along the survey lines.

**Table 5.1: Coordinates of the ERT survey on the UFS campus**

| | | Straight survey line | 22.5° angled survey line | 45° angled survey line |
|---|---|---|---|---|
| **Coordinates at 400 m of survey lines (north)** | Latitude ( S) | 29.10597 | 29.10597 | 29.10597 |
| | Longitude ( E) | 26.1696 | 26.1696 | 26.1696 |
| **Coordinates at 200 m of survey lines** | Latitude ( S) | 29.10776 | 29.10776 | 29.10776 |
| | Longitude ( E) | 26.1696 | 26.1696 | 26.1696 |
| **Coordinates at 0 m of survey lines (south)** | Latitude ( S) | 29.10957 | 29.10942 | 29.10903 |
| | Longitude ( E) | 26.1696 | 26.17029 | 26.17087 |

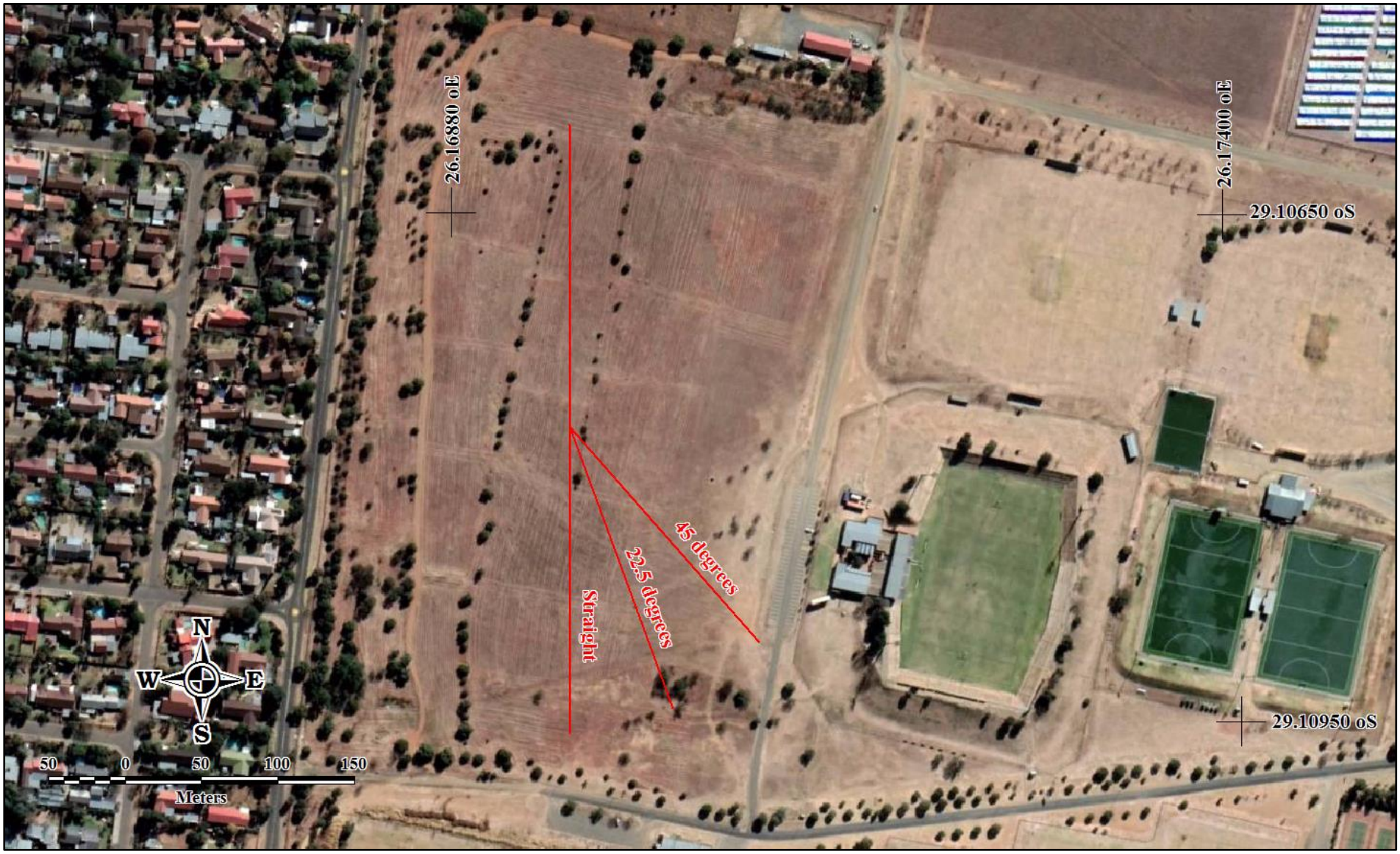


**Figure 5.4. The geometry of the ERT survey on the UFS Campus**

### 5.5.2 Results

In Figure 5.5, the pseudo-sections of the apparent resistivity data are shown for the straight and the two angled survey lines. It is clear that the introduction of angles to the survey lines resulted in distortions of the pseudo-sections. Since the erroneous apparent resistivities recorded on the angled survey lines will be used as inputs to the inversion algorithm, it can be expected that distorted resistivity models will be obtained for the data of these pseudo-sections. The inverse resistivity models are shown in Figure 5.6. All three models show the presence of four layers of distinct resistivities, namely: a thin (<5 m) layer at surface overlying a thin (<5 m) near-horizontal layer of higher resistivities which appears to pinch out towards the southern parts of the survey lines. Below this layer, a horizon of lower resistivities is seen. This layer is approximately 10 m thick and overlies a thick layer of higher resistivities (>133 Ωm). The shallow layer probably represents the topsoil while the other three layers are likely different shale and mudstone layers of the Beaufort Group.

However, when comparing the models of the angled survey lines to the model of the straight survey line, it is clear that models of the subsurface differ significantly. The following should be noted:

- Since the northern halves of all the survey lines coincide, the models for the shallow subsurface along the northern parts of the survey lines are very similar, as expected.
- Since the southern halves of the survey lines occur in different positions and are underlain by slightly different geological conditions, the southern parts of the resistivity models display differences related to the local geological conditions.
- Various artefacts are introduced to the models of the angled survey lines. The most prominent artefacts are the localised zones of low resistivity near the centres of the angled survey lines. The low resistivity zone is particularly prominent on the 45° survey line.
- The resistivity models of the angled survey lines also display resistivity values for the deepest layer that differ from the resistivities of the straight survey line. The model of the 45° survey line in particular significantly overestimates the resistivity of the deepest layer.

Since the survey geometry is known for all three survey lines, the true geometric factors ($K_{true}$) can be calculated for the displaced electrodes along the angled survey lines. The apparent resistivity values may then be corrected by multiplication with the factor $K_{true}/K_{ass}$, where $K_{ass}$ are the assumed (straight) geometric factors. The corrected pseudo-sections thus obtained are shown in Figure 5.7, while the corresponding inverse resistivity models are displayed in Figure 5.8.

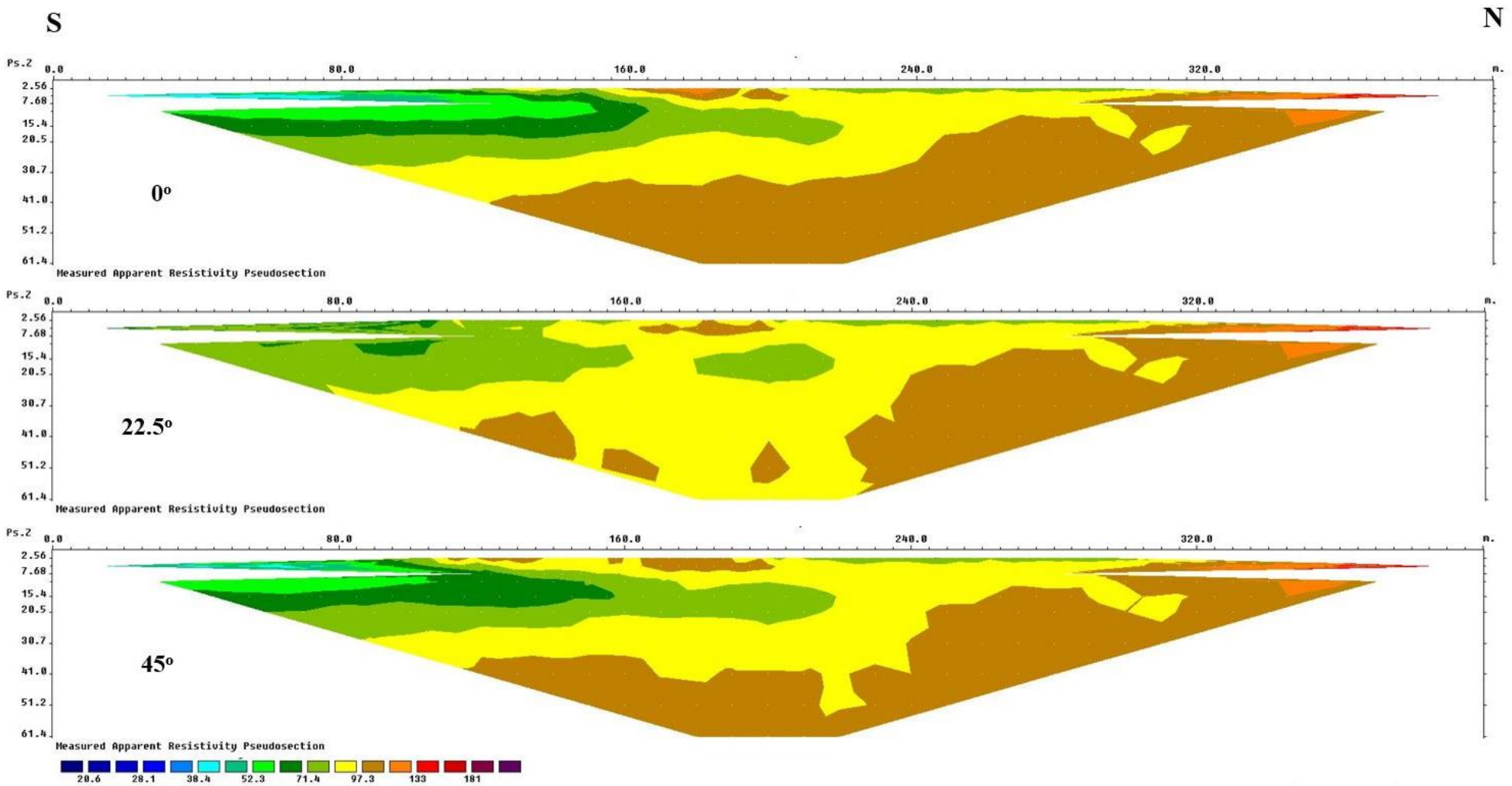


**Figure 5.5. Pseudo-sections for the survey on the UFS Campus**

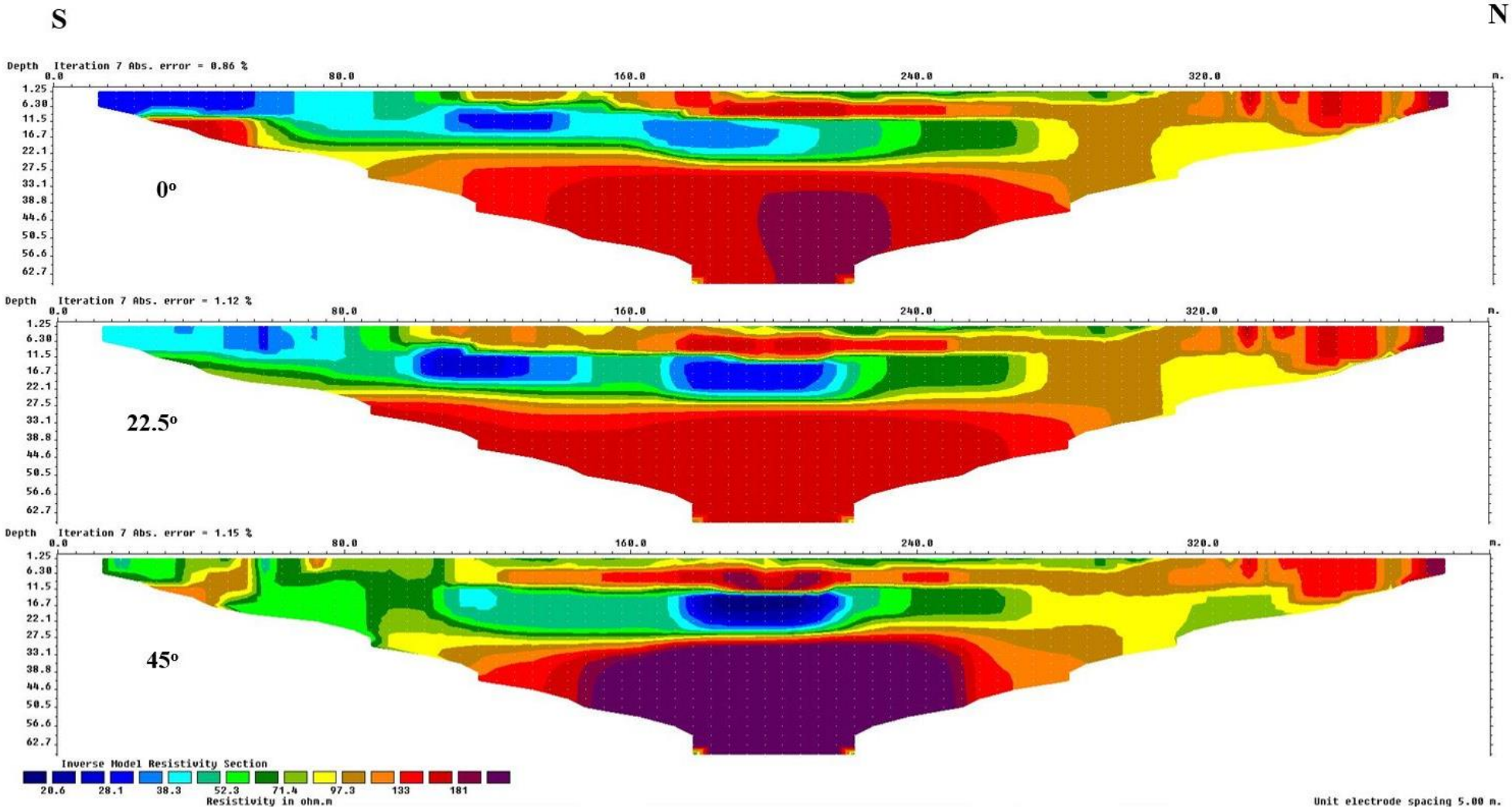


**Figure 5.6. Inverted resistivity models for the survey on the UFS Campus**

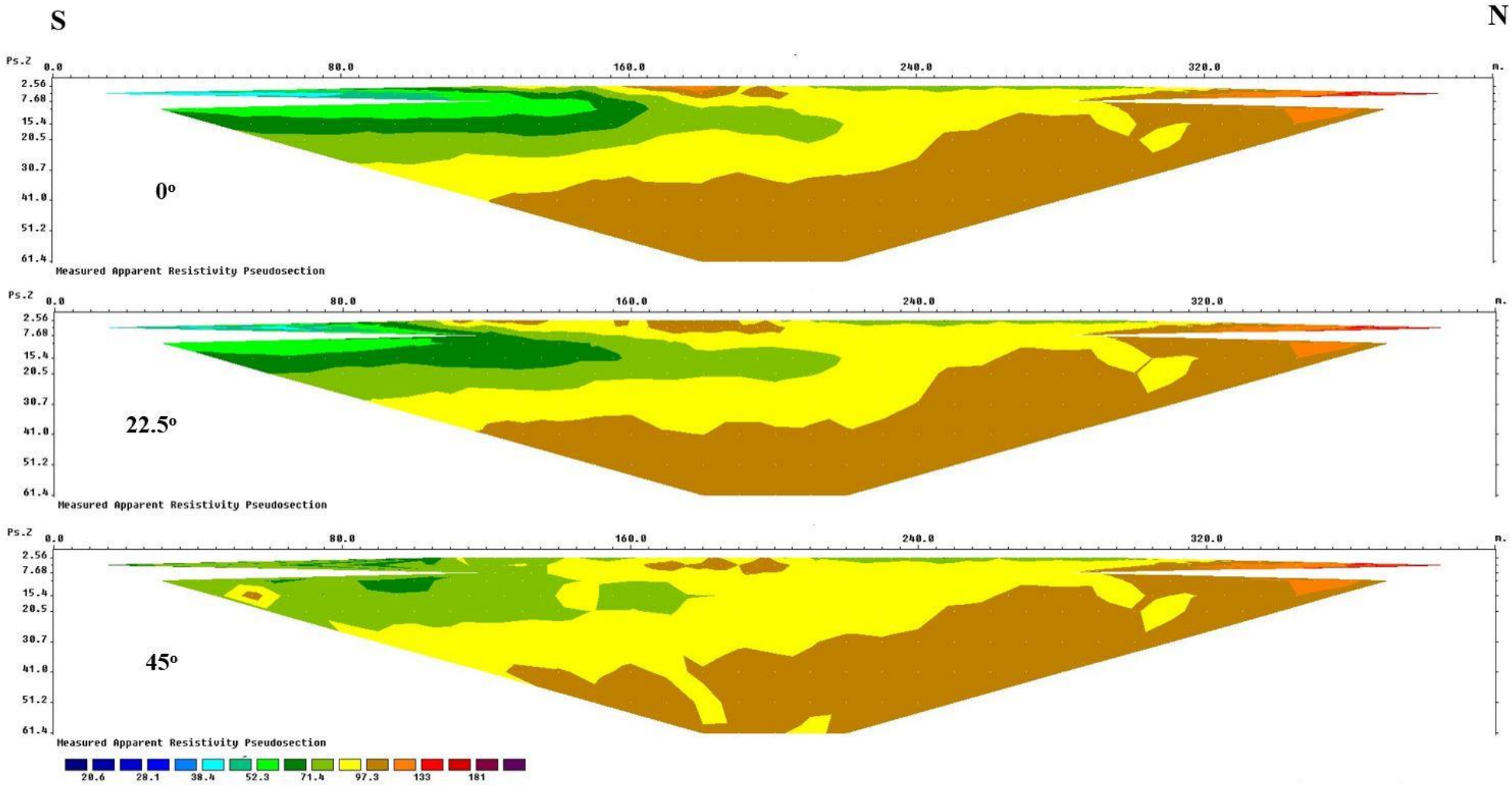


**Figure 5.7. Corrected pseudo-sections for the survey on the UFS Campus**

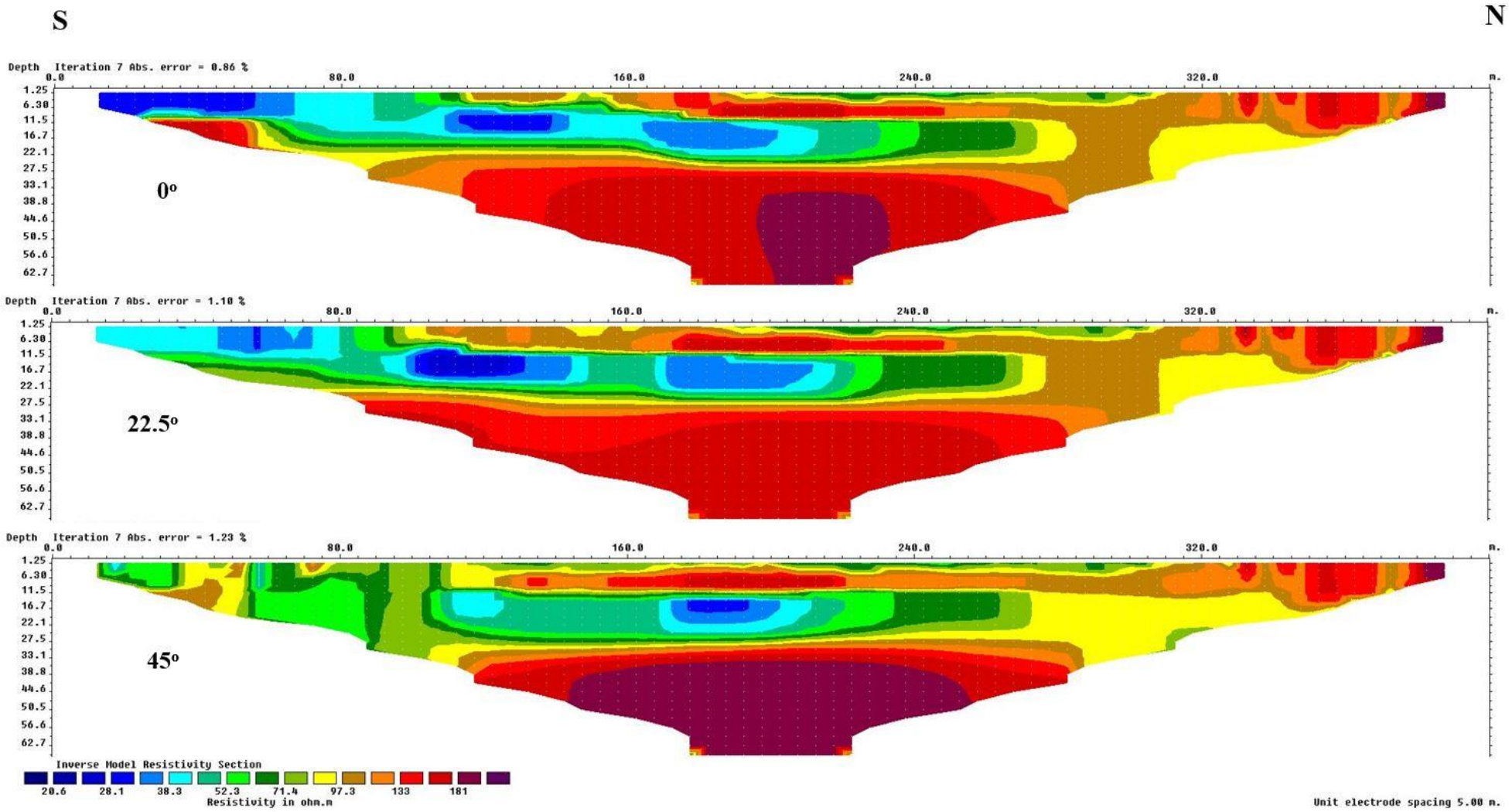


**Figure 5.8. Inverted resistivity models for the corrected pseudo-sections of the survey on the UFS Campus**

Comparing the three resistivity models in Figure 5.8 with those shown in Figure 5.6 shows that the models based on the corrected data yield better results, with both the 22.5º and 45º models agreeing better with the straight model than was the case for the uncorrected data. The low-resistivity artefacts near the centres of the angled survey lines are now much less prominent. However, it is clear that the models derived from the corrected data still differ from the model of the straight survey line. This may partly be due to the fact that correction was done for only the apparent resistivities, while the pseudo-depths of the pseudo-sections are also affected by angled survey lines. Unfortunately the inversion software used in this study (RES2DINV) calculates pseudo-depths based on assumed distances between electrodes and does not allow the user to adjust the pseudo-depths.

To further compare the models obtained for the straight and angled survey lines, the differences between the calculated subsurface resistivities (values along angled lines minus values along straight line) are shown in Figure 5.9 for the survey line making an angle of 22.5º and in Figure 5.10 for the survey line making an angle of 45º. The differences between the models for both the uncorrected and corrected data sets are shown in these figures. Only the northern halves of the survey lines are shown to isolate the effects of systematic electrode displacement on the resulting magnetic models (the southern halves occur in slightly different geological conditions with different resistivities).

Large differences are seen to occur near the centre of the survey line (200 m). For the 22.5° line, the differences range between -30 Ωm and +60 Ωm, while larger difference are found for the 45° line (-50 Ωm to +100 Ωm). For both lines, the differences are reduced when using the corrected data sets. This is particularly true for the 45° line where large positive differences in the deeper parts of the section are removed (refer to Figure 5.10) when using the corrected data set.

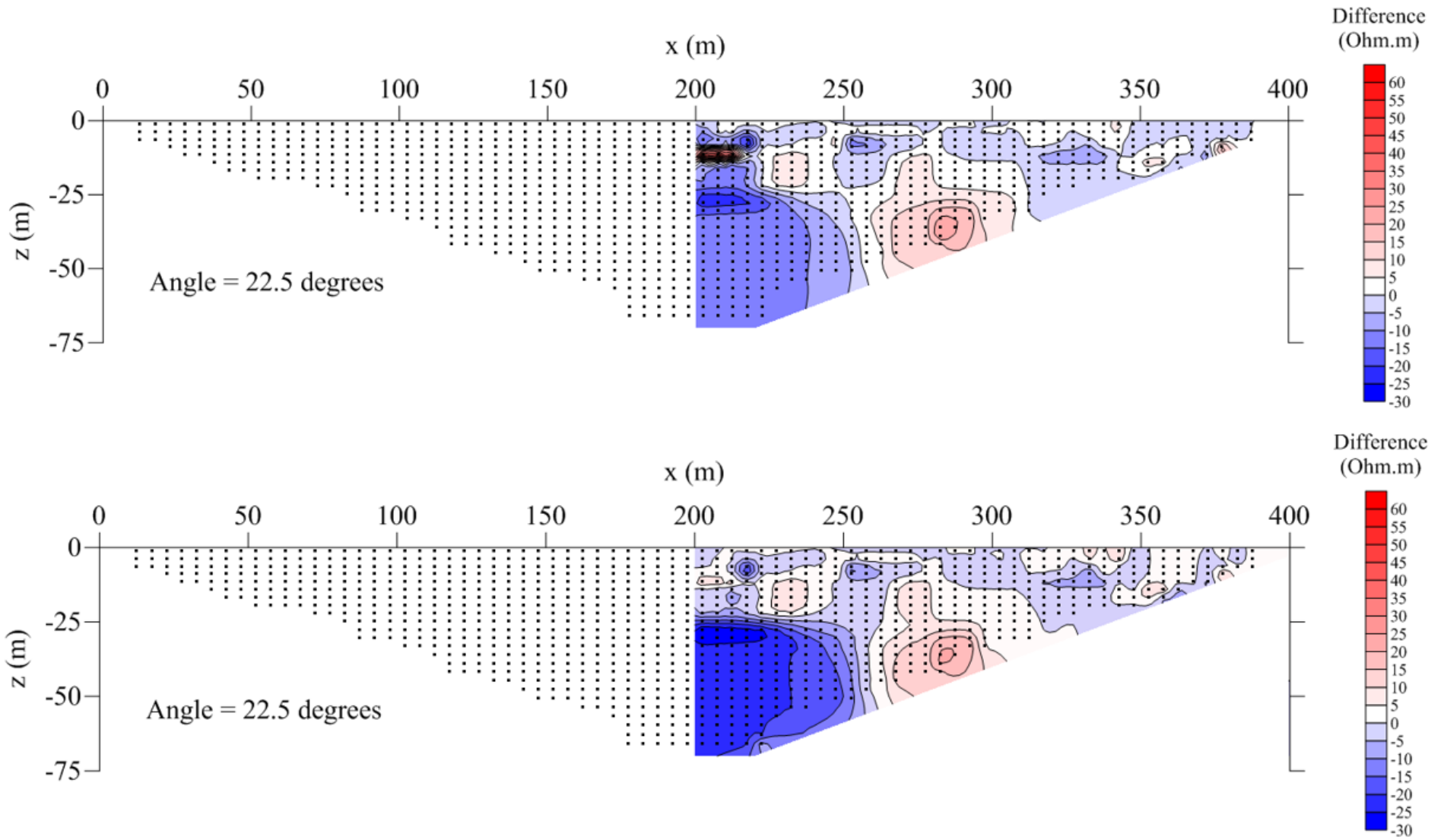


**Figure 5.9. Differences between the resistivity models along the angled survey line (22.5$^{o}$) and the straight line on the UFS Campus (top: uncorrected; bottom: corrected)**

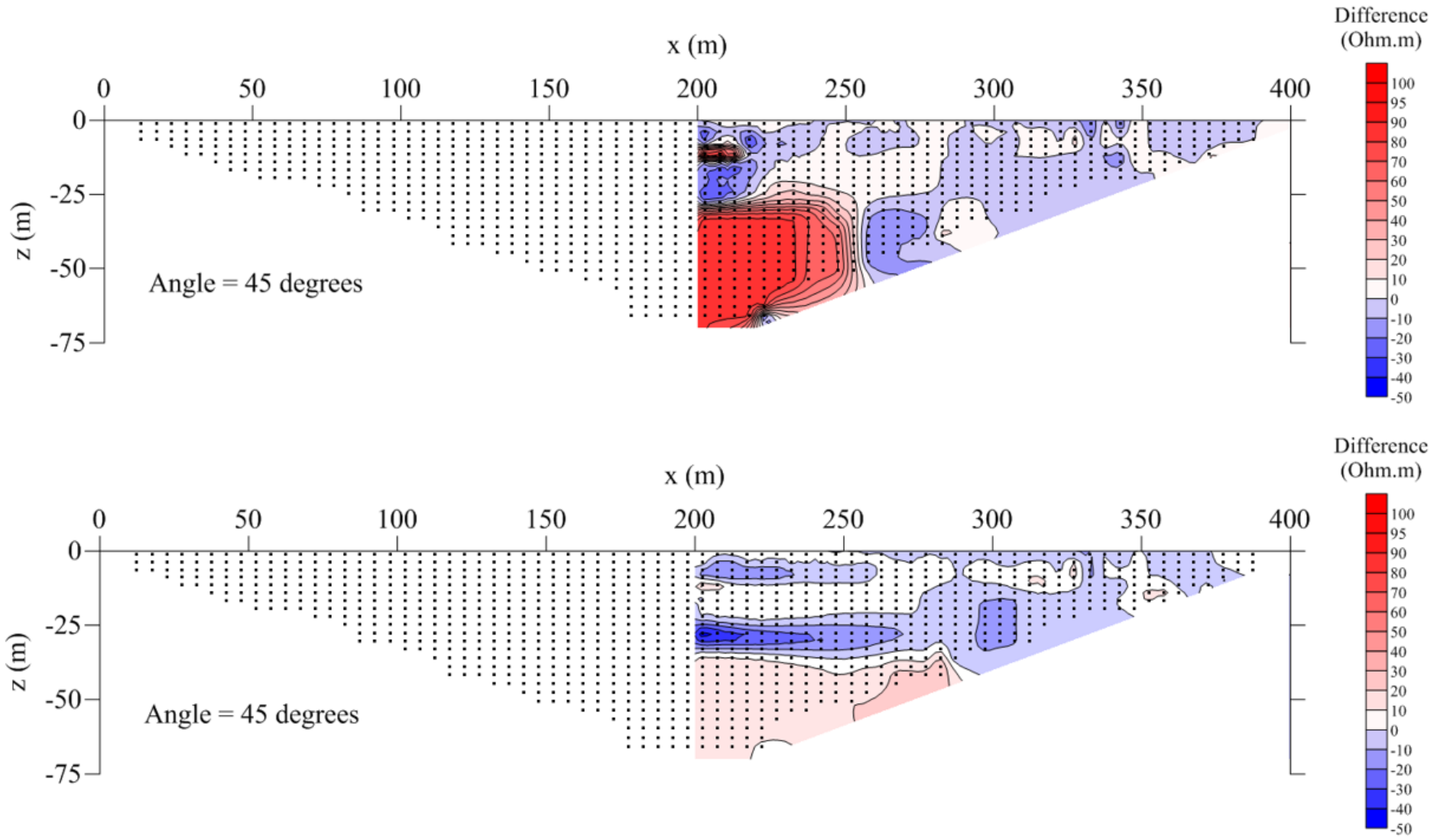


**Figure 5.10. Differences between the resistivity models along the angled survey line (45º) and the straight line on the UFS Campus (top: uncorrected; bottom: corrected)**

## 5.6 FIELD SURVEY 2 – THE COCA-COLA FACTORY

### 5.6.1 Survey geometry

Figure 5.11 is a contour map of the total magnetic field near the Coca-Cola factory. A prominent linear magnetic anomaly with a north-west/south-east strike is clearly seen in the map. This anomaly was interpreted to be due to a large dolerite dyke. ERT data were recorded across this anomaly with the centre position of the survey lines occurring approximately 100 m south-west of the anomaly. Data were again recorded on three survey lines, namely a straight line and two lines with angles of 22.5° and 45° at the centre of the lines (Figure 5.12).

The coordinates of the three profiles are listed in Table 5.2 for the endpoints (0 m, south-west; 400 m, north-east) and centre position (200 m).

**Table 5.2: Coordinates of the ERT survey near the Coca-Cola factory**

| | | Straight survey line | 22.5° angled survey line | 45° angled survey line |
|---|---|---|---|---|
| **Coordinates at 400 m of survey lines (NE)** | Latitude ( S) | 29.16479 | 29.16479 | 29.16479 |
| | Longitude ( E) | 26.21839 | 26.21839 | 26.21839 |
| **Coordinates at 200 m of survey lines** | Latitude ( S) | 29.16643 | 29.16643 | 29.16643 |
| | Longitude ( E) | 26.21756 | 26.21756 | 26.21756 |
| **Coordinates at 0 m of survey lines (SW)** | Latitude ( S) | 29.16808 | 29.16769 | 29.16703 |
| | Longitude ( E) | 26.21673 | 26.21608 | 26.21571 |

### 5.6.2 Results

The inverse resistivity models for the straight and angled survey lines are shown in Figure 5.13 (top: straight; middle: 22.5$^o$; bottom: 45$^o$), while the corresponding inverse models for the corrected data sets are shown in Figure 5.14.

The most prominent feature of the inverse models is the broad, near-vertical zone of high resistivities that corresponds to the position of the dyke as indicated by the magnetic data. This zone is well defined in the model for the straight line, and appears to have a thickness of approximately 40 m. However, in the models for the angled lines, the anomaly is less well defined and appear to be thicker than in the model for straight line. The resistivity of the dyke also appears lower in the models for the angled lines.

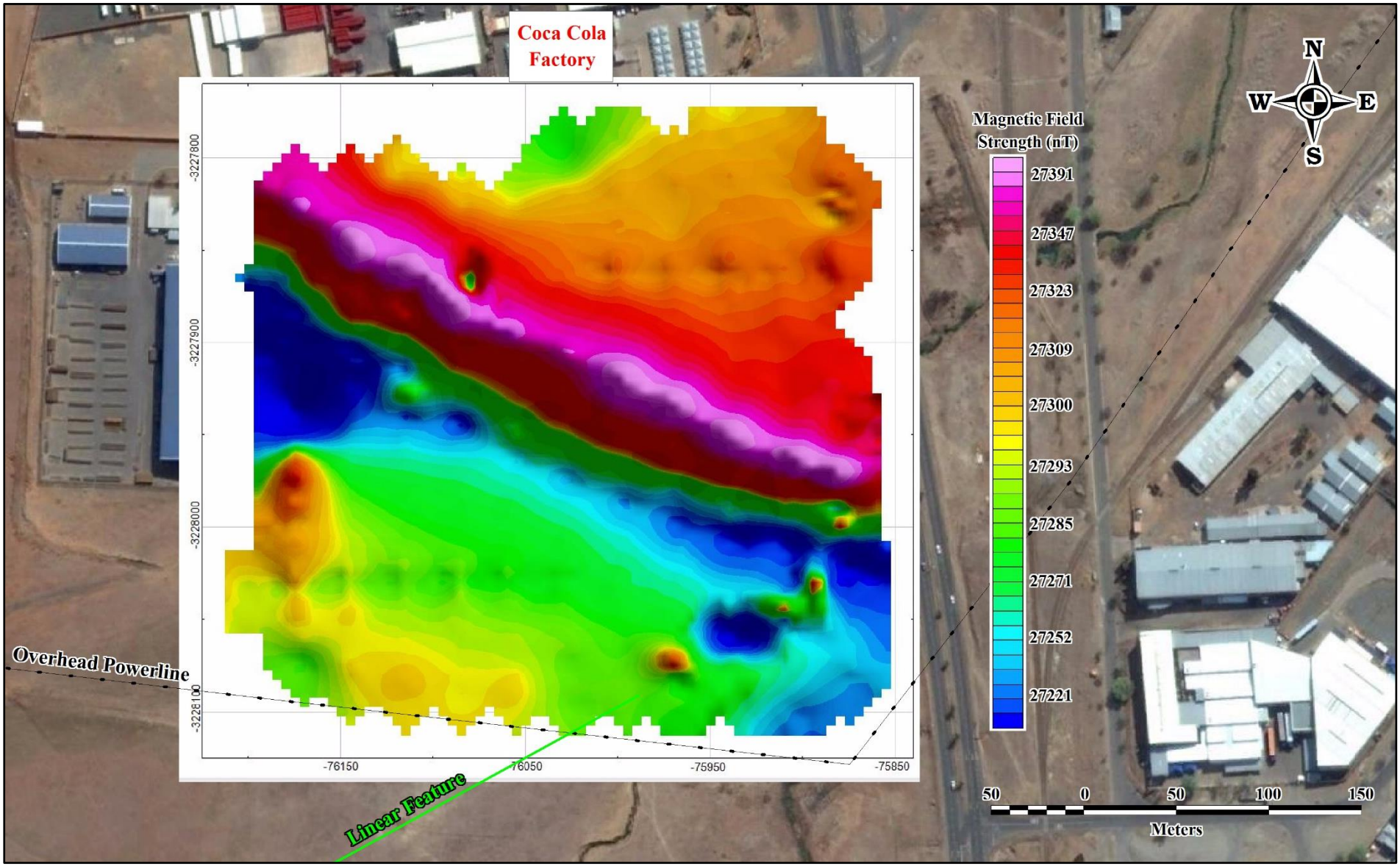


**Figure 5.11. Linear magnetic anomaly recorded near the Coca-Cola factory (projection: WGS84, LO29)**


**Figure 5.12. Geometry of the ERT survey near the Coca-Cola factory**

Also observed when comparing the different models in Figure 5.13 is the elongation of a shallow zone of high resistivity centred at position 180 m when introducing angles to the survey lines. This may be artefacts introduced by the angles, or it may be due to the fact that the southern parts of the lines occur in different positions with slightly different subsurface conditions.

Comparison of the models in Figure 5.14 shows that the artefacts introduced to the inverse resistivity models for the angled survey lines were successfully removed when using the corrected data sets. The geometry, resistivity and thickness of the dolerite dyke are now much more similar than was the case for the uncorrected data sets. In the northern parts of the models, where all three survey lines coincided, the inverse resistivity models are remarkably similar for the corrected data sets. The near-surface zone of high resistivity is now also less elongated in the models for the angled lines, although its resistivity is still overestimated. This may again be due to the fact that slightly different geological conditions occur in the southern parts of the three survey lines.

The differences between the modelled resistivity values for the straight and angled survey lines are shown in Figure 5.15 and Figure 5.16 for the 22.5° and 45° survey lines, respectively. In these figures, both the differences for the models of the uncorrected (top) and corrected (bottom) data sets are shown. From these figures it is clear that large differences occur in the vicinity of the dolerite dyke, particularly for the model of the 45° line where differences ranging between -1 200 Ωm and +1 000 Ωm are observed. These differences are, however, dramatically reduced in the models for the corrected data sets (compare the top and bottom images of Figure 5.15 and Figure 5.16).

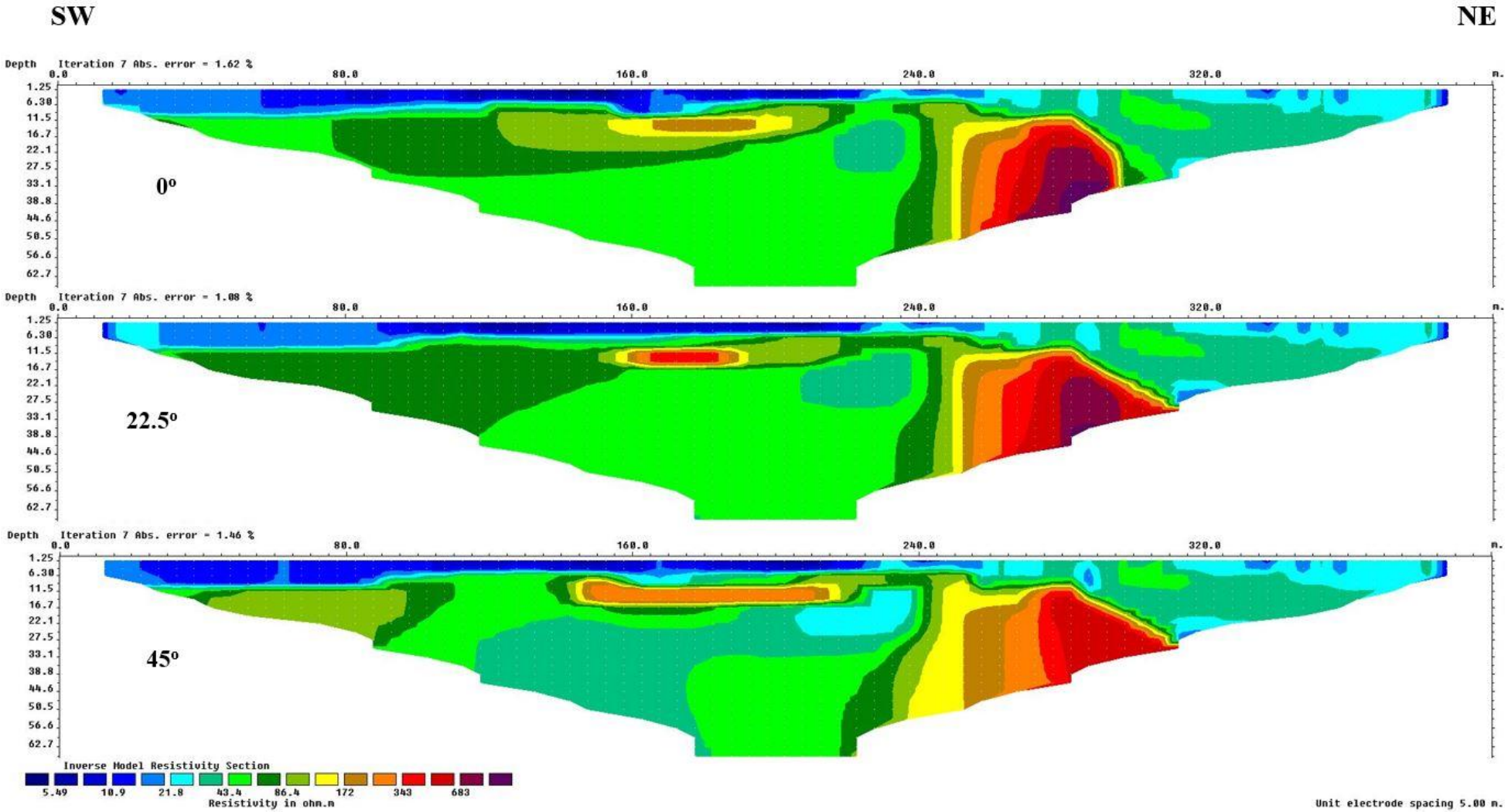


**Figure 5.13. Inverted resistivity models for the survey at the Coca-Cola Factory**

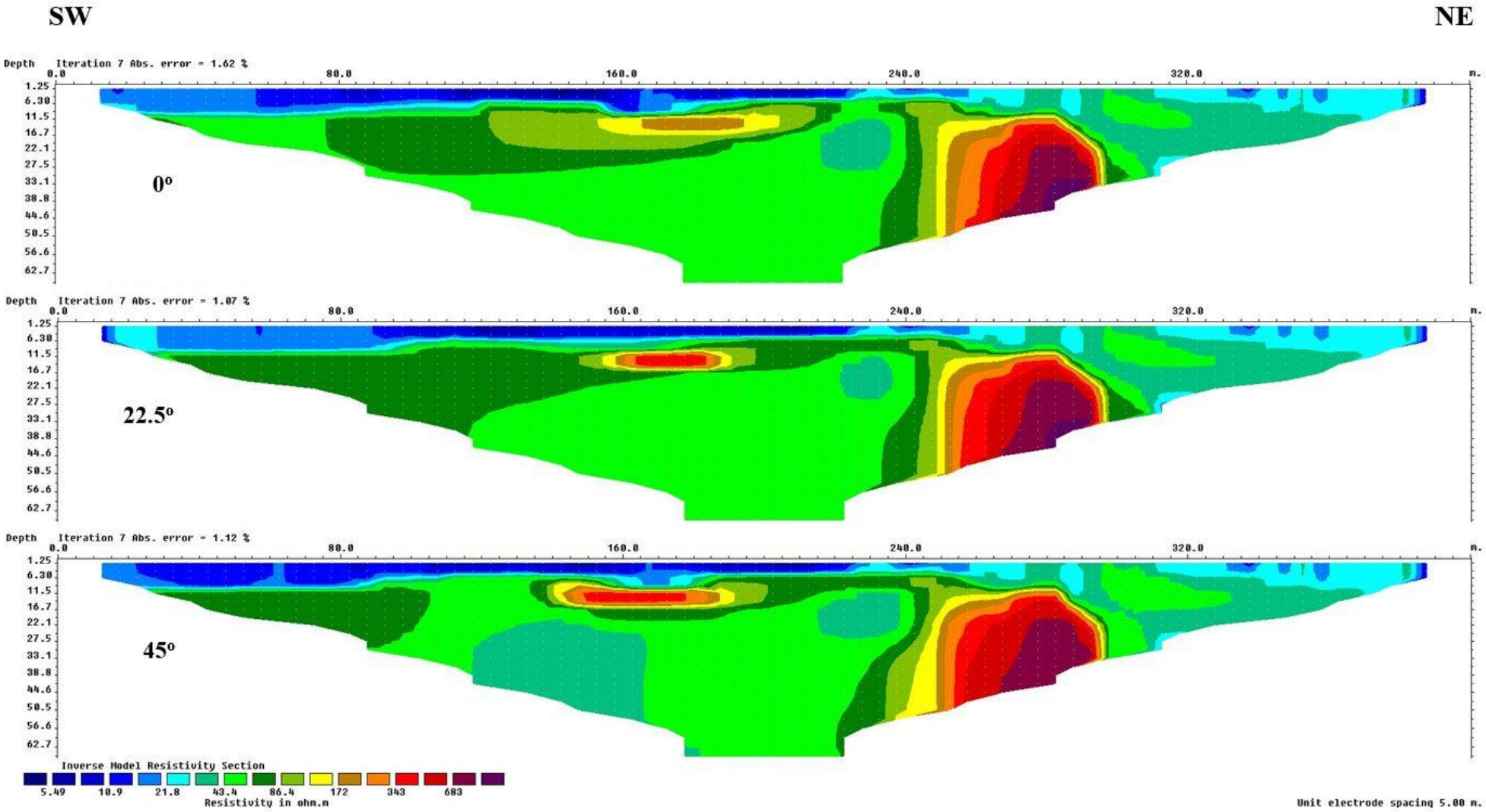


**Figure 5.14. Inverted resistivity models for the corrected pseudo-sections of the survey at the Coca-Cola Factory**

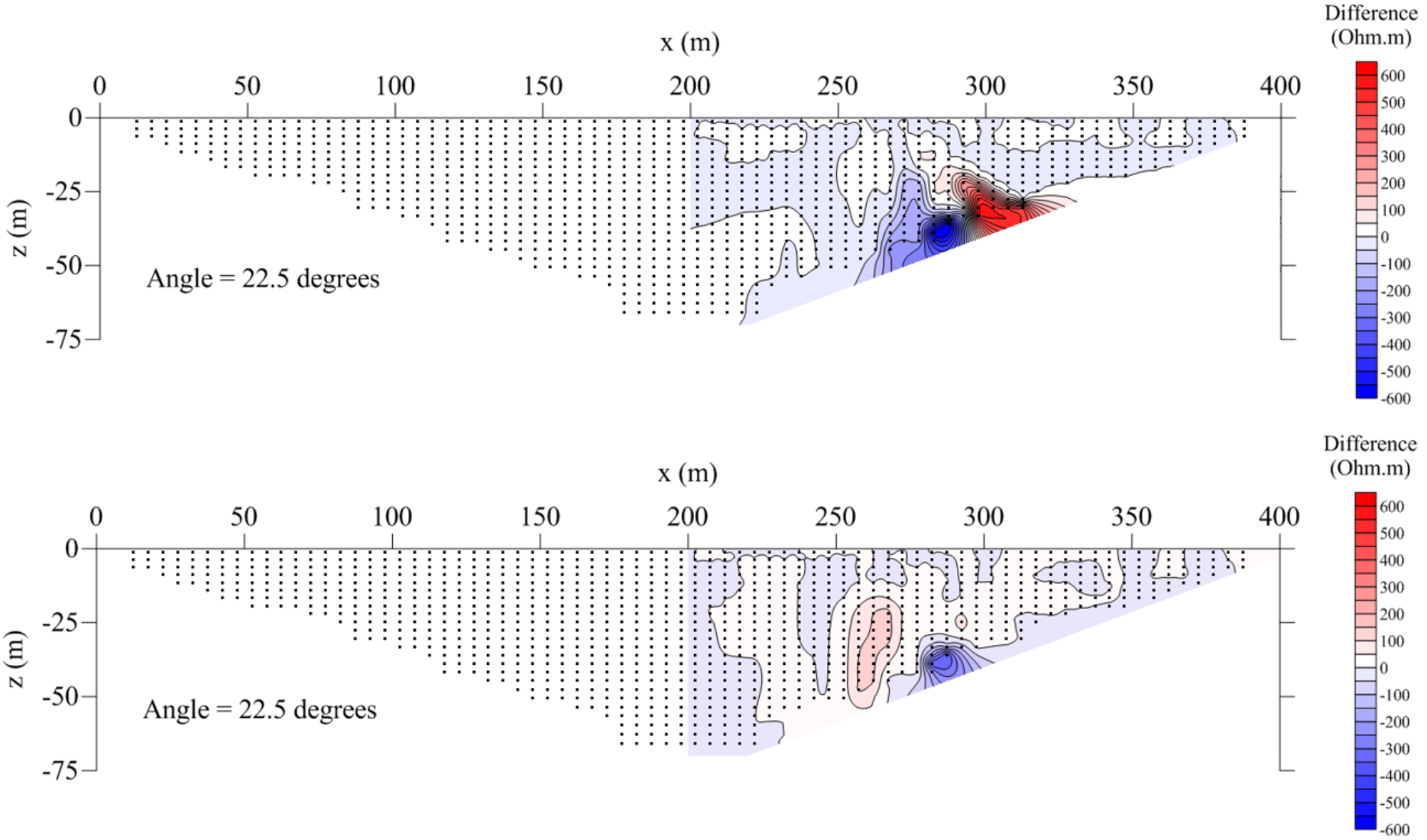


**Figure 5.15. Differences between the resistivity models along the angled survey line (22.5º) and the straight line at the Coca-Cola Factory (top: uncorrected; bottom: corrected)**

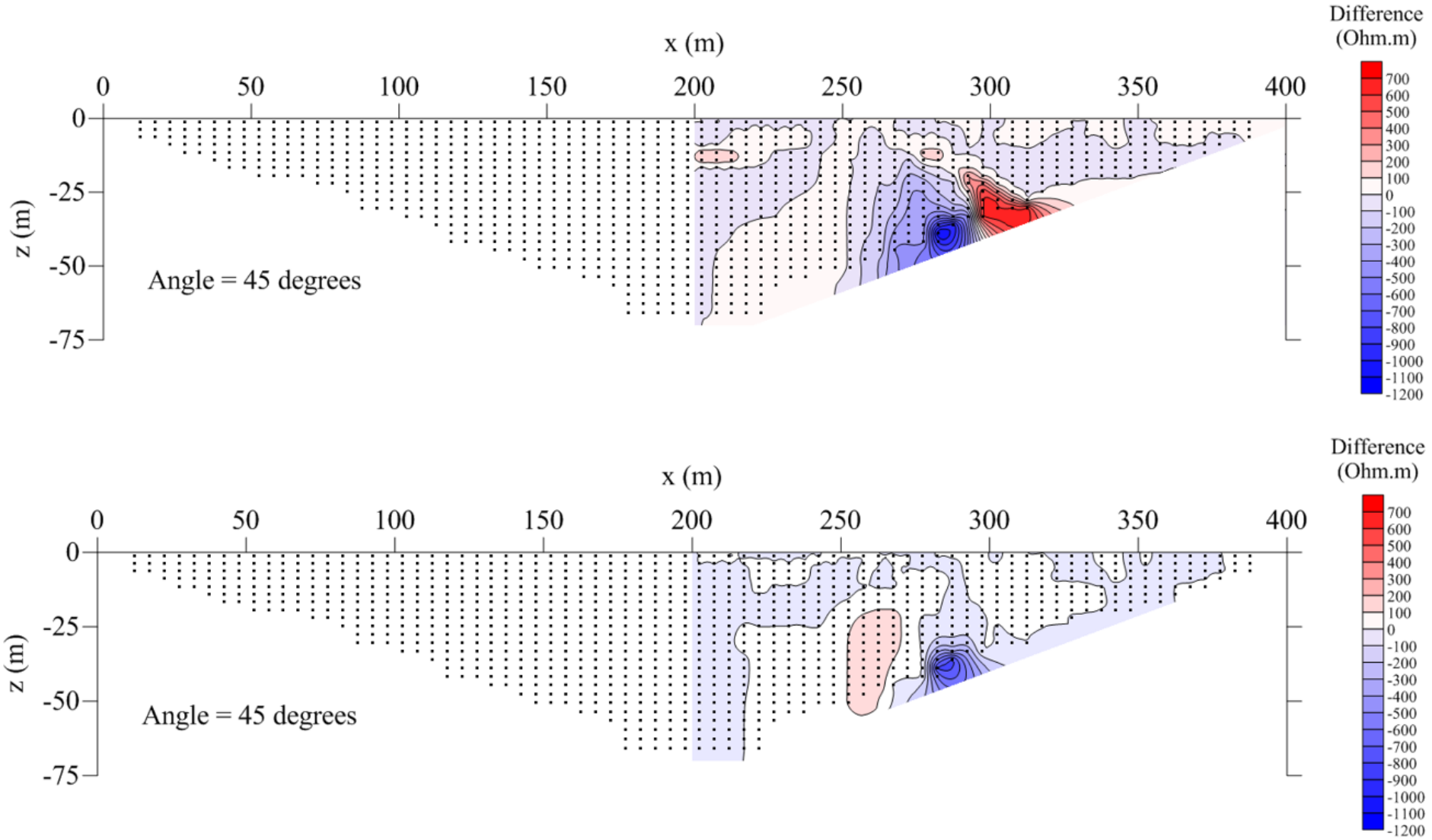


**Figure 5.16. Differences between the resistivity models along the angled survey line (45º) and the straight line at the Coca-Cola Factory (top: uncorrected; bottom: corrected)**

## 5.7 FIELD SURVEY 3 – THE FARM HEELVROEG

The ERT survey on the Heelvroeg Farm targeted a possible thin dolerite dyke that had been identified by a magnetic survey conducted by students of the IGS in 2015. Dolerite dykes are often regarded as potential targets for groundwater in the Karoo Supergroup. Since large resistivity contrasts generally exist between the intrusives and their sedimentary host rocks, ERT is well suited to detect and delineate the intrusives. However, if ERT surveys cannot be performed on straight survey lines across such intrusives, the angles in the survey lines could result in distorted pseudo-sections which will affect the accuracy of the inverse resistivity models. It is therefore important to investigate the impact of angled survey lines on the results of ERT surveys across dolerite dykes to determine how the data and resistivity models are affected.

### 5.7.1 Survey geometry

A contour map of the total magnetic field recorded on the Heelvroeg Farm is shown in Figure 5.17. A prominent linear magnetic anomaly with a west-north-west/east-south-east strike is clearly visible in the magnetic map. This anomaly was interpreted to be due to a thin dolerite dyke. Subsequent drilling confirmed this interpretation.

The geometry of the ERT survey on the Heelvroeg Farm is shown in Figure 5.18. The straight survey line extended perpendicularly across the dolerite dyke, with its centre positioned at the dyke. The southern halves of the angled survey lines coincided with the straight survey line, but the northern halves were rotated through angles of 22.5° and 45° towards the east. The lengths of the survey lines were 400 m. The coordinates for the three profiles are listed in Table 5.3. The coordinates were recorded at 0 m (SW), 200 m (centre point) and at 400 m (NE).

**Table 5.3: Coordinates of the ERT survey on the Heelvroeg farm**

| | | Straight survey line | 22.5° angled survey line | 45° angled survey line |
|---|---|---|---|---|
| **Coordinates at 0 m of survey lines (SW)** | Latitude ( S) | 28.93353 | 28.93353 | 28.93353 |
| | Longitude ( E) | 26.03993 | 26.03993 | 26.03993 |
| **Coordinates at 200 m of survey lines (centre)** | Latitude ( S) | 28.93024 | 28.93024 | 28.93024 |
| | Longitude ( E) | 26.04165 | 26.04165 | 26.04165 |
| **Coordinates at 400 m of survey lines (NE)** | Latitude ( S) | 28.93189 | 28.93069 | 28.93133 |
| | Longitude ( E) | 26.04079 | 26.04221 | 26.04256 |

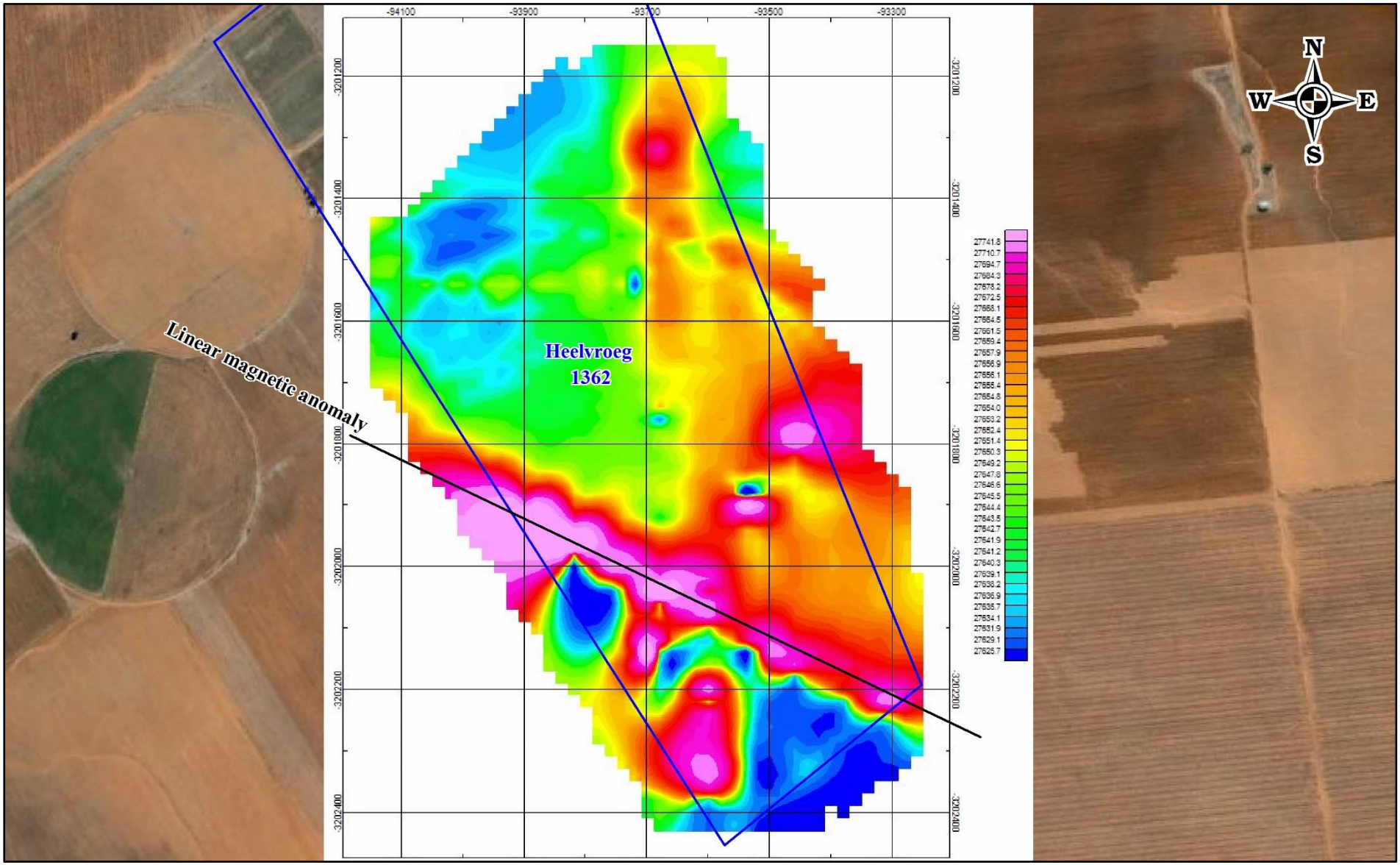


**Figure 5.17. Linear magnetic anomaly recorded on the farm Heelvroeg**

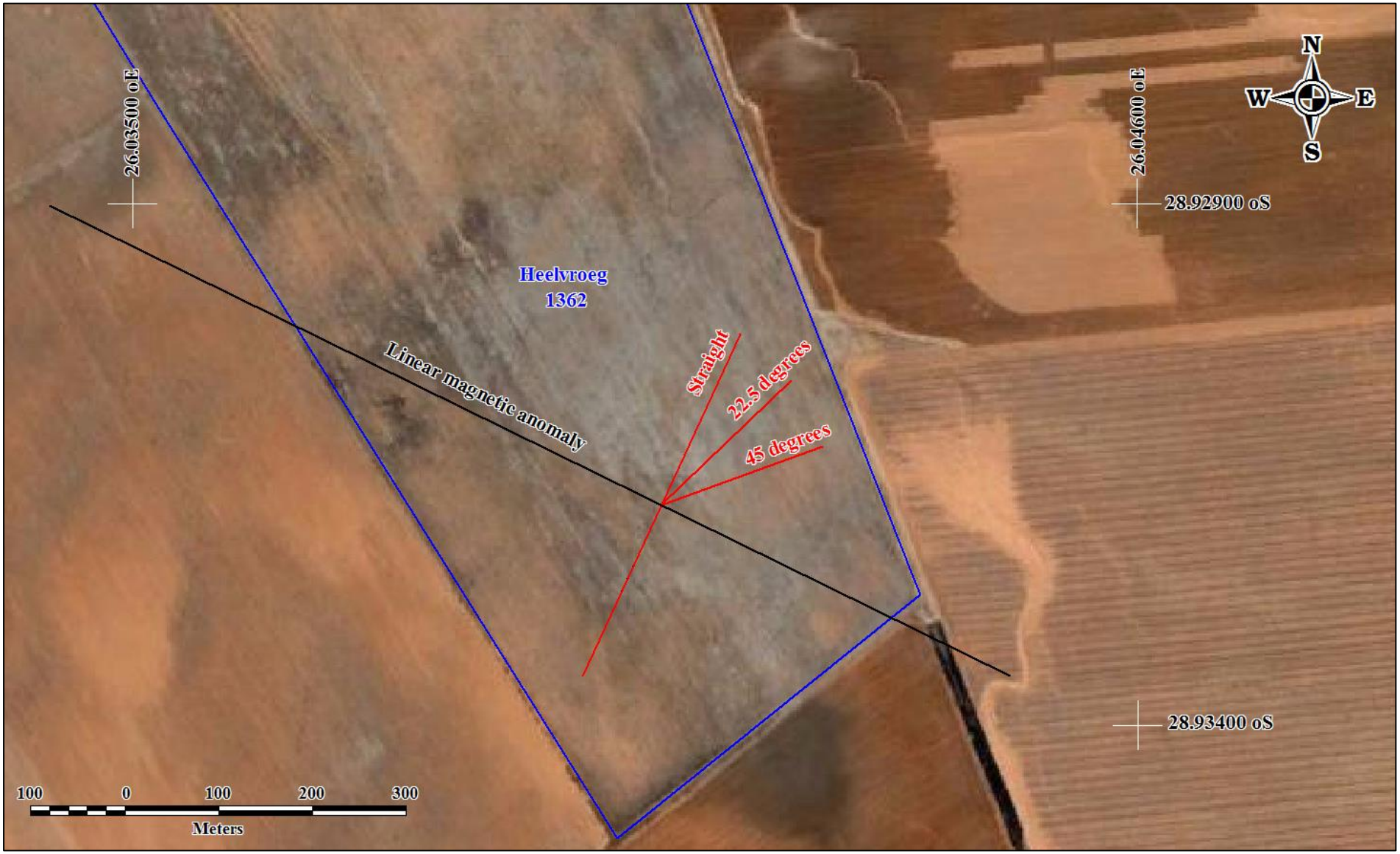


**Figure 5.18. The geometry of the ERT survey on the farm Heelvroeg**

### 5.7.2 Results

The inverse resistivity models for the uncorrected apparent resistivity data are shown in Figure 5.19 for the straight (top) and angled survey lines (middle: 22.5°; bottom: 45°). No dyke-like structure is evident in the models. The most prominent feature of the model for the straight line is the large lateral change in resistivities near position 155 m. To the left (south-west) of this position, the deeper geological units have significantly higher resistivities than to the right (north-east). The bedrock topography also seems to vary significantly with a shallower bedrock to the left of this position and a deeper bedrock to the right. It is therefore possible that the linear magnetic anomaly across which the survey was done is due to the edge of a sill, rather than a linear dyke.

However, it must be stated that the quality of the data recorded at the Heelvroeg farm was rather poor. The presence of aeolian sand at surface lead to high contact resistances between the electrodes and the earth materials. This lead to data with large standard deviations. The poor quality of the apparent resistivity data negatively affected the quality of the inverse resistivity models.

The model for the 22.5° line looks similar to the model of the straight line. Since the south-western parts of the three survey lines coincided, similar responses were to be expected in these parts, particularly for the shallower measurements not affected by the angle in the survey line. However, the bedrock resistivity in the southern part of the line is visibly higher than for the straight model. Changes in the bedrock topography along the northern parts of the survey line are also observed. This may again be partly due to the fact that the north-eastern parts of the different lines did not coincide. Slightly different geological conditions were therefore affecting the apparent resistivity measurements and the inverse resistivity models.

The model for the 45° line looks completely different from the model for the straight line, both in the south-western and north-eastern parts of the survey line. It is clear that the large angle in the survey line completely distorted the inverse model.

The inverse models for the corrected data sets (Figure 5.20) show some improvement on the models for the uncorrected data sets. However, the improvement is less significant than it was for the other two field surveys at the UFS Campus and the Coca-Cola factory. This may be due to the poor data quality at the Heelvroeg farm.

The differences between the modelled resistivity values for the straight and angled survey lines are shown in Figure 5.21 and Figure 5.22 for the 22.5° and 45° survey lines, respectively. From these figures it is clear that the models for the corrected data sets yielded inverse resistivity models that were more similar to the model for the straight line. Using corrected data sets therefore lead to more accurate resistivity models.

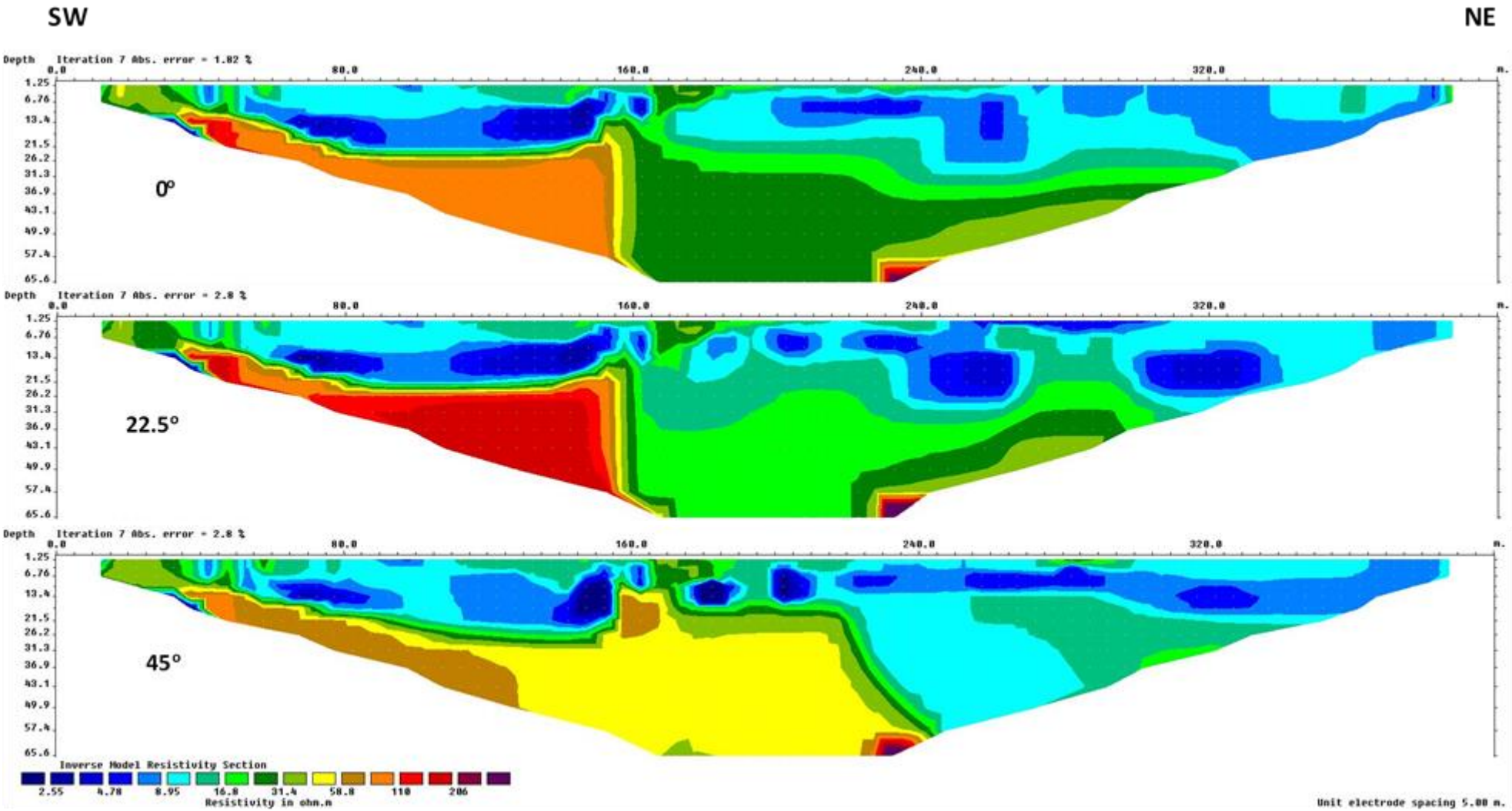


**Figure 5.19. Inverted resistivity models for the survey at the Heelvroeg farm**

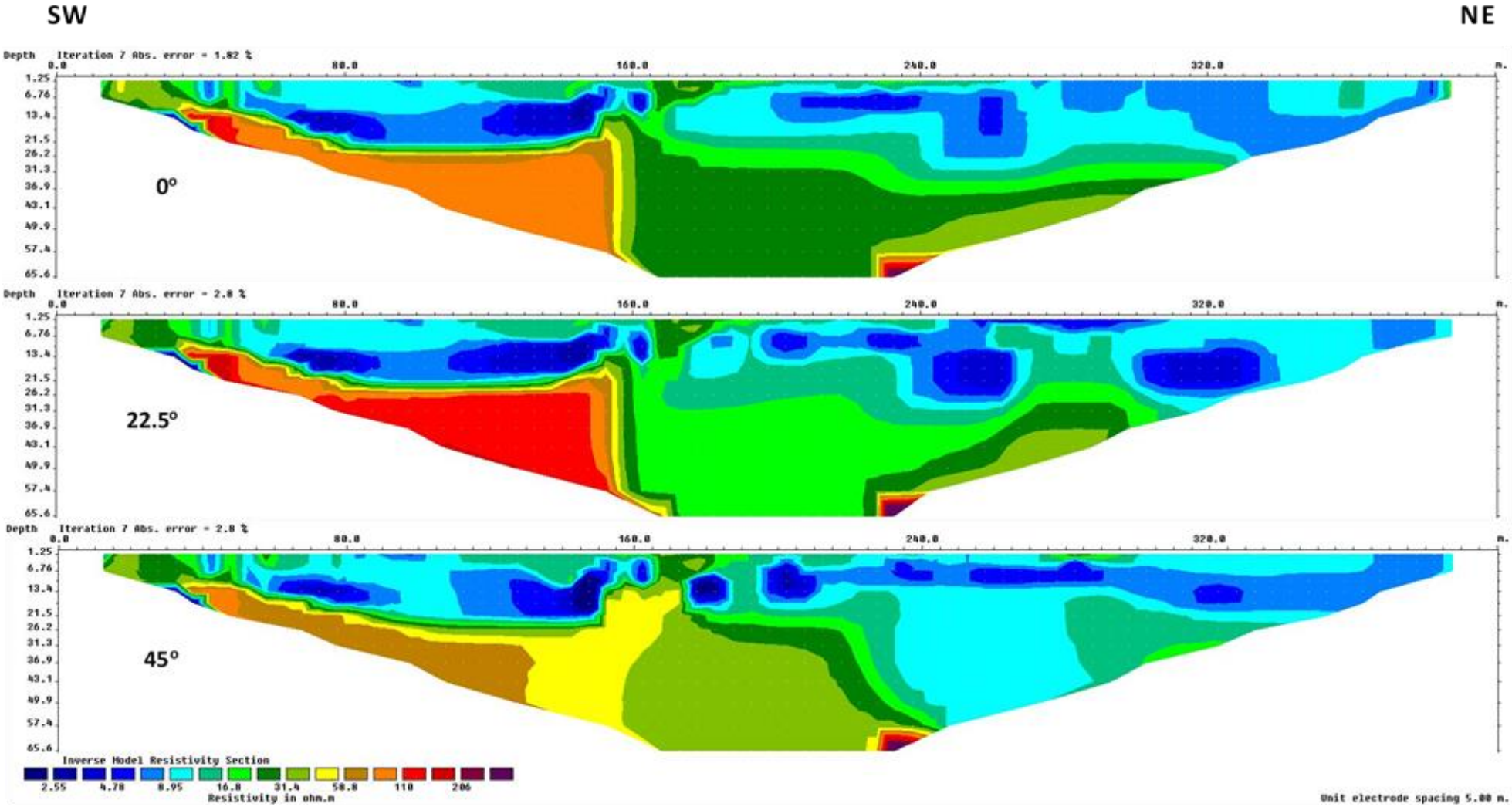


**Figure 5.20. Inverted resistivity models for the corrected pseudo-sections of the survey at the Heelvroeg farm**

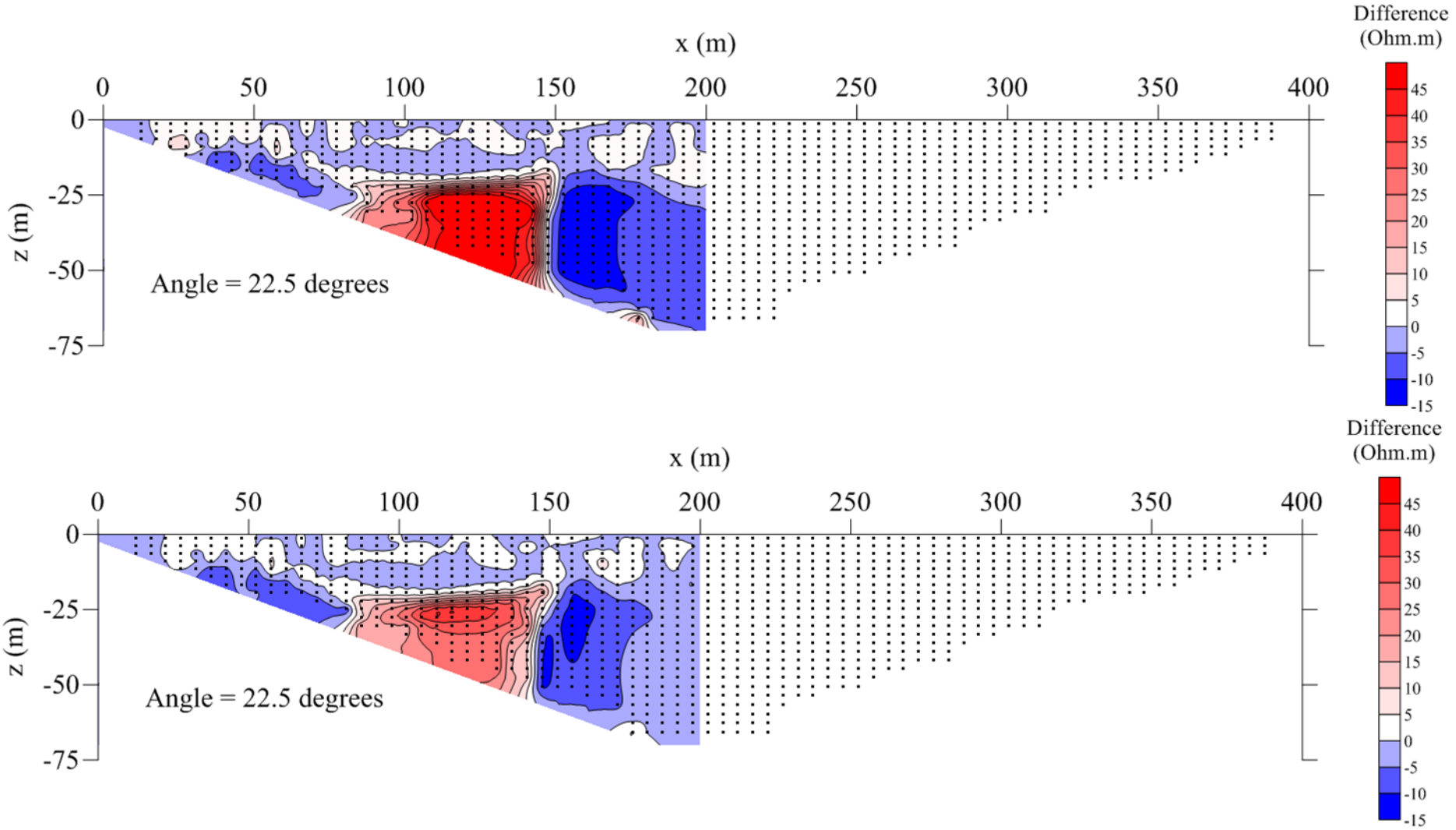


**Figure 5.21. Differences between the resistivity models along the angled survey line (22.5º) and the straight line at the Heelvroeg farm (top: uncorrected; bottom: corrected)**

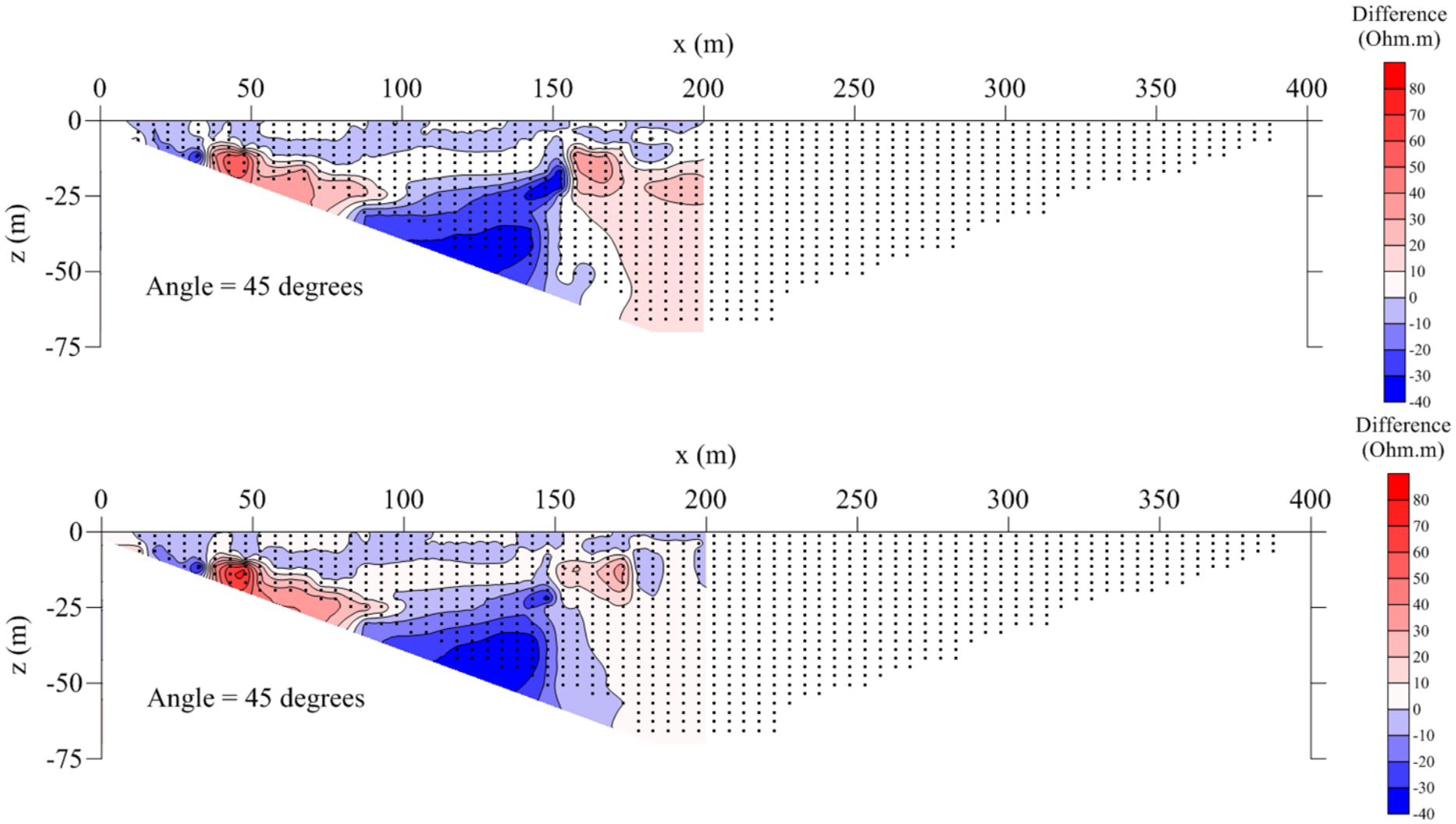


**Figure 5.22. Differences between the resistivity models along the angled survey line (45º) and the straight line at the Heelvroeg farm (top: uncorrected; bottom: corrected**

## 5.8 DISCUSSION

In this chapter the results of ERT surveys at three sites were presented. At each of the sites, data were recorded along a straight survey line, as well as along two survey lines making angles of 22.5°and 45° at their centres. The three sites all occur in areas underlain by Karoo rocks, but differ in terms of the presence or absence of dolerite intrusions. The UFS Campus site is underlain by Karoo sedimentary rocks with no known dolerite intrusives, while a prominent dolerite dyke is known to occur at the Coca-Cola site. The linear magnetic anomaly at the Heelvroeg farm site was thought to be due to a thin dolerite dyke.

The purpose of the field surveys was to obtain real field data to compare with the numerical modelling results of Chapter 4. The results of the field survey agreed with the findings of the numerical modelling in the following ways:

- The introduction of angles to the survey lines lead to distorted pseudo-sections,
- The distortion was more severe for larger angle,
- The distortion of the pseudo-sections occurred in a fan-shaped area centred at the angle in the survey line, and,
- The distorted pseudo-section lead to distorted inverse resistivity models. The distortion was more severe for the larger angle.

It was also shown in this chapter how the apparent resistivity data recorded along angled survey lines may be corrected to a degree by calculating the true geometric factors for the survey and by adjusting the apparent resistivity data accordingly. The inverse resistivity models obtained from the corrected data sets were seen to be superior to the models obtained from the uncorrected data. However, the pseudo-depths of the pseudo-sections were also affected by angled survey lines. The pseudo-depths could not be corrected since the inversion software used in this study (RES2DINV) calculates pseudo-depths based on assumed distances between electrodes and does not allow the user to make adjustments. The inverse resistivity models for the angled survey lines were therefore still affected by these errors in the pseudo-depths.

Despite the fact that no corrections could be made to the pseudo-depths, it is clear that the corrected data sets resulted in more reliable inverse resistivity models. As discussed, improved models could make the difference between siting successful or unsuccessful boreholes on subsurface geological structures. It is therefore vital that ERT data recorded along angled survey lines should be corrected before subjected to the process of inversion.

# CHAPTER 6: CONCLUSIONS AND RECOMMENDATIONS

Due to the presence of surface infrastructure and natural constraints, it is not always possible to conduct 2D ERT surveys along straight lines. Since the protocols used during 2D ERT surveys typically assume that the survey lines are straight, errors are introduced to the apparent resistivity data. In general, recording ERT data along angled survey lines affect the data in the following ways:

1) Since the true distances between the electrodes are smaller than the assumed distances for some measurements, the geometric factors and apparent resistivities are affected,

2) The true pseudo-depths for some measurements are smaller than the assumed pseudo-depths,

3) The volumes of the subsurface surveyed are displaced from the survey line and the recorded apparent resistivity data may be the representative of the subsurface at positions displaced from the survey lines.

Since the recorded resistivity data are used to obtain inverse models of the subsurface resistivity distribution, data recorded along angled survey lines will lead to distorted resistivity models. The larger the angle, the more severe the distortion. Distorted resistivity models may in turn lead to the siting of boreholes in positions that are not optimal for intersecting water-bearing structures.

In this study, the impact of angled survey lines on the data and resistivity models obtained for the Wenner ($\alpha$) array was studied by 1) considering the theory of resistivity surveys, 2) numerical model investigations, and 3) processing the data recorded during field surveys along angled survey lines. The theoretical considerations showed that both the geometric factors (and thus the calculated apparent resistivities) and the pseudo-depths are affected by angles in survey lines. In the pseudo-sections, the apparent resistivity data affected by the angles occur in fan-shaped zones centred at the angles. The errors in the apparent resistivities are, however, small. Even for a large angle of $45^{o}$, the errors do not exceed 6.5% (geometric factors and apparent resistivities) and 3.8% (pseudo-depths).

Despite the fact that the errors in the apparent resistivity data are small, numerical model studies showed that these errors could lead to severely distorted inverse resistivity models. Distorted models could lead to incorrect interpretations of the subsurface resistivity distributions. Since the contacts between different subsurface geological units are often targeted during groundwater exploration, distorted models could lead to boreholes being sited in suboptimal positions. This could affect the costs of groundwater exploration programmes because more boreholes may need to be drilled to intersect the targets.

Field surveys along angled survey lines confirmed the results of the theoretical work and the numerical modelling. It was also shown in this study that the apparent resistivity data set recorded along angled lines may be partially corrected by calculating the true geometric factors and by adjusting the apparent resistivity data accordingly. Significantly improved inverse resistivity models were found for the corrected data sets. It is therefore recommended that such corrections be done on all data sets recorded along angled survey lines, even if the errors in the apparent resistivity data are small.

No corrections could, however, be made to the affected pseudo-depths because the inversion software used in this study calculates pseudo-depths based on the assumption of straight survey lines and does not allow the user to adjust the pseudo-depths. It is therefore recommended that further studies be conducted to evaluate the effects of errors in the pseudo-depths on the inverse resistivity models and to determine whether models may be improved by correcting for these errors. This may require the use of different inversion software that allows the user flexibility to change the values of the input parameters to the inversion process.

Another direct effect of recording apparent resistivity data along angled lines is the fact that the volume of the subsurface investigated is displaced from the survey line. However, this is due to the geometry of the survey and cannot be corrected for single ERT profiles. It may be possible to account for the lateral displacement and to apply corrections to data sets consisting of several parallel ERT profiles. This warrants further investigation, but falls beyond the scope of the current research.

This study focussed on the effect of angled survey lines on the data and inverse models of the Wenner ($\alpha$) array. Many of the observations made during the study should be equally valid for other arrays, but further studies are recommended, particularly for the arrays that are dissimilar to the Wenner array in the way the electrodes are arranged. Such arrays include the pole-dipole and dipole-dipole arrays where there are often large separations between the current and potential electrode pairs.

# REFERENCES


Adli, Z.F., Musa, M.H., Arifin, M.N.K., 2010. Electrical Resistivity of Subsurface: Field and Laboratory Assessment. International Journal of Geological and Environmental Engineering 4, 422–425.

Ahiakwo, N.I., Egwuonwu, A.C., Okeke, O.C., 2018. A Review of the Geology and Mineral Resources of South Africa. International Journal of Advanced Academic Research 4, 90–121.

Ahzegbobor, P.A., 2010. 2D and 3D Geoelectrical Resistivity Imaging: Theory and Field Design. Scientific Research and Essays 5, 3592–3605.

Bernard, J., 2003. Short Note on the Depth of Investigation of Electrical Methods. Iris Instruments. Orléans, France.

Bobatchev. A., Modin, I, Shevnin, V., 2001. IPI2WIN v.2.0 - User's manual. Moscow University, Russia.

Botha, J.F., Cloot, A.H.J., 2004. Deformations and the Karoo Aquifers of South Africa. Advances in Water Resources 27, 383–398.

Botha, J.F., Verwey, J.P., van der Voort, I., Vivier, J.J.P., Buys, J., Collison, W.P., Loock, J.C., 1998. Karoo aquifers: Their geology, geometry and physical behaviour (No. 487/1/98). Water Research Commission, Pretoria, South Africa.

Catuneanu, O., Wopfner, H., Eriksson, P.G., Cairncross, B., Rubidge, B.S., Smith, R.M.H., Hancox, P.J. 2005. The Karoo Basins of South Central Africa. Journal of African Earth Sciences 43, 211–253.

Chandra, P.C., 2015. Groundwater Geophysics in Hard Rock, 1st ed. CRC Press, London.

Chevallier, L., Goedhart, M., Woodford, A.C., 2001. The Influence of Dolerite Sill and Ring Complexes on the Occurrence of Groundwater in Karoo Fractured Aquifers: A Morpho-tectonic Approach (WRC Project 937 No. 937/1/01). Water Research Commission, Pretoria, South Africa.

Dafalla, M.A., AlFouzan, F.A., 2012. Influence of Physical Parameters and Soil Chemical Composition on Electrical Resistivity: A Guide for Geotechnical Soil Profiles. International Journal of Electrochemical Science 7, 3191–3204.

Daily, W., Ramirez, A., Binley, A., LaBrecque, D., 2005. Electrical Resistance Tomography- Theory and Practice, in: Near-Surface Geophysics, Investigations in Geophysics. Society of Exploration Geophysicists, Tulsa, Oklahoma, U.S.A, pp. 573–597.

Danielsen, B.E., Dahlin, T., 2010. Numerical Modelling of Resolution and Sensitivity of ERT in Horizontal Boreholes. Journal of Applied Geophysics 70, 245–254.

Dey and Morrison, 1977. Resistivity Modelling for Arbitrarily Shaped 2-Dimentional Structure. Geophysical Prospecting 27, 1-62.

Donnenfeld, Z., Crookes, C., Hedden, S., 2018. Water Scarcity in South Africa (No. 13). Institute for Security Studies, Pretoria, South Africa.

Edwards, L.S., 1977. A Modified Pseudosection for Resistivity and IP. Geophysics 42, 1020–1036.

EPA, 2016. Resistivity Methods [WWW Document]. United States Environmental Protection Agency. URL https://archive.epa.gov/esd/archive-geophysics/web/html/resistivity_methods.html

Ferry, D.K., 2012. Ohm's Law in a Quantum World. Applied Physics, American Association for the Advancement of Science (AAAS) 335, 45–46.

Fourie, F., 2009a. The Influence of Curved and Angled Survey Lines on 2D Resistivity Surveys Employing the Wenner (α) Geometry, in: Potential Field Methods, Electrical Resistivity and Induced Polarization. Presented at the 11th SAGA Biennial Technical Meeting and Exhibition, SAGA, South Africa.

Fourie, F., 2009b. Model Studies of the Propagation of Errors During the Inversion of 2D Resistivity Data Recorded with the Wenner (α) Geometry Along Curved and Angled Survey Lines, in: Potential Field Methods, Electrical Resistivity and Induced Polarization. Presented at the 11th SAGA Biennial Technical Meeting and Exhibition, SAGA, South Africa.

Fourie, F.D., 2010. Lecture notes: The Electrical Resistivity Method. The Institute for Groundwater Studies, The University of the Free State. Bloemfontein, South Africa.

Furman, A., Ferré, P.A., Warrick, A.W., 2003. A Sensitivity Analysis of Electrical Resistivity Tomography Array Types Using Analytical Element Modeling. Vadose Zone Journal, Hydrology and Water Resources 2, 416–423.

Griffiths, D.H., Barker, R.D., 1993. Two-dimensional Resistivity Imaging and Modelling in Areas of Complex Geology. Journal of Applied Geophysics 29, 211–226.

Hassan, A.A., Nsaif, M.D., Abbas, I.M., 2015. 3D Electrical Resistivity Tomography Method for Simulating of Polygonal Soil Cracks. International Journal of Scientific & Engineering Research 6, 155–160.

Herbert, C.T., Compton, J.S., 2007. Depositional Environments of the Lower Permian Dwyka Diamictite and Prince Albert Shale Inferred from the Geochemistry of Early Diagenetic Concretions, Southwest Karoo Basin, South Africa. Sedimentary Geology 194, 263–277.

Herman, R., 2001. An Introduction to Electrical Resistivity in Geophysics. American Journal of Physics 69, 943–952.

Holland, M., 2012. Evaluation of Factors Influencing Transmissivity in Fractured Hard-rock Aquifers of the Limpopo Province. Water Research Commission 38, 379–390.

Johnson, M.R., Van Vuuren, C.J., Hegenberger, W.F., Key, R., Show, U., 1996. Stratigraphy of the Karoo Supergroup in Southern Africa: An Overview. Journal of African Earth Sciences 23, 3–15.

Kirsch, R., 2006. Groundwater Geophysics: A Tool for Hydrogeology, 1st ed. Springer, New York.

Koefoed, O., Mallick, K., 1979. Geosounding Principles: Resistivity Sounding Measurements, 1st ed, Methods in Geochemistry and Geophysics. Elsevier Scientific Publishing Company, New York.

Kumar, D., 2012. Efficacy of Electrical Resistivity Tomography Technique in Mapping Shallow Subsurface Anomaly. Journal Geological Society of India 80, 304–307.

Linol, B., de Wit, M.J., 2016. Origin and Evolution of the Cape Mountains and Karoo Basin, 1st ed, Regional Geology Reviews. Springer, Port Elizabeth, South Africa.

Loke, M.H., 1999. Electrical Imaging Surveys for Environmental and Engineering Studies: a Practical Guide to 2-D and 3-D Surveys. Penang, Malaysia.

Loke, M.H., 2002. RES2DMOD ver.3.01: Rapid 2D Resistivity Forward Modelling Using the Finite-Difference and Finite-Element Methods. Geotomo Software, Malaysia.

Loke, M.H., 2004. Tutorial: 2-D and 3-D Electrical Imaging Surveys. Geotomo Software, Malaysia.

Loke, M.H., 2011. Electrical Resistivity Surveys and Data Interpretation. In: Gupta H.K. (eds) Encyclopedia of Solid Earth Geophysics. Encyclopedia of Earth Sciences Series. Springer, Dordrecht.

Loke, M.H., Chambers, J.E., Rucker, D.F., Kuras, O., Wilkinson, B.P., 2013. Recent Developments in the Direct-Current Geoelectrical Imaging Method. Journal of Applied Geophysics 95, 135–156.

Makhokha, D., Fourie, F.D., 2016. A Systematic Approach to the Interpretation of Conductivity Anomalies Recorded with the Geonics EM34-3 Electromagnetic Instrument Across Intrusive Dolerite Dykes and Sills in the Karoo Supergroup (Master's Dissertation). University of the Free State, Bloemfontein, South Africa.

Manninen, T., Eerola, T.T., Mäkitie, H., Vuori, S., Luttinen, A., Sénvano, A., Manhiça, V., 2008. The Karoo Volcanic Rocks and Related Intrusions in Southern and Central Mozambique. Special Paper of the Geological Survey of Finland 48, 211–250.

McCarthy, T., Rubidge, B., 2005. The Story of Earth and Life, 1st ed. Struik Nature, Cape Town, South Africa.

Meinzer, O.E., 1923. The Occurrence of Ground Water in the United States, with a Discussion of Principles (USGS Numbered Series No. 489), Water Supply Paper. U.S. Government Printing Office, Washington, DC.

Milsom, J., Ericksen, A., 2011. Field Geophysics, 4th ed, The Geological Field Guide series. John Willey & Sons, West Sussex, U.K.

Mohamaden, M.I.I., Ehab, D., 2017. Application of Electrical Resistivity for Groundwater Exploration in Wadi Rahaba, Shalateen, Egypt. NRIAG Journal of Astronomy and Geophysics 6, 201–209.

Morrison, F., Gasperikova, E., 2012. DC resistivity and IP field systems, data processing and interpretation [WWW Document]. The Berkeley Course in Applied Geophysics. URL http://appliedgeophysics.berkeley.edu/ (accessed 1.11.18).

Murray, R., Baker, K., Ravenscroft, P., Musekiwa, C., Dennis, R., 2012. A Groundwater Planning Toolkit for the Main Karoo Basin: Identifying and Quantifying Groundwater Development Options Incorporating the Concept of Wellfield Yields and Aquifer Firm Yields. Water SA 38, 407–416.

Obi, J.C., 2012. The Use of Electrical Resistivity Tomography (ERT) to Delineate Water-filled Vugs Near a Bridge Foundation (Master's Thesis). Missouri University of Science and Technology, Missouri, U.S.

Okpoli, C.C., 2013. Sensitivity and Resolution Capacity of Electrode Configurations. International Journal of Geophysics 1–12.

Oldenborger, G.A., Routh, P.S., Knoll, M.D., 2005. Sensitivity of Electrical Resistivity Tomography Data to Electrode Position Errors. Geophysical Journal International 163, 1–9.

Oldenburg, D.W., 1978. The Interpretation of Direct Current Resistivity Measurements. Geophysics 43, 610–625.

Parasnis, D.S., 1986. Principles of Applied Geophysics, 4th ed. Chapman and Hall, London New York.

Pozdnyakova, L., Pozdnyakov, A., Zhang, R., 2001. Application of Geophysical Methods to Evaluate Hydrology and Soil Properties in Urban Areas. Urban Water 3, 205–216.

Reynolds, J.M., 1997. An Introduction to Applied and Environmental Geophysics, 2nd ed. John Wiley & Sons, New York.

Roy, A., Apparao, A., 1971. Depth of Investigation in Direct Current Methods. Geophysics 36, 943–959.

Sami, K., Neumann, I., Gqiba, D., de Kock, G., Grantham, G., 2002. Groundwater Exploration in Geologically Complex and Problematic Terrain – Guidelines (No. 966/1/02). Water Research Commission, Pretoria, South Africa.

Seaton, W.J., Burbey, T.J., 2002. Evaluation of Two-dimensional Resistivity Methods in a Fractured Crystalline Rock Terrane. Journal of Applied Geophysics 51, 21–41.

Singhal, B.S., Gupta, R.P., 2010. Applied Hydrogeology of Fractured Rocks, 2nd ed. Springer, London New York.

Smith, R.M.H., 1990. A Review of Stratigraphy and Sedimentary Environments of the Karoo Basin of South Africa. Journal of African Earth Science 10, 117–137.

Tankard, A., Welsink, H., Aukes, P., Newton, R., Stettler, E., 2009. Tectonic Evolution of the Cape and Karoo Basins of South Africa. Marine and Petroleum Geology 26, 1379–1412.

Truswell, J.F., 1977. The Geological Evolution of South Africa, 1st ed. Purnell & Sons, Cape Town, South Africa.

Van Tonder, G., 2012. Karoo Groundwater Atlas: February 2012 ( No. 439159) SRK Consulting, Cape Town, South Africa.

Van Wyk, W.L., 1963. Groundwater Studies in the Northern Natal, Zululand and Surrounding Areas, Geological Survey (South Africa) Memoir. Pretoria Government Printer, Pretoria, South Africa.

Vegter, J.R., 1995. An Explanation of a Set of National Groundwater Maps (No. TT74/95). Water Research Commission, Pretoria, South Africa.

Wilkinson, P.B., Chambers, J.E., Lelliott, M., Wealthall, G.P., Ogilvy, R.D., 2008. Extreme Sensitivity of Crosshole Electrical Resistivity Tomography Measurements to Geometric Errors. Geophysical Journal International 173, 49–62.

Wilkinson, P.B., Meldrum, P.I., Kuras, O., Chambers, J.E., Holyoake, S.J., Ogilvy, R.D., 2010. High-resolution Electrical Resistivity Tomography Monitoring of a Tracer Test in a Confined Aquifer. Journal of Applied Geophysics 70, 268–276.

Woodford, A.C., Chevallier, L., 2002. Hydrogeology of the Main Karoo Basin: Current Knowledge and Future Research Needs (No. TT 179/02). Water Research Commission, Pretoria, South Africa.

Yadav, G.S., 1988. Pole-Dipole Resistivity Sounding Technique for Shallow Investigations in Hard Rock Areas. Birkhäuser-Verlag 127, 63–71.

Zhou, B., Dahlin, T., 2003. Properties and Effects of Measurement Errors on 2D Resistivity Imaging Surveying. Near Surface Geophysics 1, 105–117.

## *ABSTRACT*

ERT surveying systems typically use standard protocols that assume straight survey lines and collinear electrodes. However, it is not always possible to conduct ERT surveys along straight lines due to the presence of infrastructures and other surface constraints. When survey lines are angled, the resistivity data and results may be affected for measurements where electrodes straddle the position of the angle in survey lines, since the assumed distances between some of the electrodes are larger than the actual (true) distances. This may result in 1) incorrect geometric factors and apparent resistivities, 2) incorrect estimation of the depths of investigation, and 3) the volumes of the subsurface sampled may be displaced from the survey line and the recorded apparent resistivity data may be the representative of the subsurface at positions laterally displaced from the survey lines.

This study investigates the impact of angled survey lines on 2D ERT data and results using the Wenner (α) array. The methodological approach of this study entails 1) the theoretical investigation of the influence of angled survey lines on the geometric factors, depths of investigation and the subsurface volume investigated, 2) numerical modelling of ERT responses over potential groundwater targets typically encountered in the Karoo Supergroup when using angled survey lines, and 3) the collection of field data on angled survey lines across different geological structures found in the Karoo Supergroup.

Considering the theory of resistivity surveys shows that both the geometric factors and the pseudo-depths are affected by angles in survey lines. The resulting errors in the apparent resistivities are, however, small. Even for a large angle of 45$^{o}$, the errors are smaller than 6.5% for the geometric factors and apparent resistivities, and smaller than 3.8% for the pseudo-depths.

Since the apparent resistivity data and the pseudo-depths are affected by angles in the survey lines, the inverse resistivity models, which uses the apparent resistivities and pseudo-depths as inputs, are also affected. The distorted inverse resistivity models could lead to the incorrect interpretation of the subsurface structures, which could lead to poorly sited boreholes. Numerical modelling shows that even small input errors may be propagated (both in magnitude and location) during inversion, thereby severely distorting the resulting resistivity models.

The results of field surveys show that apparent resistivity data sets recorded along angled lines may be partially corrected by calculating the true geometric factors and by modifying the apparent resistivity data accordingly. Significantly improved inverse resistivity models are found for corrected data sets. It may also be possible to improve the inverse resistivity models by correcting the affected pseudo-depths. This would, however, require the use of inversion software that allows the user

flexibility to change the values of the input parameters to the inversion process. For single ERT profiles, no corrections can be made for the fact that volume of the subsurface that is sampled is laterally displaced from angled survey lines. It may, however, be possible to account for the lateral displacement and to apply corrections to data sets consisting of several parallel ERT profiles.